The Role of the Voltage Gated Sodium Channel Gene *Scn1b* in Neuronal Excitability and Network Synchrony

by

Jacob Hull

A dissertation submitted in partial fulfillment
of the requirements for the degree of
Doctor of Philosophy
(Neuroscience)
in the University of Michigan
2019

Doctoral Committee:

Professor Lori L. Isom, Chair
Professor Richard I. Hume
Professor Geoffrey G. Murphy
Professor Jack M. Parent
Professor Leslie L. Satin
Research Assistant Professor Yukun Yuan

Jacob Hull

hulljm@umich.edu

ORCID iD: 0000-0003-1812-0214

© Jacob Hull 2019

Acknowledgments

This thesis marks a milestone in my lifelong dream of being a scientist. There have of course been numerous people who have made this possible.

I would first and foremost like to thank my doctoral advisor, Lori Isom, for her sage wisdom in all areas of science. Secondly I would like to thank my life coach, Lori Isom, for her sage wisdom in being a functional adult while also doing science. Thirdly, I would like to thank the scientific Scully to my scientific Mulder, Lori Isom, for listening to and indulging my scientific conspiracy theories. Fourthly, I would like to thank my writing partner, Lori Isom, without whom my babbling incoherency would forever remain so. The completion of this thesis marks quite an accomplishment for Lori in developing such a willful and often scattered student into a scientist.

I would also like to thank those who have taught me in and out of the lab at the University of Michigan. Luis Lopez-Santiago, Yukun Yuan, and Rene Caballero-Floran have been the optimal guides in becoming an electrophysiologist, teaching me how to cut through the electrophysiological voodoo as a technique and getting down to the real science (i.e. defining the action potential threshold). I would like to thank those in both the systems and integrative physiology training grant and the neural networks group who expanded my horizons so immensely, particularly Victoria Booth who has guided me during my computational neuroscience adolescence. I would like to thank Chunling Chen for the times we put our heads together to answer important questions and the enthusiasm with which she addressed them. I would like to thank my other lab members as well who helped me to grow and evolve in my thinking and scientific communication.

In particular, I would like to thank the students I helped train, who taught me as much as I did them. Of them, I must profusely thank Nick Denomme for his enthusiasm and perspectives on what I was doing. He was often the only person to feel the same

sense of wonder and was thus an immense source of validation and support. I would like to thank those on my doctoral committee, whose roles as a committee was incidental to the training and perspectives they provided otherwise

I would also like to thank my undergraduate research advisors, Christine Aikens and Bruce Schultz, for allowing me to start being a scientist at such an early point in my education. Not only was I surprised to be allowed in the lab doing research they even paid me to do it full-time. The financial support they provided marks the boundary where my science dreams became reality. They were also both terrific mentors and shaped the way I think as a scientist. The work in this thesis is largely an amalgamation of the computational physics approaches I learned with Christine and the electrophysiological and experimentalist approaches I learned with Bruce.

There are also numerous friends and family members along the way who I am forever indebted to in terms of shaping who I am and in their support in doing science. My sister: my earliest teacher, protector, and role model is in large part responsible for my love of science and education in general. She forced me to play pretend school almost every day of my childhood and thereby tricked me into thinking I have been on a giant playground this entire time. My mother refocused the chaotic child I was away from destruction and into creation. She instilled a love of knowing, of work, and alongside my brother, the value of principles and duty to others. My grandmother not only provided me with a home but also taught me that a job half-finished may as well be a job just begun. Numerous friends along the way have aided me through understanding and support of my sporadic absences throughout this process, many of them are already mentioned above. While science often interfered with our time together, the support is well appreciated. I must lastly thank those friends closest to me; my dog Roxy and my friend-turned-girlfriend-turned-family Jen, who were both there at every stage of graduate school and loved, supported, and taught me along the way.

Table of Contents

Acknowledgements..... ii

List of Figures..... vi

List of Tables..... vii

Abstract.....viii

Chapter I. **The Power Outside the Pore: Beyond Conduction in Voltage Gated Sodium Channels**.....1

Structure of VGSCs.....2

VGSC α Subunit Structure.....3

Structure of VGSC β subunits and the Heterotrimeric VGSC Signaling Complex.....6

VGSCs in Physiology and Development.....12

Expression Profile of the VGSC α Subunits.....12

VGSCs in the Initiation of Action Potentials.....14

Expression Profile of the VGSCs β Subunits.....16

β Subunits Alter VGSC Properties.....19

In Vivo Effects of β subunits on VGSC Function.....22

β Subunits Affect Trafficking and Expression of VGSC α subunits *In Vivo*.....244

Non-excitable Signaling Pathways of VGSCs Through Proteolytic Processing of β subunits.....288

Beyond Hodgkin-Huxley, Alternative Gating Schemes in VGSCs.....29

Neuromodulation of Voltage-gated Sodium Channel α Subunits.....32

β Subunit Crosstalk.....35

β Subunits Modulate Potassium Channels.....36

VGSCs in Structural Brain Development.....37

Differential Effects of VGSC β Subunits in Excitability.....39

VGSCs in Epilepsy and Intellectual Disability.....42

SCN1A.....43

SCN8A.....45

SCN2A.....47

SCN3A.....48

SCN1B.....49
Antiepileptic Drugs and VGSCs 52
Conclusion.....53
Chapter II. **Deletion of the epilepsy-associated gene, *Scn1b*, leads to network location specific disinhibition and pyramidal neuron dysfunction.....55**
Introduction.....55
Results 58
Discussion.....77
Methods 83
Chapter III. **Voltage Gated Sodium Current Diversity Suppresses Synchrony While Preserving Spike Timing Reliability in Pyramidal Neurons 95**
Introduction.....95
Results 97
Discussion.....119
Methods 124
Chapter IV. **Conclusions 138**
References **.....156**

List of Figures

Fig. 1.1 Topology of the VGSC α and β subunits. 3
Fig. 1.2 A multitude of functions of VGSC β subunits in the nervous system.....25
Fig. 2.1 PV-, but not CAMK2α-, dependent Cre deletion of *Scn1b* results in early lethality. 59
Fig. 2.2. *Scn1b* deletion results in cortical PV+ neuron hypoexcitability.....60
Fig. 2.3. Scn1b deletion reduces INa density in dissociated cortical PV+ neurons. 62
Fig. 2.4. Scn1b deletion results in network location and network activity dependent pyramidal neuron hyperexcitability 66
Fig. 2.5. *Scn1b* deletion differentially impacts spontaneous inhibitory post synaptic currents in layer 5 and layer 6 pyramidal neurons. 69
Fig 2.6. *Scn8a* haploinsufficiency does not rescue *Scn1b*$^{-/-}$ mice. 71
Fig. 2.7. Scn1b deletion reduces INa density and density diversity in nucleated patches from cortical layer 6 and subicular pyramidal neurons. 74
Fig. 2.8. Scn1b deletion does not impact VGKC density or voltage dependence in layer 6 pyramidal neurons. 76
Fig. 3.1. *Scn1b* deletion causes increased spike synchrony and impaired firing rate heterogeneity to fluctuating input. 98
Fig. 3.2. Altering INa desynchronizes spiking without affecting spike reliability.....102
Fig. 3.3. g_{Na} variability desynchronizes spiking in response to fluctuating synaptic conductances in a computational model. 106
Fig. 3.4. g_{Na} diversity suppresses spontaneous network synchrony. 110
Fig. 3.5. Asynchrony increases with increasing CV-g_{Na}, with weak dependence on mean g_{Na}. 112
Fig. 3.6 High CV-g_{Na} displaces the network coupling requirements to support synchrony. 115
Fig. 3.7 High CV-g_{Na} displaces the network coupling requirements to support synchrony in networks with heterogeneous connection probability. 118
Fig. 4.1. I_{Na} Variability and Synchrony. 148

List of Tables

Table 2.1 Scn1b deletion impairs excitability of PV+ neurons. 61
Table 2.2. Effects of Scn1b deletion on INa density and voltage-dependence in PV+ cortical neurons.....63
Table 2.3. *Scn1b* deletion alters excitability in subpopulations of pyramidal neurons in a network activity dependent manner.....68
Table 2.4. Effects of Scn1b deletion on INa density and voltage-dependence in layer 6 and subicular pyramidal neurons. 75
Table 2.5 Effects of *Scn1b* deletion on current density and voltage dependence of transient and non-inactivating IK. 77
Table 3.1. High CV-gNa suppresses synchrony across multiple cellular conditions. .113

Abstract

How organisms gather and respond to information is a fundamental process of life. In animals, the nervous system is an information processing system that performs operations with remarkable speed and efficiency. The primary currency of information in the nervous system, and the medium by which it is processed and transmitted, is electrical in nature. At the forefront of acting on the information contained in the neuronal membrane potential are voltage gated sodium channels (VGSCs). These channels convert membrane potential information into an explosive depolarization, in the form of an action potential. In combination with the work of our laboratory and others, this thesis work is directed at understanding the modularity and complexity of VGSCs, not only in the firing of action potentials, but in the powerful role they play in neuronal dynamics and pathophysiology of the nervous system. Chapter 1 of this thesis provides an introduction to VGSC biochemistry, physiology, and their role in epilepsy. Chapter 2 presents work directed at understanding the origins of hyperexcitability and epilepsy in a model of developmental and epileptic encephalopathy (DEE). DEEs are epileptic disorders with additional debilitating dysfunctions including intellectual disability. Mutations in several VGSC genes result in DEEs. One such gene, *SCN1B*, encodes a non-pore forming beta subunit of the VGSC signaling complex. *Scn1b*$^{-/-}$ mice model DEE and it has been proposed that epilepsy in this model results from altered development. Chapter 2

characterizes the origins of hyperexcitability in this mouse model. We found that, rather than a developmental origin, hyperexcitability in this model results from impaired inhibition in subsets of pyramidal neurons. We found impaired excitability and VGSC current (I_{Na}) in inhibitory neurons expressing parvalbumin and location specific disinhibition in pyramidal neurons. Under blockade of network activity, *Scn1b*$^{-/-}$ pyramidal neurons are not intrinsically hyperexcitable. We additionally found that I_{Na} is impaired in cortical layer 6 and subicular pyramidal neurons of Scn1b$^{-/-}$ mice. Strikingly, the impairment of I_{Na} is due to a loss of high I_{Na} density patches rather than a global shift in mean I_{Na}, greatly impairing I_{Na} heterogeneity. The impact of I_{Na} heterogeneity on firing pattern and network synchrony forms the subject of Chapter 3. We found that, when a fluctuating stimulus is presented to *Scn1b*$^{-/-}$ layer 6 pyramidal neurons, they have impaired response heterogeneity between neurons relative to *Scn1b*$^{+/+}$ mice while spike train reliability is unimpaired. We then tested the capacity of altering I_{Na} to change the firing pattern of neurons with the VGSC blocker tetrodotoxin, finding that altering I_{Na} is sufficient to alter firing pattern to levels between different neurons while preserving spike train reliability. We then investigated the role of I_{Na} heterogeneity in small networks computationally, finding that heterogeneous I_{Na} between neurons raises the network connectivity requirements to support spontaneous network synchronization. Altogether, this thesis work expands our understanding of the role of VGSCs in both physiology and pathophysiology. The enhanced understanding of the origins of hyperexcitability in *Scn1b*$^{-/-}$ mice provides important insights into the specific networks impacted in DEE and provides potential avenues for targeted therapeutics. The work here also expands our understanding of the biophysical mechanisms of neuronal heterogeneity and its

pathophysiological relevance, advancing our understanding of nervous system function and presenting an entirely novel avenue for treatment of epilepsy and intellectual disability.

Chapter I. The Power Outside the Pore: Beyond Conduction in Voltage Gated Sodium Channels

(Portions of this chapter have been published in Neuropharmacology 2018 doi: 10.1016/j.neuropharm.2017.09.018 and Pharmacol Rev 10.1124/pr.118.016592)

Voltage gated sodium channels (VGSCs) were first identified functionally in terms of their role in the upstroke of the action potential (AP) (Hille 2001). The underlying proteins were later identified as saxitoxin and scorpion toxin receptors consisting of α and β subunits (Hartshorne, Messner et al. 1982, Messner and Catterall 1985). We now know that VGSCs are heterotrimeric complexes consisting of a single pore forming α subunit joined by two β subunits; a noncovalently linked β1 or β3 and a covalently linked β2 or β4 subunit (Isom and De Jongh 1992, Isom, Ragsdale et al. 1995, Morgan, Stevens et al. 2000, Yu, Westenbroek et al. 2003). Mammalian genomes contain 9 VGSC α subunits, encoded by the *SCN(1-10)A* genes, and 5 β subunits, encoded by the *SCN(1-4)B* genes (Catterall WA and Waxman 2005). VGSC α subunits contain all the machinery necessary for channel cell surface expression, ion conduction, voltage sensing, gating, and inactivation, in one central, polytopic, transmembrane protein (Auld, Goldin et al. 1988).

Consequently, early electrophysiological results led to the misconception that β subunits are simple accessories to α subunits (Goldin, Snutch et al. 1986).

However, in the 25 years since the original cloning of the first β subunit, their role has expanded immensely (Isom and De Jongh 1992). VGSC β subunits stand at the forefront of the modularity of VGSCs, conferring unique gating mechanisms, regulating cellular excitability, affecting brain development, and even having functions that are independent of the α subunits. The vast array of functions of these proteins stems from their special station in the channelome: being the only known constituents that are cell adhesion and intra/extracellular signaling molecules in addition to being part of channel complexes (Isom, De Jongh et al. 1994, Brackenbury and Isom 2011). This functional trifecta and how it goes awry demonstrates the power of VGSC signaling complexes, broadening our understanding of VGSCs in the nervous system beyond the upstroke of an action potential.

Structure of VGSCs

VGSCs transition between several basic conformations through the course of an action potential including closed, open, and inactivated states. The predominant state of the channel at resting membrane potential is the closed state, where no Na^+ ions are conducted. Upon sufficient membrane depolarization, channels undergo a conformational change to the open state, where Na+ ions enter the cell and drive further depolarziaiton. After transition to the open state, fast inactivation is enhance, where intracellular residues (the inactivation gate) occule the inside face of the channel, blocking further conduction. Such fast inactivation (recovery time constants on the scale of milliseconds), is distinct from slow inactivation (recover time constants on the scale of hundreds milliseconds to

seconds) which is discussed in more detail below. The comparatively slower rate of inactivation to activation and deactivation allows for timely termination of depolarization during an action potential and supports the refractory period between action potentials (Hille 2001).

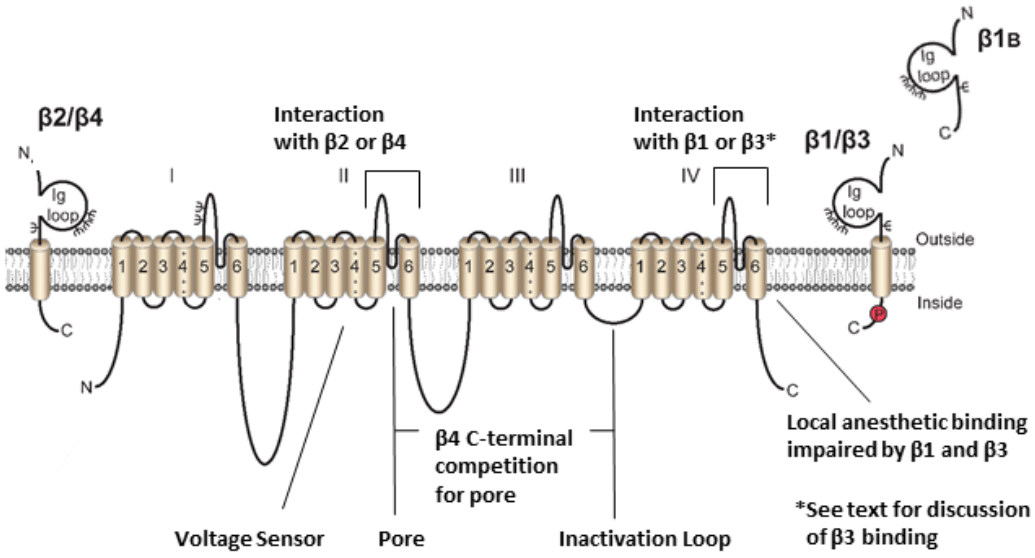


Fig. 1.1 Topology of the VGSC α and β subunits. VGSCs contain a pore-forming α subunit consisting of four homologous domains of six transmembrane segments (Catterall 2012). Segment 4 contains the voltage sensor. VGSCs also contain one or more β subunits. β1, β2, β3, and β4 contain an extracellular immunoglobulin (Ig) loop, transmembrane domain, and an intracellular C-terminal domain (O'Malley and Isom 2015). β1B also contains an Ig loop, but has a different C-terminus lacking a transmembrane domain, and is thus a soluble, secreted protein (Patino, Brackenbury et al. 2011). β1 contains a tyrosine phosphorylation site in its C-terminus (Malhotra, Thyagarajan et al. 2004) ψ, glycosylation sites. β1 and β3 are non-covalently linked to α, whereas β2 and β4 are covalently linked through disulfide bonds (O'Malley and Isom 2015). Figure was modified from (Brackenbury and Isom 2011).

VGSC α Subunit Structure

VGSC α-subunits can be divided into two classes based on their sensitivity to tetrodotoxin (TTX). $Na_v1.1$-1.4, $Na_v1.6$ and $Na_v1.7$ are 'TTX-sensitive', as half-maximal

block of Na^+ conduction by TTX occurs at concentrations between 1 and 25 nM (Catterall, Perez-Reyes et al. 2005). $Na_v1.5$, $Na_v1.8$, and $Na_v1.9$ are referred to as 'TTX-resistant', requiring >1 μM TTX for block of half-maximal conduction. All the human VGSC α subtypes share greater than 75% amino acid sequence identity(Catterall, Perez-Reyes et al. 2005). The different conformational states of VGSC α subunits rely on the activity of distinct regions of the channel. VGSC α subunits consist of 4 homologous domains, each composed of 6 transmembrane segments (see Fig. 1.1).

Segments 1-4 (S1-S4) are primarily involved in voltage dependent activation and deactivation. The S4 segment in particular is crucial to voltage sensing, containing four to eight positively charge amino acid motifs (R/K) which are primarily involved in voltage sensing (Bezanilla 2000, Catterall 2010). Segments S1-S3 form a gating canal using polar and negative residues that promote the movement of the S4 segment upon depolarization (Catterall 1986, Catterall 1986, GuY and Seetharamulu 1986). Site directed mutagenesis studies in the S4 segment shows a reduction of the steepness in voltage sensitive gating with mutations in the S4 Arginine residues, supporting the view of their role as gating charges (Stühmer, Conti et al. 1989, Kontis, Rounaghi et al. 1997). The electromechanical coupling of voltage sensing to the opening of the pore domain is thought to occur through a sliding-helix mechanism, a view supported by a recent cryo-EM structure of the resting state of the ancestral bacterial sodium channel (Vargas, Yarov-Yarovoy et al. 2012, Wisedchaisri, Tonggu et al. 2019).

S5-S6 form the pore, which is necessary for ion conduction following voltage dependent activation. This region was first identified through the residues necessary for forming the binding site of the VGSC pore blocker tetrodotoxin. Mutations in these residues were later shown to control ion selectivity of the channel (Noda, Suzuki et al. 1989, Terlau, Heinemann et al. 1991, Heinemann, Terlau et al. 1992). The residues responsible for fast inactivation were discovered using site directed mutagenesis and targeted antibody studies (Vassilev, Scheuer et al. 1988). It was found that the fast inactivation gate consists of a short loop on the intracellular side of the channel linking domains III and IV. Fast inactivation occurs through occlusion of the intracellular face of the pore blocking ion conduction. The amino acid motif IFM was found to be critical, with synthetic peptide with this motif restoring fast inactivation to mutant channels (Eaholtz, Scheuer et al. 1994). Selectivity of Na^+ over other ions is an essential function for the action of VGSCs. This is achieved by the precise architecture of a VGSC region known as the selectivity filter. Approximately 4.6 Å in size, the selectivity filter is composed of an inner and outer ring of charged residues. The asymmetric charge distribution of each ring coordinates the solvated Na^+ ions as they flow through the pore (Catterall 2012). Through mutagenesis and subsequent electrophysiological analysis, four key residues (D: aspartate, E: glutamate, K: lysine, and A: alanine), each present in one of the domains, were identified as the inner ring of the mammalian VGSC selectivity filter(Lipkind and Fozzard 2008). The DEKA motif found in human VGSCs is conserved across all isoforms. Mutating the KA (lysine and alanine) of the DEKA motif to glutamate (EE) abolishes Na^+ selectivity of the channel and allows Ca^{2+} ions to pass through the pore.(Heinemann, Terlau et al. 1992)

Structure of VGSC β subunits and the Heterotrimeric VGSC Signaling Complex

VGSCs are heterotrimers in brain. While the β subunits do not conduct ions or perform voltage sensing, the assembly of the VGSC signaling complex between α and β subunits is critical for VGSC function (Hull and Isom 2018). Excluding β1b, the VGSC β subunits have type 1 membrane protein topology consisting of an extracellular N-terminal domain, a single transmembrane segment, and a C-terminal tail (Fig. 1.1) (Isom and De Jongh 1992, Isom, Ragsdale et al. 1995, Kazen-Gillespie, Ragsdale et al. 2000, Morgan, Stevens et al. 2000, Yu, Westenbroek et al. 2003). The array of functions and interactions imparted by the assembly of the VGSC complex relies on the function of each of the β subunit domains, making β subunits immensely powerful for such small proteins. This section will examine the structure and sites of interactions of β subunits in forming the VGSC signaling complex

Each VGSC β subunit features an extracellular N-terminal domain that contains homology to V-type immunoglobulin (Ig) loops common to the Ig superfamily of cell adhesion molecules (CAMs) (Isom and De Jongh 1992, Isom, Ragsdale et al. 1995, Kazen-Gillespie, Ragsdale et al. 2000, Morgan, Stevens et al. 2000, Yu, Westenbroek et al. 2003). In the β subunits, these domains are capable of both interaction with VGSC α subunits and cell adhesion (Brackenbury and Isom 2011). Each Ig domain consists of antiparallel β sheets stabilized by an intrasubunit disulfide bond (McCormick, Isom et al. 1998, Gilchrist, Das et al. 2013, Namadurai, Balasuriya et al. 2014, Das, Gilchrist et al. 2016, Shimizu, Miyazaki et al. 2016). Early on, β subunit structure was modeled based

on the crystal structure of the extracellular domain of myelin P0, a protein containing a single V type Ig loop and single transmembrane domain with modest homology to β1 and β3 (Isom, Ragsdale et al. 1995, McCormick, Isom et al. 1998, Morgan, Stevens et al. 2000). Crystal structures of β2, β3, and β4 were recently solved in isolation or in complexes with each other. (Gilchrist, Das et al. 2013, Namadurai, Balasuriya et al. 2014, Das, Gilchrist et al. 2016). Subsequently the crystal structure of β1 in complex with $Na_v1.4$ from electric eel was solved (Yan, Zhou et al. 2017). These structures inform and confirm many insights into β subunit Ig domains garnered from previous biochemical work and show that each subunit contains unique structural features. Approximately one-third of the molecular mass of each β subunit is due to N-linked glycosylation moieties in the extracellular domain (Isom and De Jongh 1992, Isom, Ragsdale et al. 1995, McCormick, Isom et al. 1998, Morgan, Stevens et al. 2000, Yu, Westenbroek et al. 2003, Johnson, Montpetit et al. 2004). Sialic acid terminated glycosylation is necessary for modulation of α subunit gating by β1, suggesting that electrostatic interactions with voltage sensing domains may occur through modification of these residues (Johnson, Montpetit et al. 2004).

VGSC β1 and β3 subunits share the highest percentage of sequence identity to each other, while β2 and β4 share a higher percentage of sequence identity to each other than to either β1 or β3 (Isom and De Jongh 1992, Isom, Ragsdale et al. 1995, Morgan, Stevens et al. 2000, Yu, Westenbroek et al. 2003). Studies using chimeric subunits revealed that β1 modulates the gating of $Na_v1.2$ via association with the extracellular domain IV S5-S6 region of that α subunit (McCormick, Srinivasan et al. 1999, Qu, Rogers

et al. 1999). This may extend to β3, given its high sequence similarity to β1, although see (Namadurai et al. 2014). The site of association between β1 and Nav1.4 was localized to the S5-S6 segments, at the interface of domains I and IV, implicating channel specific regions of interaction (Makita, Bennett et al. 1996). This was recently confirmed with the crystal structure of β1 in complex with $Na_v1.4$ with additional interaction sites in the transmembrane and intracellular segments of β1 (Yan, Zhou et al. 2017). β2 and β4 bind to VGSC α subunits differently than β1 and β3. A key difference between the Ig loops of the β subunits is the presence of an exposed free cysteine residue in β2 and β4 that forms a disulfide bond with α subunits (Isom, Ragsdale et al. 1995, Yu, Westenbroek et al. 2003). Mutation of this residue in β2 or β4 abolishes α subunit interactions (Chen, Calhoun et al. 2012, Gilchrist, Das et al. 2013). The cysteine residues in β2 (Cys-26) or β4 (Cys-58) responsible for covalent association with α were determined to bind to a corresponding cysteine residue in $Na_v1.2$ located in the domain II S5-S6 loop (Das, Gilchrist et al. 2016). This residue is absent from the tetrodotoxin-resistant (TTX-R) α subunits Nav1.5, Nav1.8 and Nav1.9, although Nav1.5 and $\beta2$ have been shown to associate through disulfide bonds in cardiac tissue and β2 modifies Nav1.5 currents in heterologous systems and *in vivo* (Malhotra, Chen et al. 2001, Johnson and Bennett 2006, Bao, Willis et al. 2016). β2 and β4 differentially affect channel modulation of α subunits by extracellular μ-, μO- and μO§-conotoxins relative to β1 and β3 (Wilson, Zhang et al. 2011, Zhang, Wilson et al. 2013, Gajewiak, Azam et al. 2014, Wilson, Zhang et al. 2015). In the case of μO§-conotoxins, association with α subunits occurs through the same cysteine through which these subunits covalently bind to VGSC α subunits. β1 and β3 have no influence on μO§-conotoxin effects (Gajewiak, Azam et al. 2014). Thus, as

expected from early data showing that VGSCs in brain are heterotrimers, these results suggest that the binding sites for β1 and β3 vs β2 and β4 on α subunits are mutually exclusive.

In addition to channel modulation, β subunits, in particular β1, participate in homophilic and heterophilic cell adhesion through their extracellular Ig domains. This property allows β subunits to interact with a wide variety of proteins in both *cis* and *trans* configurations, including with identical β subunits in the same membrane or on adjacent cells (Brackenbury and Isom 2011). Importantly, β subunit-mediated cell adhesive interactions can occur both in the presence and absence of VGSC α subunits (Malhotra, Kazen-Gillespie et al. 2000). β subunit-mediated cell adhesion is most well characterized for β1, which associates homophilically *in vitro* in *trans*, and heterophilically with the Ig CAMs VGSC β2, contactin-1, Nf-186, and NrCam, with the adhesion molecule N-cadherin, and with the extracellular matrix molecule tenascin-R (Isom and Catterall 1996, Malhotra, Kazen-Gillespie et al. 2000, Kazarinova-Noyes, Malhotra et al. 2001, Ratcliffe, Westenbroek et al. 2001, McEwen and Isom 2004). β2 associates homophilically as well as heterophilically with β1 and tenascin-C, but not with contactin (Srinivasan, Schachner et al. 1998, Xiao, Ragsdale et al. 1999, McEwen and Isom 2004). β4 engages in homophilic cell-cell adhesion but its ability to function as a heterophilic CAM has not been tested (Shimizu, Miyazaki et al. 2016). Crystal structure guided photocrosslinking experiments with β1 and β4 revealed the specific residues responsible for homophilic cell adhesion, further elucidating the structure of VGSC complexes (Shimizu, Miyazaki et al. 2016). Interestingly, β3 is predicted to form trimeric complexes that would obscure the

analogous residues necessary for *trans* homophilic adhesion (Namadurai, Balasuriya et al. 2014). These results are consistent with earlier data showing that, while β1 or β2 subunit expression in *Drosphila* S2 cells resulted in the formation of high affinity aggregates, β3 expression did not (McEwen, Chen et al. 2009). Overall, however, data on the cell adhesive properties of β3 are conflicting, possibly as an effect of differential trimerization based on expression system (Yereddi, Cusdin et al. 2013).

β subunits contain a single, α helical transmembrane domain that can confer unique functional properties. For example, the structure of the β3 transmembrane domain is proposed to mediate *cis* homophilic interactions allowing for trimerization (Namadurai, Balasuriya et al. 2014). Trimeric β3 complexes are capable of forming oligomers with Nav1.5, a departure from the canonical heterotrimeric VGSC structure (Namadurai, Balasuriya et al. 2014). Interaction with the third voltage sensing domain of $Na_v1.4$ occurs through the transmembrane domain of β1, providing an additional potential means for modification of voltage sensing (Yan, Zhou et al. 2017). For *Scn1b*, retention of intron 3 through alternative splicing results in the polypeptide β1b, a secreted, soluble CAM. In place of a transmembrane domain, β1b contains an alternate C-terminus with an amino acid sequence that is species specific (Kazen-Gillespie, Ragsdale et al. 2000). β1b acts as an extracellular CAM ligand. It is also capable of modulation of $Na_v1.5$ but not $Na_v1.1$ or $Na_v1.3$ in heterologous systems (Watanabe, Koopmann et al. 2008, Patino, Brackenbury et al. 2011). β subunits can also shed their Ig domain following sequential cleavage by β-Site APP-cleaving enzyme 1 (BACE1) and γ-secretase (Wong, Sakurai et

al. 2005, Gersbacher, Kim et al. 2010). The resulting soluble extracellular fragment is likely to behave similarly to β1b.

β subunit intracellular C-terminal domains are short sequences predicted to have disordered structure (Cusdin, Nietlispach et al. 2010, Lewis and Raman 2011, Namadurai, Balasuriya et al. 2014). Along with the transmembrane segment, the intracellular tails confer additional interactions with VGSC α subunits. Co-expression of β1 or β3 with Nav1.3 in heterologous cells attenuates lidocaine binding to the channel, suggesting that the β subunit C-terminal domains may occlude the α subunit local anesthetic binding site, located on the S6 helix of domain IV, and accessible only from the intracellular side (Lenkowski, Shah et al. 2003, Catterall 2012). Mutations in *Scn1a* identified an additional α-β1 subunit interaction site in the β1 C-terminal tail (Spampanato, Kearney et al. 2004). The crystal structure of the $Na_v1.4$- β1 complex suggests the C-terminal tail may modify inactivation through an allosteric blocking mechanism (Yan, Zhou et al. 2017). The intracellular domain of β2 modulates Nav1.5 gating and the C-terminal tail of β4 contains residues capable of intracellular blockade of α subunits to generate resurgent sodium current (I_{Na}) (described in section 2) (Grieco, Malhotra et al. 2005, Zimmer and Benndorf 2007). β subunit intracellular domains may also impart intracellular regulatory control of α and β subunit activity. For example, phosphorylation of β3 residue S161 is necessary for modulation of $Na_v1.2$ I_{Na} (Merrick, Kalmar et al. 2010). The β1 intracellular tyrosine residue Y181 is required for β1 association with the scaffolding proteins ankyrin-B and ankyrin-G at points of cell-cell contact following *trans* homophilic cell adhesion (Malhotra, Kazen-Gillespie et al. 2000, Merrick, Kalmar et al. 2010).

Phosphorylation of this residue prevents ankryin binding (Malhotra, Koopmann et al. 2002).

VGSCs in Physiology and Development

VGSCs exhibit cell type specific expression, interactions with other proteins, and unique subunit structural features that are important for cell type, subcellular domain, and brain region specific control of excitability and development. In the following section we will examine the physiological function of VGSCs at the level of control of individual neuronal excitability, β subunit modulation of VGSC α subunits and voltage gated potassium (VGKC) channel currents, and in the structural development in the nervous system.

Expression Profile of the VGSC α Subunits

Each VGSC α subtype is differentially distributed within and across cell and tissue types, indicating that regional enrichment or cell type selective function is important in specific neuronal functions. Each subtype has distinctive kinetic and voltage sensing properties. VGSC subtypes are strategically expressed based on these properties to maximize physiological function. $Na_v1.1$-1.3 and $Na_v1.6$ are the most prominent central nervous system VGSCs, while the $Na_v1.7$-1.9 isoforms are mainly expressed in the peripheral nervous system. $Na_v1.4$ and $Na_v1.5$ are mainly expressed in skeletal and cardiac muscle, respectively (Catterall, Goldin et al. 2005). The different VGSCs expressed in brain exhibit isoform enrichment in a cell type and subcellular region directed

manner. In the adult brain $Na_v1.1$, $Na_v1.2$, and $Na_v1.6$ are the predominant VGSCs while $Na_v1.3$ is highly expressed in the soma of neurons during development but shows low expression in the adult brain (Frank and Catterall 2003). In the forebrain, $Na_v1.1$ mRNA and protein are highly expressed in GABAergic inhibitory interneurons, although weaker expression exists in pyramidal neurons of the cortex and hippocampus (Westenbroek, Merrick et al. 1989, Gong, Rhodes et al. 1999, Van Wart, Trimmer et al. 2007, Okaty, Miller et al. 2009). In interneurons, subcellular localization of $Na_v1.1$ protein is enriched in the cell body and to a greater degree in the axon initial segment (AIS) (Ogiwara, Miyamoto et al. 2007). Na_v 1.2 expression is enriched in the axons of somatostatin- but not parvalbumin (PV)-positive interneurons of the cortex, showing further cellular subtype enrichment in VGSC expression (Li, Tian et al. 2014). Na_v 1.2 is also expressed highly in the proximal AIS of pyramidal neurons and, during development, highly at nodes of Ranvier. $Na_v1.2$ expression is present but weaker in the cell body and dendrites of pyramidal neurons (Hu, Tian et al. 2009). Na_v 1.6 protein is highly expressed in the axons of parvalbumin expressing (PV+) neurons and in the distal AIS of pyramidal neurons and in nodes of Ranvier (Hu, Tian et al. 2009, Li, Tian et al. 2014). Na_v 1.6 is also expressed in the cell body and dendrites of pyramidal neurons (Caldwell, Schaller et al. 2000, Krzemien, Schaller et al. 2000, Lorincz and Nusser 2010). The three major adult CNS VGSCs show both pre- and post-synaptic localization at synaptic terminals in the hippocampus (Johnson, Herold et al. 2017). Such localization appears to be regional/cell class specific, with the central hilus of the dentate gyrus showing predominantly presynaptic Na_v 1.1 immunoreactivity, while in the stratum radiatum of CA1, Na_v 1.1, 1.2, and 1.6 exhibit stronger post-synaptic localization in spines and dendrites (Johnson,

Herold et al. 2017). Although most of the work studying the cell type and sub-regional specific VGSC expression and function has focused on cortex and hippocampus, investigation has expanded to thalamic and subthalamic regions of the brain (Kalume, Oakley et al. 2015, Makinson, Tanaka et al. 2017). Although the study of VGSCs in most subcortical regions is nascent, cell type and regional effects of specific VGSCs in these regions are also likely to be highly relevant for circuit function.

VGSCs in the Initiation of Action Potentials

The specific role of VGSCs in the upstroke of the action potential was first characterized by Hodgkin and Huxley in squid axon (Hille 2001). Since this seminal work, many nuances to action potential initiation and propagation have been uncovered along with other roles of VGSCs which are crucially dependent on the localization of channels as described above.

Though there are VGSCs throughout the entire structure of most neurons in the CNS, action potentials are usually first initiated in the AIS (Lai and Jan 2006, Bean 2007). This AIS is is traditionally ~50 µm from the soma, though this can vary widely between neurons of different types and within the same types(Jones and Svitkina 2016). This is an important facet of neuronal excitability, as excitatory inputs in the dendrites and soma, are usually distant to the site of AP initiation. Importantly however, Na+ spikes in dendrites do occur and are suspected to have important physiological functions. AIS localization of AP initiation relies heavily on the differences in the density and properties of VGSCs in different subcellular compartments of neurons. Here we will focus on pyramidal neuron

APs, predominantly layer 5 pyramidal neurons, which have been more extensively studied than other neurons. Theoretical studies suggest that the density of VGSCs in the axon initial segment are required to be of 20 to 1,000 fold higher density than in the soma and dendrites in order to have such AIS biased initiation (Dodge and Cooley 1973, Moore, Stockbridge et al. 1983, Mainen, Joerges et al. 1995, Rapp, Yarom et al. 1996). Experimental evidence of such a distribution was first uncovered using VGSC antibodies (Wollner and Catterall 1986). This has largely been confirmed by Na+ imaging studies and axonal and somatic outside out patch clamp recordings (Kole, Ilschner et al. 2008, Hu, Tian et al. 2009, Fleidervish, Lasser-Ross et al. 2010).

The high density of axonal channels is an important aspect of VGSCs in the axon initial segment but there are also differences in channel properties and in the type of channels expressed in the AIS. In the proximal AIS, there is a high density of $Na_v1.2$ channels which is gradually decreased with distance along the AIS and replaced by Nav1.6. The voltage dependent properties of the proximal and distal AIS channels are also distinct, with distal channels having hyperpolarized activation relative to somatic and proximal AIS channels(Hu, Tian et al. 2009). While this result is consistent with the hyperpolarized activation of $Na_v1.6$, it has been recently found *Scn8a* deletion in excitatory neurons does not affect the distal position of AIS spike initiation and that the distal AIS of these mice maintain the normal low threshold of axonal VGSCs activation.(Katz, Stoler et al. 2018) These results suggest additional clarifying work into the distal AIS VGSC properties needs performed including the role of local cytoskeletal environment and the action of β subunits. VGSC location to the AIS is crucially dependent

on ankryin-G, particularly the giant 480 kDa form, with deletion of ankryin-G preventing the clustering of Na_vs in the AIS membrane(Nelson and Jenkins 2017).

VGSCs in the proximal AIS, predominantly $Na_v1.2$, have similar voltage dependent properties to somatic VGSCs and are important in AP backpropagation into the soma and dendrites(Hu, Tian et al. 2009). Importantly, the relative depolarization in the voltage dependence of activation in proximal AIS channels keep initiation localized to the distal AIS. In early in development, $Na_v1.2$ is the predominant VGSC throughout the AIS, and is gradually replaced during development by $Na_v1.6$ (Boiko, Van Wart et al. 2003, Osorio, Alcaraz et al. 2005). Somatic and dendritic VGSCs are largely a mix of many channel types, and are important in the role of the backpropagating APs in learning and memory. Additional roles of these channels in interaction with the voltage dependent Ca+ and K+ channels specialized to these compartments may be critical for other functions in pyramidal neuron excitability as well.

Expression Profile of the VGSCs β Subunits

β subunits differ in their expression and posttranslational modifications within different stages of development, in different tissues, between cell types, and in subcellular locations. This imparts a specificity that is crucial for normal development and excitability. β subunits are expressed in both excitable and non-excitable cells in brain (O'Malley and Isom 2015). In whole brain, β1b and β3 mRNA and protein expression are high during the prenatal and early postnatal period in mammals (Kazen-Gillespie, Ragsdale et al. 2000, Shah, Stevens et al. 2001, Patino, Brackenbury et al. 2011). These subunits then

give way to increased expression of β1, β2, and β4 mRNA protein in the first postnatal week and this expression persists through adulthood (Sutkowski and Catterall 1990, Isom and De Jongh 1992, Isom, Ragsdale et al. 1995, Sashihara, Greer et al. 1996, Lein, Hawrylycz et al. 2007). Different cell types in the brain express different β subunits at various levels. *In situ* hybridization and immunohistochemistry show that *Scn1b* and β1 expression, respectively, are ubiquitous throughout the brain but with modest heterogeneity (Sashihara, Greer et al. 1996, Blackburn-Munro and Fleetwood-Walker 1999, Lein, Hawrylycz et al. 2007, Brackenbury and Isom 2011, Wimmer, Harty et al. 2015). β1 immunohistochemical studies show subcellular localization in similar patterns to that found for α subunits, with high density at axon initial segments (AISs) and nodes of Ranvier in myelinated axons (Chen, Westenbroek et al. 2004, Wimmer, Reid et al. 2010, Kruger, O'Malley et al. 2016). This subcellular localization pattern allows for specialized functions. Exemplary of the importance of subcellular localization is the action of β1 at nodes of Ranvier. β1 is highly enriched in the nodal gap where it is presumed to modulate VGSC α subunit cell surface expression and gating. However, in the paranodal region β1 is engaged in a trimeric axonal-glial cell adhesion complex consisting of axonal β1, contactin, and Caspr binding in *trans* to glial neurfascin-155 in the absence of VGSC α subunits (Kazarinova-Noyes, Malhotra et al. 2001, McEwen and Isom 2004). β1 expression at the growth cones of developing neurons mediates several important functions where it is proposed to act both as a CAM and as a modulator of I_{Na} (Brackenbury, Calhoun et al. 2010). *Scn1b* is also the mostly highly expressed β subunit gene in the peripheral nervous system (PNS), where it is particularly enriched in medium

and large diameter A fibers with lower expression in C fibers (Blackburn-Munro and Fleetwood-Walker 1999, Lopez-Santiago, Pertin et al. 2006, Zhao, O'Leary et al. 2011).

Scn2b expression is similarly ubiquitous in adult brain as assessed through *in situ* hybridization (Blackburn-Munro and Fleetwood-Walker 1999, Lein, Hawrylycz et al. 2007). Similar to β1, β2 protein is highly expressed at the AIS and nodes of Ranvier. *Scn2b* is also expressed in the PNS, where its deletion results in loss of responsiveness to inflammatory and neuropathic pain but not mechanosensation, again suggesting cell type specific functions (Lopez-Santiago, Pertin et al. 2006, Zhao, O'Leary et al. 2011).

While *Scn3b* mRNA and protein are expressed ubiquitously throughout the developing CNS, in adult mice expression is greatly attenuated except in specific structures, most highly in hippocampus and others (Morgan, Stevens et al. 2000, Lein, Hawrylycz et al. 2007). This differs in human brain, where *SCN3B* expression remains highly expressed through adulthood similarly to *SCN3A* (Chen, Dale et al. 2000, Lein, Hawrylycz et al. 2007). PNS expression of *Scn3b* is especially high in unmyelinated C fibers and is low in the other fiber types (Lopez-Santiago, Pertin et al. 2006, Zhao, O'Leary et al. 2011).

Scn4b is the most restricted of the β subunits in its expression profile. *Scn4b* mRNA and protein are highly expressed in several neuronal populations, many of which are known for spontaneous or burst firing APs (Lein, Hawrylycz et al. 2007, Lewis and Raman 2014). The highest expression of β4 protein and *Scn4b* mRNA are found in the

striatum and cerebellar purkinje neurons but are also highly expressed in other restricted brain regions (Lein, Hawrylycz et al. 2007, Miyazaki, Oyama et al. 2014). β4 subcellular localization is similar to that of the other β subunits, being enriched at the AIS, nodes of Ranvier, and along the length unmyelinated axons (Buffington and Rasband 2013, Miyazaki, Oyama et al. 2014). In the PNS β4 is most highly expressed in medium and large A fibers (Lopez-Santiago, Pertin et al. 2006, Zhao, O'Leary et al. 2011).

While not much is known about the localization of β subunits into the axon, this process likely involves interactions with VGSC α subunits. Disruption of the disulfide bond between α subunits and β2 or β4 impairs the ability of β subunits to traffic to axons and nodes of Ranvier (Chen, Calhoun et al. 2012, Buffington and Rasband 2013). Similarly, an *Scn1b* mutation that interferes with α-β1 association results in failure of the mutant β1 to traffic from the soma to the AIS and nodes of Ranvier (Kruger, O'Malley et al. 2016). This suggests β1 subunit enrichment in axonal domains is dependent on trafficking of α–β complexes rather than to β subunit independent trafficking. This would imply dynamic association of β1 with α subunits, as β1 in the paranode of nodes of Ranvier is not associated with α subunits (Kazarinova-Noyes, Malhotra et al. 2001, McEwen and Isom 2004). β subunits are also expressed in various glia where they may function as cell adhesion guides and cues for neurodevelopment, including coordinating neurite outgrowth, axonal fasciculation, and neuronal migration (Brackenbury and Isom 2011).

β Subunits Alter VGSC Properties

The β subunits have specific effects on VGSC gating states and contribute unique gating mechanisms. Early work expressing α subunits in heterologous systems showed that α subunits alone contain all the machinery necessary for the basic VGSC gating processes (Noda, Ikeda et al. 1986, Tomiko, Rosenberg et al. 1986, Recio-Pinto, Duch et al. 1987). However, the activation and inactivation kinetics of TTX-sensitive α subunits expressed in Xenopus oocytes without β subunits are slower than properties observed for native VGSC expression. The voltage dependence of I_{Na} is also altered (Goldin, Snutch et al. 1986, Auld, Goldin et al. 1988, Trimmer, Cooperman et al. 1989, Joho, Moorman et al. 1990). The first indication that β subunits were necessary to reconstitute native channel properties was found by coinjection of low molecular weight brain mRNA (containing β subunit transcripts) with high molecular weight mRNA (containing α subunit transcripts). The low molecular weight mRNA fraction conferred native kinetics and voltage dependence on I_{Na} expressed by the high molecular weight mRNA fraction (Krafte, Snutch et al. 1988). Cloning of *Scn1b* and *Scn2b* cDNAs and their coexpression with α subunits in *Xenopus* oocytes revealed that β subunits are indeed responsible for these differences as well as promotion of the surface expression of α subunits (Isom and De Jongh 1992, Isom, Ragsdale et al. 1995).

The effects of β subunits on channel cell surface expression, activation, and inactivation are dependent on the particular β subunit expressed, the chosen experimental expression system, and which α subunit is coexpressed. Such effects are predicted to provide high modularity and specificity to VGSC dynamics. An overview of the effects of β subunits on channel gating and trafficking in heterologous cells is provided

in (Calhoun and Isom 2014). Some possible reasons for these differences include background expression of other β subunits in some heterologous cell lines and cell line dependent differential posttranscriptional processing of β subunits. Sialic acid terminated glycosylation in particular seems to be important for modulation of α subunit gating by β1. Sialic acid terminated glycosylation on residues within the β1 Ig loop may confer electrostatic interactions with residues in α subunit voltage sensing domains. In addition, the presence of a high degree of sialic acid terminated glycosylation in $Na_v1.4$ is thought to confer resistance to modulation by or association with β1. This is restored by mutating *Scn4a* cDNA to contain non-glycosylatable residues. This modification is also necessary for the effects of β subunits in promoting $Na_v1.4$ cell surface expression, and thus may facilitate intersubunit association rather than mediate gating differences in skeletal muscle (Johnson, Montpetit et al. 2004). Differential sialic acid modification was also found to affect β2 modulation of Nav1.5 while, in the same study, Nav1.2 was modulated regardless of α subunit sialylation status (Johnson and Bennett 2006). The epilepsy-linked β1-C121W mutation in *Scn1b* results in decreased β1 subunit glycosylation and loss of its capacity to modulate VGSC properties and to traffic out of the soma to the axon in mouse neurons (Meadows, Malhotra et al. 2002, Tammaro, Conti et al. 2002, Kruger, O'Malley et al. 2016). This raises the possibility that control of glycosylation of β subunits, especially sialyation, may be important in subcellular targeting and α-β subunit association. Interestingly β1 and β3 oppositely affect glycosylation of Nav1.7 in heterologous systems, showing β subunits can also control gating of α subunits via regulation of their posttranscriptional processing (Laedermann, Syam et al. 2013). Modulation of I_{Na} by β subunits is also dependent on phosphorylation status.

Phosphorylation of S161 in the C-terminal tail of β3 is necessary for modulation of Nav1.2 I_{Na} in heterologous cells (Merrick, Kalmar et al. 2010). Phosphomimetic mutation of residue Y181, located in the β1 C-terminal tail, results in the loss of β1's capacity to modulate Nav1.2 mediated I_{Na} and surface expression, without interfering with α-β subunit association (McEwen, Meadows et al. 2004). Tyrosine phosphorylation of β1 is likely functionally relevant in neurons, as the β1 intracellular domain is known to interact with receptor protein tyrosine phosphatase β (RPTP-β) and likely *Fyn* kinase in mouse brain, as *Fyn* null neurons lack β1-mediated neurite outgrowth (Ratcliffe, Qu et al. 2000, Brackenbury, Davis et al. 2008). In contrast to β1, β2 does not interact with RPTP-β, suggesting β subunit specificity of association with certain phosphorylation enzymes (Ratcliffe, Qu et al. 2000). Thus, differential posttranscriptional modifications to β subunits, including glycosylation and phosphorylation, may lend modularity to channel activity in a cell type and subcellular region specific manner.

In Vivo Effects of β subunits on VGSC Function

Surprisingly, despite high expression throughout the hippocampus and large effects on I_{Na} in heterologous systems, acutely dissociated *Scn1b* null whole hippocampal pyramidal neurons or CA3 bipolar neurons show no changes in I_{Na} density or voltage dependent properties (Chen, Westenbroek et al. 2004, Patino, Claes et al. 2009). This may be due to the process of dissociation, compensation by other β subunit gene expression, or only subsets of neurons being affected by *Scn1b* deletion. The latter is likely, since the mix of several pyramidal neuron populations present in whole

hippocampal neuron dissociations could obscure differences in specific hippocampal fields. Notably, in *Scn1b* null CA3 but not CA1 pyramidal neurons or dentate granule neurons, there is a reduction in the expression of $Na_v1.1$ and an increase in the expression of $Na_v1.3$ measured by immunohistochemistry (Chen, Westenbroek et al. 2004). Fittingly, acutely dissociated dentate granule neurons and CA1 pyramidal neurons show no changes in I_{Na} density, kinetics, or voltage dependent properties (Uebachs, Opitz et al. 2010, Uebachs, Albus et al. 2012). In contrast, acutely dissociated *Scn1b* null dorsal root ganglion (DRG) neurons show a depolarizing shift in the voltage dependence of TTX-S I_{Na} inactivation, reduced cell surface expression of $Na_v1.9$, and a prolonged recovery from inactivation of TTX-R I_{Na} compared to wildtype (WT) (Lopez-Santiago, Brackenbury et al. 2011). While cultured cerebellar granule neurons show no change in the amount or voltage dependence of transient I_{Na}, they do have differences in α subunit expression and decreased resurgent I_{Na}, as discussed in more detail in section 2 parts 3 and 4 (Brackenbury, Calhoun et al. 2010).

Scn2b deletion also shows cell type dependent effects in native neurons. Cultured hippocampal neurons from *Scn2b* null mice have reduced surface expression of TTX-S VGSCs. Acutely dissociated *Scn2b* null hippocampal pyramidal neurons, but not dentate granule neurons, have reduced I_{Na} density (Chen, Bharucha et al. 2002, Uebachs, Opitz et al. 2010). *Scn2b* deletion also affects the gating properties of VGSCs, slowing the kinetics of activation and inactivation in dissociated hippocampal neurons. *Scn2b* null small fast DRG neurons show a 50% reduction in transient I_{Na}, reduced $Na_v1.7$ expression, and slowed kinetics of activation and inactivation. These effects of *Scn2b*

appear to be specific to TTX-S channels, as TTX-R I_{Na} in the PNS are unchanged, perhaps due to the lack of β2-binding cysteine residues in the TTX-R PNS channels Nav1.8 and Nav1.9, as discussed in section 1 (Lopez-Santiago, Pertin et al. 2006). Differential effects of *Scn2b* deletion on VGSC α subunit subtypes within the same neuron demonstrate that β subunits modulate channels in precise ways *in vivo*.

The effects of β3 in the nervous system *in vivo* are not well studied, however *Scn3b* deletion results in reduced transient I_{Na} and hyperpolarized voltage dependence of inactivation in cardiomyocytes, suggesting the effects of β3 observed in heterologous system may hold *in vivo* (Hakim, Gurung et al. 2008).

Scn4b knockdown in cultured cerebellar granule neurons results in reduced transient I_{Na} and hyperpolarization of the voltage dependence of transient I_{Na} availability (Bant and Raman 2010). *Scn4b* null mice show no changes in transient I_{Na} in striatum, but see below for effects on special gating schemes (Miyazaki, Oyama et al. 2014). Overexpression of *Scn4b* cDNA in cultured hippocampal CA3 neurons, which do not natively express β4, hyperpolarizes and decreases the slope factor of the voltage dependence of availability, suggesting effects of β4 in heterologous systems may translate to neurons (Aman, Grieco-Calub et al. 2009).

β Subunits Affect Trafficking and Expression of VGSC α subunits *In Vivo*

The early heterologous expression studies of β1 and β2 revealed that, in addition to modulation of gating, these subunits also impact channel surface expression, largely

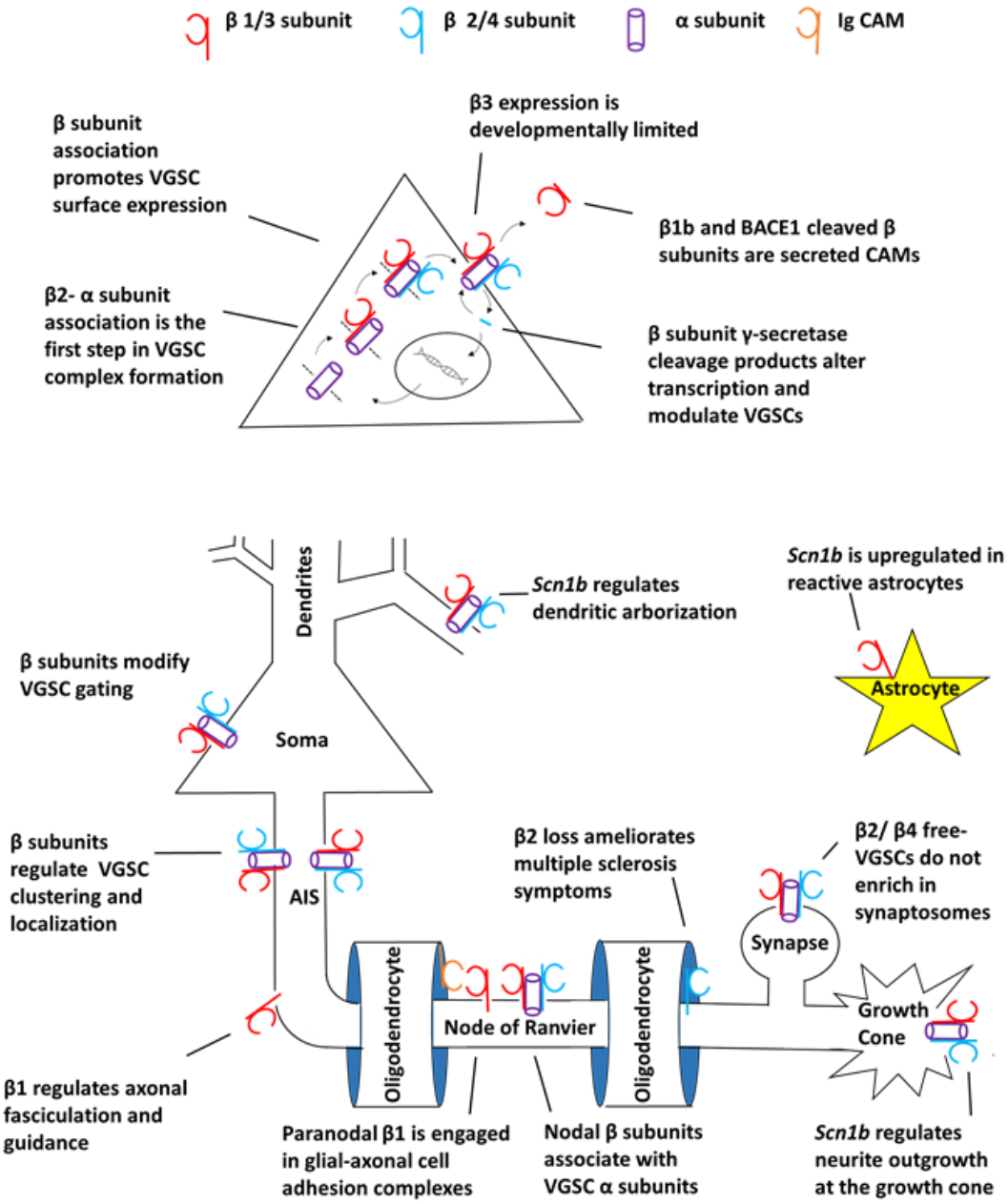


Fig. 1.2 A multitude of functions of VGSC β subunits in the nervous system. β subunits modulate VGSC trafficking to the cell surface (Brackenbury and Isom 2011). Sequential cleavage by BACE 1 and γ secretase alters transcription, including VGSC a subunits, and releases the Ig loop (similar to β1B) as an

extracellular signaling molecule (Wong, Sakurai et al. 2005, Gersbacher, Kim et al. 2010, Patino, Brackenbury et al. 2011). **B**. Each β subunit has been shown to modulate VGSC gating. β subunits alter the AIS localization of specific α subunits and can mediate clustering of α subunits (Brackenbury, Calhoun et al. 2010, Namadurai, Balasuriya et al. 2014). Loss of β1 expression alters axonal fasiculation and targeting (Chen, Westenbroek et al. 2004). β1 in nodes of ranvier associate with α subunits, likely modifying their function. β1 in paranodes is engaged in heterophilic cell adhesion complexes independnetly of α subunits (Kazarinova-Noyes, Malhotra et al. 2001, McEwen and Isom 2004). Loss of β2 ameliorates symptoms of multiple sclerosis, likely through axonal-oligodendrocyte interaction (O'Malley, Shreiner et al. 2009). α subunits in the absence of β2 or β4 fail to enrich in synaptosomes, suggesting roles in VGSC expression at the synapse (Schmidt, Rossie et al. 1985, Schmidt and Catterall 1986). β1 facilitates neurite outgrowth at growth cones, requiring I_{Na} (Brackenbury, Calhoun et al. 2010) Mutation of β1 decreases dendritic arborization, influencing input resistance and excitability (Reid, Leaw et al. 2014). β1 is upregulated in reactive astrocytes (Aronica, Troost et al. 2003).

through effects on trafficking and cell surface half-life of channels rather than through their transcriptional control (but see below) (Schmidt, Rossie et al. 1985, Schmidt and Catterall 1986, Isom and De Jongh 1992, Isom, Ragsdale et al. 1995). Association with β2 is the final step in VGSC biosynthesis, promoting α subunit insertion into the plasma membrane (Schmidt, Rossie et al. 1985, Schmidt and Catterall 1986). In contrast, "free" α subunits not associated with a disulfide-linked β subunit are located inside the cell and are inactive (Schmidt, Rossie et al. 1985). In addition, α subunits covalently associated with β subunits are removed from the cell surface more slowly than free α subunits (Schmidt and Catterall 1986). Consistent with these data, hippocampal neuron cultures from *Scn2b* null mice show a reduction in α subunits expressed at the cell surface (Chen, Bharucha et al. 2002).

Interestingly, the function of β2 on VGSC surface expression in mammalian cells appears to be dependent on β1, and this point is discussed in more detail in the next section. In contrast to β2, β4 does not appear to contribute to surface expression of α

subunits; *Scn4b* null neurons show no apparent reductions in transient sodium current (Miyazaki, Oyama et al. 2014).

Scn1b impacts α subunit expression and trafficking in an isoform specific manner *in vivo*. In CGNs, *Scn1b* deletion in mice causes a reduction in Nav1.6 and an increase in $Na_v1.1$ expression at the CGN AIS, leaving total current density unchanged (Brackenbury, Calhoun et al. 2010). In rat brain, while "free" α subunits not disulfide linked to β subunits account for 21% of VGSCs in the soma, they are wholly undetectable in synaptosomes. This suggests that β2 or β4 subunits may play roles in directing α subunits to the synapse (Schmidt, Rossie et al. 1985, Schmidt and Catterall 1986). More recent work shows that β3 mediates clustering of $Na_v1.5$ channels in heterologous systems, possibly through *cis* homophilic interactions resulting in β3 trimer formation (Namadurai, Balasuriya et al. 2014). VGSC α subunit single molecule tracking microscopy in fetal rat hippocampal neuron cultures showed that VGSCs exist in clustered microdomains (Akin, Solé et al. 2016). While the role of β subunits in this clustering is unknown, data showing the effects of β3 on VGSC clustering in culture may lend important insights into this process, since β3 is highly expressed in fetal and postnatal rodent brain. β3 also may affect α subunit expression through masking of an endoplasmic reticulum retention/retrieval motif, although this effect may be limited to $Na_v1.8$ (Zhang, Li et al. 2008). *Scn4b* deletion does not affect axonal expression of $Na_v1.2$ in striatal projection neurons, suggesting that it may not play roles in channel trafficking but instead its function may be limited to specialized impacts on persistent and resurgent sodium currents (Miyazaki, Oyama et al. 2014).

β subunits can affect VGSC α subunit transcription or translation. In *Scn1b* null hippocampus, CA3, but not CA1 or dentate gyrus, pyramidal neurons have reduced $Na_v1.1$ and increased $Na_v1.3$ expression (Chen, Westenbroek et al. 2004). In addition, $Na_v1.9$ protein is reduced in *Scn1b* null DRGs (Lopez-Santiago, Brackenbury et al. 2011). β2 is also able to affect expression of specific α subunits. In DRGS, mRNA for $Na_v1.7$, $Na_v1.6$ and $Na_v1.3$ is reduced, while $Na_v1.1$ and $Na_v1.7$ protein are reduced, with no change in $Na_v1.6$ (Lopez-Santiago, Pertin et al. 2006). Many of these effects on specific VGSC α subunit expression may be due to transcriptional regulatory effects of β subunits, discussed below.

Non-excitable Signaling Pathways of VGSCs Through Proteolytic Processing of β subunits

VGSC β subunits extend neuronal signaling beyond the role of VGSCs in membrane potential dynamics. VGSC β subunits are targets for proteolytic cleavage, with the resulting products demonstrating specific autonomous functions independent of α subunits. The β subunits contain cleavage sties for sequential cleavage by BACE1 and γ-secretase (Wong, Sakurai et al. 2005, Gersbacher, Kim et al. 2010). β2, and likely the other β subunits, contains an additional cleavage site for α-secretase enzyme ADAM10 in the extracellular portion (Kim, Ingano et al. 2005). BACE1 cleavage results in shedding of the extracellular β subunit domain. For β1, this cleaved polypeptide fragment is thought to be capable of functioning as a ligand for cell adhesion, similar to β1b (Kim, Ingano et al. 2005, Wong, Sakurai et al. 2005). Interestingly, while expression of full-length β4

subunits with α subunits in heterologous systems does not recapitulate resurgent I_{Na}, cleavage of β4 by BACE1 slows the decay of resurgent I_{Na}, suggesting that proteolytic processing of β4 may be involved in generation of resurgent I_{Na} (Huth, Rittger et al. 2011). Because the β4 residues responsible for generating resurgent I_{Na} are located within the C-terminal tail, sequential cleavage by γ-secretase, following the action of BACE1, may also be important in this mechanism. Formation and nuclear translocation of the γ-secretase cleaved β2 C-terminal fragment has been shown to lead to increased $Na_v1.1$ subunit mRNA and protein expression in neurons, suggesting a role for β subunits in the regulation of α subunit transcription (Kim, Carey et al. 2007). While similar roles for the other β subunits have not been investigated, their processing by this cleavage pathway and effects on specific α subunit expression may suggest similar mechanisms. Thus, β subunits may also affect neuronal firing through the modulation of channel transcription.

Beyond Hodgkin-Huxley, Alternative Gating Schemes in VGSCs

VGSCs exhibit several alternative gating schemes that differ from the traditional transient I_{Na} described by Hodgkin and Huxley (Hille 2001). Resurgent I_{Na} is a specialized current in which traditional inactivation is impaired by blockade of the intracellular face of the pore, which is relieved more quickly by hyperpolarization than traditional inactivation. Upon membrane potential repolarization, the channel is able to quickly convert to the open state without the prolonged recovery interval imparted by traditional inactivation. This current activates quickly upon repolarization during an AP and promotes cell type dependent spontaneous, repetitive, or burst firing of APs (Lewis and Raman 2014). The C-terminal tail of β4 is the only known endogenous molecule to generate resurgent I_{Na}

(Grieco, Malhotra et al. 2005, Lewis and Raman 2014). The residues KKLITFILKKTREK in the C-terminal tail of the mouse β4 subunit are required for resurgent I_{Na} in cerebellar purkinje and granule neurons (Grieco, Malhotra et al. 2005). Consistent with this result, *Scn4b* null mice lose resurgent I_{Na} in striatal projection neurons (Miyazaki, Oyama et al. 2014). While β4 is the only identified mediator of resurgent I_{Na} to date, there are neuronal populations that express this current but do not express β4, suggesting the involvement of other proteins (Lewis and Raman 2014). The ability of β4 to generate resurgent I_{Na} is α subunit dependent, with $Na_v1.6$ carrying proportionally more than the other α subunits (Lewis and Raman 2014). *Scn1b* null cultured granule neurons have reduced resurgent I_{Na}, likely due to decreased expression of this α subunit (Brackenbury, Calhoun et al. 2010).

Another specialized current carried by VGSCs is persistent I_{Na}, which confers a depolarizing drive at the resting membrane potential, and extends VGSC signaling into the regulation of subthreshold excitability. Persistent sodium current results from incomplete channel inactivation, accounting for up to 5% of total sodium current. Such currents are known to increase repetitive firing (Kiss 2008). Additionally, persistent I_{Na} facilitates the summation of excitatory postsynaptic currents and contributes to determination of firing threshold (Crill 1996). $Na_v1.6$ disproportionality caries persistent I_{Na} relative to other α subunits but all subtypes carry at least some persistent current (Lewis and Raman 2014). In addition to reduced resurgent I_{Na}, *Scn4b* null striatal projection neurons also have reduced persistent I_{Na} (Miyazaki, Oyama et al. 2014). Knockdown of β4 in cultured cerebellar granule neurons reduced both resurgent and

persistent I_{Na} (Aman, Grieco-Calub et al. 2009). Inclusion of the C-terminal β4 peptide restored resurgent I_{Na} in these neurons and induced it in neurons that do not typically have resurgent I_{Na} (Grieco, Malhotra et al. 2005). Interestingly, in contrast to the β4 C-terminal peptide, expressing the full-length β4 protein does not generate resurgent I_{Na} in heterologous systems. It does, however, destabilize inactivation; tripling persistent I_{Na} amplitude (Aman, Grieco-Calub et al. 2009). β4 is not unique in its ability to impact persistent I_{Na}. β3, but not β1 or β2, when coexpressed in heterologous systems with $Na_v1.2$, increases persistent I_{Na} (Qu, Curtis et al. 2001). *Scn1b* has effects on both persistent and resurgent I_{Na} *in vitro* and *in vivo*. *Scn1b* null CGNs have reduced resurgent I_{Na} and *Scn1b* null DRGs have reduced persistent TTX-R I_{Na} (Brackenbury, Calhoun et al. 2010, Lopez-Santiago, Brackenbury et al. 2011).

In addition to the two pro-excitatory gating schemes above, VGSCs also exhibit use dependent slow inactivation of channels, an excitability mitigating mechanism. Entry into the slow inactivated state requires repetitive or sustained depolarization which accumulate channels in the slow inactivated state over the course of numerous action potentials (Schauf, Pencek et al. 1976). Recovery from the slow inactivated state is much slower than entry, supporting longer lasting effects on the channel than fast inactivation, which is limited to affecting fewer individual action potentials due to its fast recovery time constant. VGSC slow inactivation has the interesting property that at the depolarized potentials that support spiking (i.e. -70 mV), the recovery from slow inactivation is slow, while at hyperpolarized potentials (i.e. -80 mV), the recovery is much faster (Fleidervish, Friedman et al. 1996, Jung, Mickus et al. 1997). Importantly, this property confers a

mechanism of autoregulation of excitability to neurons based on previous activity. This voltage dependent effect is highly relevant to neuromodulation as discussed in below. Slow inactivation utilizes molecular mechanisms that differ from fast inactivation. Mutations that impair fast inactivation do not prevent slow inactivation, (Rudy 1978, Featherstone, Richmond et al. 1996, Vedantham and Cannon 1998, Todt, Dudley Jr et al. 1999, Mitrovic, George et al. 2000, Ong, Tomaselli et al. 2000). Although numerous mutations in VGSCs have been found to affect slow inactivation, the S6 segments contain highly conserved asparagine residues that, when mutated to hydrophobic residues, completely blocks slow inactivation (Carr, Day et al. 2003, Chen, Frank et al. 2006).

In summary, VGSC gating schemes are used to modulate neuronal excitability and firing patterns, often in a cell type specific manner, conferred by slow inactivation of channels and the levels of persistent and resurgent I_{Na}. (Krahe and Gabbiani 2004, Paul, DeWoskin et al. 2016).

Neuromodulation of Voltage-gated Sodium Channel α Subunits

VGSCs are affected by the action of various neuromodulators including acetylcholine, monoamines, neuropeptides, and glutamate (Cantrell and Catterall 2001). Such modulation by neurotransmitters, which are involved in a vast array of functions, may represent a key means of controlling excitability and network dynamics through control of VGSCs. Administration of the cholinergic agonist carbachol reduces peak I_{Na} and slows fast inactivation in dissociated hippocampal neurons(Cantrell, Ma et al. 1996). This modulation was shown to act via a protein kinase C (PKC) dependent

phosphorylation of VGSCs with similar effects in cortical pyramidal neurons. Cholinergic input to the hippocampus suppresses bursting activity and promotes tonic firing (Azouz, Jensen et al. 1994, Alroy, Su et al. 1999). The nucleus basalis, a major driver of cholinergic tone in the cortex, shifts cortical spiking from bursting to tonic firing, potentially utilizing modulation of VGSCs as describe above (Metherate, Cox et al. 1992). Dopaminergic modulation of VGSCs is also observed. Activation of D1-like dopamine receptors, which stimulate adenylyl cyclase activity, decreases I_{Na} in acutely isolated hippocampal neurons (Cantrell, Smith et al. 1997, Cantrell, Scheuer et al. 1999). This modulation was shown to be protein kinase A (PKA) dependent. Alternatively, activation of D2 receptors, which are coupled to inhibition of adenylyl cyclase, increases I_{Na} in medium spiny neurons, but has an overall inhibitory effect through activation of a PKC mediated pathway. Both PKA and PKC phosphorylate VGSCs to mediate a reduction in I_{Na}. Effects on I_{Na} are limited to depolarized potentials, with similar features to slow inactivation as described above, leading to the proposal that PKC and PKA modulation acted on the slow inactivation process (Carr, Day et al. 2003). Indeed, it was found that mutation of an asparagine in S6 required for slow inactivation to alanine increased slow inactivation and potentiated the effects of PKC and PKA modulation while mutation to aspartate blocked slow inactivation and prevented modulation by PKA and PKC. Modulation of VGSCs by PKA and PKC exhibits synergistic modulation (Li, West et al. 1993, Scheuer 2011). Those residues which are phosphorylated by PKC but not PKA, when mutated to block phosphorylation, also blocked the reduction in I_{Na} by PKA activation. In the absence of PKC modulation, PKA requires membrane depolarization for effective modulation, while in the presence of PKC modulation, PKA modulation occurs

at all potentials(Cantrell, Ma et al. 1996). This interface between neuromodulation and activity dependence provides a rich environment for mechanisms of action for dynamic control of excitability, linking neuronal activity patterns and neuromodulatory tone in the brain.

It is important to note the effects of phosphorylation on VGSC activity are specific to the cellular environment in which they are studied. Careful attention is required to understand the influence that an experimental expression system may have on the resulting VGSC modulation observed. Not surprisingly, given the high degree of differential expression of the VGSCs in cell type and subcellular domains, the different VGSC α subunits also exhibit differential sensitivity to neuromodulation by PKA and PKC. $Na_v1.6$ is far less sensitive to PKA and PKC modulation than $Na_v1.2$. ((Maurice, Tkatch et al. 2001, Chen, Frank et al. 2008). Recent work has found that activation of 5-HT_{1A} receptors in prefrontal cortical layer 5 pyramidal neurons differentially decreases I_{Na} in the proximal axon attributable to $Na_v1.2$ while not impacting those in the distal axon, attributable to $Na_v1.6$, showing subcompartment-specific action of neuromodulators on VGSC function. As described above for PKA and PKC modulation, the effect of 5-HT_{1A} receptor activation on reducing I_{Na} could be attributed to enhancing slow inactivation and depolarizing the voltage dependence of channel activation(Yin, Rasch et al. 2017). The importance of neuromodulation in regulating VGSC availability may provide insights into how the disruption or potentiation of such effects are involved in the mechanism of various physiological and pathophysiological contexts.

β Subunit Crosstalk

VGSC β subunits can also impact the actions of each other. Coexpression of β1 and β2 in oocytes with $Na_v1.2$ increases I_{Na} density greater than either β subunit alone, suggesting synergistic action (Isom, Ragsdale et al. 1995). In Chinese hamster lung fibroblasts, β2 expression does not increase the surface expression of $Na_v1.2$ unless β1 is also expressed (Kazarinova-Noyes, Malhotra et al. 2001, McEwen, Meadows et al. 2004). This seem to be the case for endogenous expression as well; mice that are homozygous for both the *Scn1b* and *Scn2b* null alleles have reduced I_{Na} density in cerebellar purkinje neurons but I_{Na} density is not different in mice null for *Scn1b* or *Scn2b* alone (Grieco, Malhotra et al. 2005). This result suggests there is a capacity for β1 and β2 to compensate for each other *in vivo*, in spite of evidence that these subunits bind to different locations on α subunits. This may be the case for other subunits as well. *Scn3b* null mice have apparently normal nervous system development, suggesting compensatory *Scn1b* expression (Hakim, Gurung et al. 2008, Hakim, Brice et al. 2010). Coexpression of β1 with β4 overcomes β4 induced persistent I_{Na} in heterologous cells and neurons. Additionally, the β4 mediated hyperpolarized activation and inactivation of Nav1.1 I_{Na} are antagonized by β1. In contrast, β1 functions appear to be relatively unaffected by β4 co-expression, as cells expressing both subunits match the electrophysiological profile of β1 expression alone. These data suggest opposing roles of β1 and β4 in the same trimeric channel complex, with β4 acting as an excitation accelerator and β1 acting as an overriding brake (Aman, Grieco-Calub et al. 2009). While the binding sites on α subunits for β1 and β3 are predicted to be competitive, there is

evidence that β1 and β3 coexpression can generate properties not present with either alone when coexpressed with Nav1.5 (Ko, Lenkowski et al. 2005). This may be specific to the α subunit, as similar experiments with Nav1.8 show the opposing shifts in channel availability with β1 and β3 seem to cancel when coexpressed in the same oocyte. In the same study, β1 and β2 coexpression revealed a depolarizing voltage shift in availability, contrary to the hyperpolarizing shift of β1 alone or the absence of effect of β2 alone (Vijayaragavan, Powell et al. 2004). β subunits can also affect expression of other β subunits *in vivo*. Quantification of β subunit proteins in *Scn4b* null mice showed increased expression of β1 and reduced β2 in spinal cord and cerebellum, with no effect on their expression levels in striatum or cortex (Miyazaki, Oyama et al. 2014). In DRG neurons, *Scn2b* null mice have decreased expression of *Scn3b* and *Scn4b* but not *Scn1b* mRNA (Lopez-Santiago, Pertin et al. 2006). This cell type specific regulation of β subunit mRNA expression by other β subunits further highlights the precise control of β subunit function in vivo.

β Subunits Modulate Potassium Channels

β subunits also affect some potassium currents (I_K), creating the potential for cross-talk between VGKCs and VGSCs. β1 subunits interact with K_V4.2 and Kv4.3, major contributors to A-type I_K in brain. This interaction was first uncovered in heterologous expression studies (Deschênes and Tomaselli 2002). Later, an unbiased proteomic approach designed to discover novel K_V4.2 interacting partners in rodent brain identified VGSC β1. In the same study, investigators found that heterologous co-expression of β1

with $K_v4.2$ increases I_K density. In addition, shRNA knockdown of β1 in cultured cortical neurons decreased A-type I_K (Marionneau, Carrasquillo et al. 2012). β1 also modulates several other VGKCs when co-expressed in *Xenopus* oocytes, including $K_v4.3$, $K_v1.1$, $K_v1.3$, $K_v1.6$, and $K_v7.2$. β1 did not, however, modulate Kv3.1 in this study, suggesting that interactions are moderately specific to channel type (Nguyen, Miyazaki et al. 2012). It will be important to test these interactions in native neurons and cardiomyocytes because β1 interactions are known to be dependent on cell type and these interactions may be limited to heterologous overexpression systems. VGKC modulation by β1 may be cell type dependent as well. CA1 pyramidal neurons express a high level of $K_v4.2$ mediated A-type I_K but their excitability is largely unaffected in *Scn1b* null or homozygous mutant neurons (Chen, Yuan et al. 2006, Patino, Claes et al. 2009, Uebachs, Opitz et al. 2010, Reid, Leaw et al. 2014). *Scn1b* null mice exhibit reduced transient outward I_K in DRG neurons, demonstrating that the effects of β1 on VGKCs is not limited to the brain (Lopez-Santiago, Brackenbury et al. 2011). Potential effects of other VGSC β subunits on VGKCs in the nervous system have not been investigated, however, large effects on I_K in *Scn2b* null mouse cardiomyocytes suggest that other β subunits may also modulate VGKC function (Bao, Willis et al. 2016).

VGSCs in Structural Brain Development

VGSCs function in nervous system development on several levels, including neurite outgrowth, axonal pathfinding, dendritic arborization, neuronal patterning, and cell migration. Importantly, the interface between the cell adhesion aspects of the β subunits and the ion conducting aspects of α subunits provides a mechanism for the conversion of

electrical function into the structure of the neuron. Neurite extension of WT CGNs plated on β1 expressing fibroblast monolayers is increased compared to control monolayers and requires β1- β1 *trans* homophilic cell adhesion. In contrast, β2 expressing fibroblast monolayers reduce neurite outgrowth of WT CGNs and β4 has no detectable effects. β1 function in neurite outgrowth requires both cell-cell adhesion and VGSC conduction, particularly current carried by $Na_v1.6$. Deletion of *Cntn1*, *Fyn*, or *Scn8a* or the addition of TTX abrogated β1-mediated neurite outgrowth in CGNs. Unlike other CAMs, β1 dependent neurite outgrowth is independent of the FGF mediated neurite outgrowth pathway. *Scn1b* null mice have several nervous system structural defects that may be directly related to altered neurite outgrowth. These include cerebellar parallel fiber defasiculation, CGN axonal mistargeting, dentate granule neuron axonal mistargeting, corticospinal tract defasiculation, and decreased dendritic arborization in pyramidal neurons of the subiculum (Brackenbury, Davis et al. 2008, Brackenbury, Calhoun et al. 2010, Brackenbury, Yuan et al. 2013, Reid, Leaw et al. 2014). Structural defects in *Scn1b* null brain go beyond the regulation of neuronal process extension, also impacting cell migration, proliferation, and neuronal patterning defects. In the cerebellum there is an expansion of the external germinal layer and in the hippocampus there is increased proliferation of dentate granule neurons, ectopic Prox1 positive neurons, and increased thickness of the dentate gyrus granule cell layer with a reduction in dentate granule neuron number (Brackenbury, Davis et al. 2008, Brackenbury, Yuan et al. 2013). Interestingly, while the majority of focus of VGSCs in development have been on the cell adhesion function of the β subunits, $Na_v1.3$ is also crucially involved in cortical development, with pathogenic variants of *SCN3A* resulting in disrupted cortical folding.

This may in fact be due to the highly developmental nature of $Na_v1.3$ expression in the CNS relative to the other VGSC α subunits.

Differential Effects of VGSC β Subunits in Excitability

While the effect of a reduction in VGSC α subunits in general decreases excitability of the neurons in which they are expressed, the effects of β subunits is less clear. Note however, that deletion of α subunit genes need not follow such a simple relationship, as it is known that *Scn1a* deletion can actually increase I_{Na} in pyramidal neurons and upregulate $Na_v1.3$. The wide array of β1-mediated effects on neuronal excitability is consistent with the multi-functionality of β1. Several of these effects can be linked directly to modulation of VGSC α subunit expression and function, while others are attributable to VGKC modulation or altered neuronal morphology. *Scn1b* deletion in mice results in differential effects on excitability at the single neuron level with some populations showing increased excitability, some decreased, and others unaffected. Cultured *Scn1b* null CGNs show a decrease in the number of APs fired in response to depolarizing current injections compared to WT (Brackenbury, Calhoun et al. 2010). There are no measureable changes in the level of transient I_{Na} in these cells, but instead a decrease in the level of resurgent I_{Na}, which is known to be important in repetitive firing of these neurons (Brackenbury, Calhoun et al. 2010, Lewis and Raman 2014). Many *Scn1b* null neuron populations, including dentate granule neurons, CA1 pyramidal neurons, and hippocampal interneurons, have unaffected excitability profiles compared to WT (Patino, Claes et al. 2009, Uebachs, Opitz et al. 2010, Uebachs, Albus et al. 2012). *Scn1b* null optic nerve

has reduced speed of the fastest component of the compound AP, suggesting decreased excitability (Chen, Westenbroek et al. 2004).

The reported differential effects on excitability appear to be dependent on different functions of *Scn1b*. *Scn1b* null cortical layer 5 pyramidal neurons fire more APs compared to WT with an increased action potential half width, indicating loss of β1 modulation of $K_v4.2$ may be a factor (Marionneau, Carrasquillo et al. 2012). However, in homozygous knockin mice expressing the epilepsy causing *Scn1b*-C121W mutation, this population is unaffected (Reid, Leaw et al. 2014). While these results are seemingly at odds, they may provide clues to even more nuanced differences in the effects of *Scn1b* on neuronal excitability. The β1-C121W mutation interferes with both α subunit interaction and cell adhesion but with unknown impact on modulation of VGKCs (Meadows, Malhotra et al. 2002, Kruger, O'Malley et al. 2016). This may indicate subpopulations of the same neuron type in different regions of cortex may be affected in different ways or that C121W mutants may modulate excitability differently than total loss of *Scn1b*. The latter may be the case because C121W heterozygous mice have increased seizure susceptibility relative to *Scn1b*$^{+/-}$ mice (Kruger, O'Malley et al. 2016). Hyperexcitability has been found in layer 2/3 pyramidal neurons and pyramidal neurons of the subiculum in mice homozygous for the β1-C121W mutation. These increases in excitability can be attributed to differences in structural development of these neurons, as they have increased input resistance and reduced cell surface area, measured by whole cell capacitance and immunohistochemistry, respectively (Reid, Leaw et al. 2014). Interestingly, this may be a

way that reductions in VGSC function can drive hyperexcitability via cross-talk between I_{Na} and neuronal development.

The effects of *Scn2b* on excitability are not as well studied as those of *Scn1b*. We do know, however, that *Scn2b* null mice have increased threshold and reduction in amplitude of extracellularly recorded compound APs in the optic nerve, suggesting that reduced levels of VGSCs at the cell surface result in reduced excitability. *Scn2b* deletion also increases susceptibility to pilocarpine-induced seizures, suggesting aberrant neuronal excitability elsewhere in the CNS (Chen, Bharucha et al. 2002). While the effects of *Scn2b* deletion on DRG AP firing have not been measured, altered VGSC function and reduced pain sensitivity in *Scn2b* null mice suggest reduced DRG neuron excitability (Lopez-Santiago, Pertin et al. 2006).

The effects of *Scn3b* on nervous system excitability have not been reported, but there is extensive work showing impacts on cardiomyocyte excitability (Hakim, Gurung et al. 2008, Hakim, Brice et al. 2010).

Scn4b's effects on neuronal excitability appear to be largely related to its role in regulating persistent and resurgent I_{Na}. *Scn4b* null mice have reduced repetitive firing of APs in striatal projection neurons and *Scn4b* knockdown in cultured CGNs causes reduced excitability, suggesting that reductions in resurgent I_{Na} impact excitability (Bant and Raman 2010, Miyazaki, Oyama et al. 2014). In a similar manner, reduced persistent

and resurgent current in *Scn1b* null CGNs decrease excitability (Brackenbury, Calhoun et al. 2010).

VGSCs in Epilepsy and Intellectual Disability

VGSCs play important roles in both the mechanism and treatment of several disorders of the nervous system. The underlying links between VGSC gene mutations and these disparate diseases result from the numerous biochemical and physiological functions outlined in sections 1 and 2. Some can be linked to effects on neuronal and network excitability, while others may be associated with other effects of VGSCs such as in brain development. Here we will focus on VGSCs in epilepsy and intellectual disability which are commonly interrelated in VGSC gene mutations but both dysfunctions can both be found independently as a result of VGSC gene mutations. Epilepsy is a condition characterized by unprovoked recurrent seizures (Fisher, Acevedo et al. 2014). Up to 40% of epilepsy cases have unknown origin (Beck and Elger 2008). Exceptions to this are the genetic epilepsies, which can often be linked directly to specific ion channel gene mutations. The majority of epilepsy resulting from VGSC gene mutations occurs from mutations in *SCN1A*, but there are also numerous patients with mutations have been found in *SCN2A*, *SCN3A*, *SCN8A*, and *SCN1B(Meisler and Kearney 2005)*. Importantly, many of the epileptic disorders discussed here have significant overlap with intellectual disability and are partially defined by the associated poor outcomes in regard to intellectual disability. Alternatively, diseases like autism spectrum disorders (ASDs) and intellectual disability are also found to be associated with VGSCs independently of epilepsy.

SCN1A

Mutations in *SCN1A* are predominantly associated with genetic epilepsy with febrile seizures + (GEFS+) and Dravet syndrome (DS). DS a severe developmental and epileptic encephalopathy (DEE). DS is characterized by early pediatric seizures associated with fever followed by febrile and afebrile seizures. DS is a disorder of epilepsy, ataxia, intellectual disability, ASD, sleep abnormalities, and a high risk of sudden unexpected death in epilepsy (SUDEP) (Scheffer, Zhang et al. 2010, Skluzacek, Watts et al. 2011). More than 70% of DS cases are caused by *de novo* loss-of-function mutations in *SCN1A*. (Patino, Claes et al. 2009, Scheffer, Zhang et al. 2010, Ogiwara, Nakayama et al. 2012, Ramadan, Patel et al. 2017). Recently, gain-of-function mutations in *SCN1A*, that result in a more severe disorder than traditional DS, have been reported but are comparatively rare compared to loss of function mutations. By what means does the loss of function of a VGSC α subunit, proteins promoting single neuron excitability, result in the hyperexcitability observed in epilepsy?

Scn1a DS models are the most heavily studied VGSC epilepsy models. *Scn1a* deletion or the introduction of the nonsense mutation R1407X results in a DS phenotype with severe seizures, ataxia, and (SUDEP) (Frank, Mantegazza et al. 2006, Ogiwara, Miyamoto et al. 2007). Early work showed that heterozygous or homozygous deletion of *Scn1a* reduced I_{Na} and excitability in dissociated hippocampal bipolar shaped neurons but not pyramidal neurons (Frank, Mantegazza et al. 2006). Bipolar morphology is commonly used to identify GABAergic neurons in neuronal dissociations. Around this period, work investigating *Scn1a* R1470X knock-in mice, found that PV+ fast spiking

interneurons in these mice were hypoexcitable and that $Na_v1.1$ expression was highest in PV+ interneuron axons (Ogiwara, Miyamoto et al. 2007). These results combined to form a framework for understanding DS as a disorder of impaired interneuron excitability, with a particular emphasis on PV+ neurons. This view has been supported by several other animal studies, where heterozygous *Scn1a* deletion has been targeted to subclasses of neurons. Vesicular GABA transporter (VGAT)-Cre driven *Scn1a* heterozygous deletion, targeting GABAergic neurons, results in increased phenotypic severity than in global *Scn1a* deficient mice. Furthermore, when combined with empty spiracles homolog 1 (Emx1)-Cre, targeting excitatory neurons, the VGAT-Cre heterozygous knockout mice exhibited disease severity similar to that of the global Scn1a+/- mice. Additionally, in this work it was found that PV targeted heterozygous deletion was sufficient to generate spontaneous seizures (Ogiwara, Miyamoto et al. 2007). PV+ hippocampal and cortical neurons, are not the only interneuron class affected however, with other classes of interneurons exhibiting hypoexcitability in *Scn1a* heterozygous mice (Tai, Abe et al. 2014, Goff and Goldberg 2019). Interestingly, it has been found that the PV+ neuron hypoexcitability in DS mice is developmentally limited (Favero, Sotuyo et al. 2018). Furthermore, there exists a developmental and mouse strain dependent increase in pyramidal neuron I_{Na} and excitability (Mistry, Thompson et al. 2014). The understanding the *Scn1a* DS landscape becomes even more complicated however as in human induced pluripotent stems cells, interneuron hypoexcitability is variably reported to be both increased and decreased (Higurashi, Uchida et al. 2013, Liu, Lopez-Santiago et al. 2013). These results show that despite extensive work, there exist further nuances in the pathophysiology of excitability in DS.

Many epilepsy patients have comorbidities including autism, intellectual disability, impaired sleep, and mood disorders (Steffenburg, Gillberg et al. 1996, Levisohn 2007, Louis 2011, Lau, Ettinger et al. 2012) but DS in particular is characterized as having high incidences of autism and intellectual disability. *Scn1a*$^{+/-}$ mice model ASD (Han, Tai et al. 2012, Villeneuve, Laguitton et al. 2014). It is unclear to what extent seizures and neuronal damage play in the intellectual disability and ASD in DS. The mechanisms may be similar however as treatment of *Scn1a*$^{+/-}$ mice with a clonazepam, a positive allosteric modulator of $GABA_A$ receptors rescued several social deficits in these mice. Furthermore, there may be a mutual link in the cell type dependence of PV+ interneurons in causing both ASD and epilepsy in DS (Higurashi, Uchida et al. 2013).

SCN8A

Mutations in the other major brain VGSCs can also result in epilepsy and epileptic encephalopathies (EEs). In contrast to *SCN1A*, EE mutations in *SCN8A* are commonly missense mutations that increase channel activity (Meisler, Helman et al. 2016). Several different de novo mutations and effects are observed in cases of *SCN8A* associated epilepsies, with over 150 cases having been reported. Within cases of epileptic encephalopathies associated with SCN8A, patients have been diagnosed with different syndromes including unclassified epileptic encephalopathy or a Dravet like phenotype, but are predominantly diagnosed with early infantile epileptic encephalopathy 13 (EIEE13) (Veeramah, O'Brien et al. 2012, De Kovel, Meisler et al. 2014, Blanchard, Willemsen et al. 2015, Larsen, Carvill et al. 2015, Mercimek-Mahmutoglu, Patel et al.

2015). The clinical presentation of *Scn8a* EE patients includes multiple seizure types and early age of onset with an average age of 4 months. In contrast to DS, the seizures do not usually have a febrile component. Intellectual disability and ASD, as in DS is severe in patients with EE related *SCN8A* mutations. Unlike in *SCN1A* associated DS, EEs related to *SCN8A* appear to be primarily reliant on excitatory neurons, likely reflecting the increased expression of $Na_v1.6$ in excitatory neurons relative to GABAergic interneurons. Of the functionally evaluated *SCN8A* EE mutations, the majority have demonstrated altered channel properties consistent with increasing neuronal excitability. Effects include enhanced channel activation, impaired inactivation, increased resurgent I_{Na}, and increased persistent I_{Na} (Veeramah, O'Brien et al. 2012, O'Brien and Meisler 2013, De Kovel, Meisler et al. 2014, Estacion, O'Brien et al. 2014, Wagnon and Meisler 2015). There exists however a cases of *SCN8A* related EE where current amplitude was reduced in heterologous cells, though there may be a property that reveals this too may be a gain of function mutation(De Kovel, Meisler et al. 2014). Mouse models of *Scn8a* EE mutations support the view that increased excitability of pyramidal neurons is the primary mediator of epilepsy in these mice. Persistent I_{Na} is increased in *Scn8a*$^{+/R1872W}$ mice in both pyramidal and bipolar neurons of the hippocampus and persistent and resurgent I_{Na} is increased in neurons of medial entorhinal cortex (Lopez-Santiago, Yuan et al. 2017, Ottolini, Barker et al. 2017). Conditional expression of the R1872W mutant channels in excitatory neurons using Emx1-Cre resulted in epilepsy and early lethality, while neither glutamic acid decarboxylase 2-cre (Gad2-Cre) or disal-less homeobox 5a cre (Dlx5a-Cre), both inhibitory neuron promoters, resulted in any overt abnormalities. These results

support the view that the primary neurons involved in epileptogenesis in *SCN8A* EE are excitatory (Bunton-Stasyshyn, Wagnon et al. 2019).

SCN8A mutations have been identified that do not result in EE. Sixteen patients with benign infantile seizures and paroxysmal dyskinesia have been found to harbor the E1483K mutation in *SCN8A*. These patients in contrast to *SCN8A* EE patients, do not typically exhibit cognitive or severe developmental motor disorders (Gardella, Becker et al. 2016). Cases of loss of function mutations in *SCN8A* have been found to result in intellectual disability or ASD without seizures, and cases of myoclonus without seizures or intellectual disability(Wagnon, Barker et al. 2017). Another mutation in *SCN8A, G1451S,* that causes a complete loss of function results in epilepsy with absence and generalized tonic-clonic seizures (Blanchard, Willemsen et al. 2015). A heterozygous *Scn8a* null allele is known to result in an absence seizure phenotype, particularly through its action on PV+ thalamic reticular neurons.(Papale, Beyer et al. 2009, Makinson, Tanaka et al. 2017)

SCN2A

Scn2a is associated both with a varied array of epilepsies and is among the most common monogenetic causes of intellectual disability. The first human epilepsies associated with *Scn2a* were GEFS+ and benign familial neonatal/infantile seizures (BFNIS), though an *SCN2A* origin of GEFS+ or familial neonatal or infantile seizures is much less common than mutations in *SCN1A* and *KCNQ2* or *PRRT2* respectively(Sugawara, Tsurubuchi et al. 2001, Heron, Crossland et al. 2002, Grinton,

Heron et al. 2015). *SCN2A* mutations in BFNIS have largely been found to consist of missense mutations, with impaired channel inactivation and increased persistent I_{Na} (Kearney, Plummer et al. 2001, Liao, Anttonen et al. 2010, Lauxmann, Boutry-Kryza et al. 2013). It has been found that early onset (before 3 months) cases of disease are associated with gain of function mutations, while loss of function mutations are associated with later disease onset (Wolff, Johannesen et al. 2017). Mutations associated with milder epilepsy are typically inherited while the more severe cases are typically de novo mutations. *SCN2A*'s involvement in various EEs is relatively fragmentary, with *SCN2A* variants having been described in West syndrome, Ohtahara syndrome, DS, and in unclassified EEs (Nakamura, Kato et al. 2013, Matalon, Goldberg et al. 2014) While the EE patients with *SCN2A* mutations exhibit intellectual disability, *SCN2A* is strongly involved in intellectual disability independently and stands out in whole exome sequencing studies identifying ASD and intellectual disability related genes (De Ligt, Willemsen et al. 2012, Neale, Kou et al. 2012, O'Roak, Vives et al. 2012, Rauch, Wieczorek et al. 2012, Sanders, Murtha et al. 2012). Variants associated with ASD have been shown to be largely non-conducting or have decreased function (Ben-Shalom, Keeshen et al. 2017).

SCN3A

In contrast to the other major α subunit genes expressed in brain, detection of involvement of *SCNAB* in epilepsy has been less pronounced. Scattered cases of *SCN3A* mutations have been found in patients with cryptogenic partial epilepsy and several patients with focal epilepsy have been reported with variable functionality of the mutant

channels including both increased I_{Na} and impaired transient I_{Na}. (Holland, Kearney et al. 2008, Estacion, Gasser et al. 2010, Wang, Du et al. 2017). In these cases there was no found association with intellectual disability. However, four cases of *SCN3A* related epileptic encephalopathy have been described with de novo gain of function mutations and 2 patients with inherited mutations, which included increased persistent I_{Na}, hyperpolarized activation, and slowed inactivation. Age of onset was usually within the first year of life, with one patient with disease onset at 18 months (Zaman, Helbig et al. 2018). Interestingly, *SCN3A* mutations have been found which impair cortical development, without causing epilepsy and also exhibiting increased persistent I_{Na}. These mutations impaired cortical folding and resulted in speech and oral motor dysfunction (Smith, Kenny et al. 2018).

SCN1B

One of the first identified mutations linked to human epilepsy was *SCN1B*-C121W that results in GEFS+ (Wallace, Wang et al. 1998). There are also *SCN1B* associated DS cases, the first identified was a loss of function mutation, *SCN1B*-R125C that results in failure of β1 subunits to traffic to the cell surface (Patino, Claes et al. 2009). Simple loss-of-function is a viable explanation for the mechanism of *SCN1B*-linked DS, as *Scn1b* null mice recapitulate the full DS phenotype, including frequent spontaneous seizures, ataxia, developmental delay, and early lethality (Chen, Westenbroek et al. 2004). This phenotype is more severe than is found in *Scn1a* DS mice and the outcome of patients with *SCN1B* associated DEE are correspondingly more severe than with *SCN1A* cases, indicating it may be a distinct disorder. 100% of *Scn1b* null mice die by postnatal day (P)21, which

may explain the limited detection of patients with homozygous *SCN1B* mutations in the human population (Chen, Westenbroek et al. 2004). Even though β1-C121W polypeptides are expressed at the neuronal cell surface, mice homozygous for the GEFS+ mutation, *Scn1b*-C121W, recapitulate the phenotype of *Scn1b* null mice, suggesting loss-of-function of a cell surface expressed subunit (Reid, Leaw et al. 2014, Kruger, O'Malley et al. 2016). Interestingly, mice heterozygous for the *Scn1b*-C121W allele have increased susceptibility to febrile seizures compared to mice heterozygous for the *Scn1b* null allele (Kruger, O'Malley et al. 2016). Differences in excitability at the single neuron level are not always consistent between the *Scn1b* null and *Scn1b*-C121W homozygous mouse models (Marionneau, Carrasquillo et al. 2012, Reid, Leaw et al. 2014). Several defects in AP waveforms in *Scn1b*-C121W heterozygous mice are absent in *Scn1b*-C121W homozygous mice (Wimmer, Reid et al. 2010, Reid, Leaw et al. 2014). Thus, *SCN1B* associated GEFS+ and DS likely have distinct mechanisms.

A *SCN1B* mutation specific to β1b, G25R, was identified in multiple pedigrees with idiopathic epilepsy (Patino, Brackenbury et al. 2011). Excluding this mutation, all the *SCN1B* epilepsy-causing mutations are within or near the Ig domain, which is important in both α subunit modulation and cell adhesion as described in section 1. Importantly, in the *Scn1b* null mouse, developmental defects appear prior to the onset of seizures or evidence of altered neuronal excitability, suggesting a causative effect of aberrant brain development on altered excitability (Brackenbury, Yuan et al. 2013). Altered CNS development in *Scn1b* null mice may predict a role in intellectual disability independently of seizures (Brackenbury, Yuan et al. 2013). As described in section two, the

hyperexcitability of homozygous *Scn1b*-C121W subicular pyramidal neurons and cortical layer 2/3 pyramidal neurons appears to be a result of decreased cell size (Reid, Leaw et al. 2014). Importantly, specific deletion of *Scn1a* in forebrain GABAergic interneurons is sufficient to phenocopy DS in mice (Cheah, Frank et al. 2012, Ogiwara, Iwasato et al. 2013). Little is known about altered interneuron function in *Scn1b* models of DS, but initial experiments in hippocampal interneurons suggest that they are not affected (Patino, Claes et al. 2009, Reid, Leaw et al. 2014). Given the brain region and cell type specificity of β1 subunit expression discussed in section 2, it is important to expand our understanding of β1 function in the CNS to different neuron types. This may be a useful guide for understanding the exact microcircuit components that are altered in DS and GEFS+ and help us to understand how similar epileptic phenotypes may arise from different mechanisms in specific cell populations. In contrast to the gain or loss of function mutations in *SCN1A* and *SCN8A* EEs, where the predominant expression of the channel is in different neuronal populations and predicts a disease mechanism, β1 is expressed ubiquitously in the CNS and may be involved in numerous pathogenic mechanisms in multiple cell types.

VGSC β subunit expression is differentially impacted in several forms of epilepsy. In pilocarpine induced seizures, there is a downregulation of *Scn1b* and *Scn2b* mRNA following status epilepticus with impacts on sodium current consistent with known functions of these two subunits (Gastaldi, Robaglia-Schlupp et al. 1998, Ellerkmann, Remy et al. 2003). This result may be model or species dependent, as there is no evidence for similar increases in temporal lobe epilepsy patients (Gassen, Koen et al.

2008). There is however, a reduction in *SCN3B* and β3 expression in the hippocampus of temporal lobe epilepsy patients and increased *SCN1B* and β1 in reactive astrocytes of both epileptic and non-epileptic brain trauma patients. (Gorter, Van Vliet et al. 2002, Aronica, Troost et al. 2003, Gassen, Koen et al. 2008, Das, Wallace et al. 2012).

Antiepileptic Drugs and VGSCs

Approximately 30% of epilepsy patients lack adequate seizure control with existing antiepileptic drugs (AEDs) for unknown reasons (Kwan and Brodie 2000). Many antiepileptic drugs target VGSCs, the general effect of which is to reduce excitability through inhibition of VGSCs. The drugs phenytoin and carbemazapine are seminal VGSC inhibitors with many newer drugs sharing this mechanism. While most VGSC AEDs target fast inactivation, lacosamide is notable in that it enhances slow inactivation(Clare, Tate et al. 2000, Errington, Stöhr et al. 2008). Importantly, many of the genetic VGSC disorders above are pharmacoresistant and exhibit differential sensitivity to VGSC targeting AEDs, with some paradoxically being exacerbated by these drugs. In DS, seizures are made worse by giving VGSC acting drugs(Wallace, Wirrell et al. 2016). In *SCN2A* and *SCN8A* EEs, there is a mixed response but no counter indication in responses (Boerma, Braun et al. 2016, Dilena, Striano et al. 2017). The actions of β subunits affect the efficacy of two known AEDs, carbamazepine and phenytoin (Lucas, Meadows et al. 2005, Uebachs, Opitz et al. 2010, Uebachs, Albus et al. 2012). A GEFS+-linked *SCN1B* mutation causes a reduction in the efficacy of phenytoin, attenuating the drug's effects on frequency dependent block of sodium current (Lucas, Meadows et al. 2005). The effects of carbamazepine are also affected by β subunits. *Scn1b* null neurons show a paradoxical

increase in persistent current when treated with carbamazepine, abolishing the usual spiking attenuation caused by this drug (Uebachs, Opitz et al. 2010, Uebachs, Albus et al. 2012). Recently, a case study of a family with benign familial infantile epilepsy identified an *SCN1B* splicing variant as a disease modifier or part of an oligogenic predisposition in this family (Usluer, Kayserili et al. 2017). As many of our AEDs target VGSCs, the diverse function of VGSCs, and the broadly pharmacoresistant nature VGSC related epilepsies, VGSCs may be components in understanding why so many AEDs fail to adequately control seizures.

Conclusion

VGSCs are key players in the development and excitability of the nervous system. The targeted expression and properties of these channels are crucial to normal nervous system function. While VGSCs are traditionally thought of as all or none mediators of action potentials, the precise control of their expression and properties have both physiological and pathophysiological consequences. β subunits, more than simple accessories of the pore-forming α subunits, instead confer several unique properties to VGSCs. β subunit multifunctionality allows for crosstalk between several excitability mechanisms for the control of neuronal excitability within and between cells. The cell adhesive properties of β subunits link neuronal development to excitability. Sodium current impacts brain development through β subunit dependent pathways and defects in structure resulting from β subunit gene deletion can influence excitability. The cell type dependent properties and unique pharmacology of the different VGSC subunits are also

emerging targets for guiding our understanding of nervous system function and disease mechanisms.

In the following chapters I will present my work investigating the role of β1 subunits in the control of VGSC function in specific neuronal cell types and in communication between neurons. In Chapter 2 I describe my work investigating the role of *Scn1b* in single neuron and network hyperexcitability. In Chapter 3 I describe my work characterizing the role of heterogeneity of I_{Na} density between neurons in the control of patterning network activity. Together this work constitutes a significant advancement in our understanding of the role of VGSCs in both the pathophysiology of epilepsy and in the patterning of neuronal activity.

Chapter II. Deletion of the epilepsy-associated gene, *Scn1b*, leads to network location specific disinhibition and pyramidal neuron dysfunction

This chapter has been submitted for publication to the Journal of Neuroscience[1]

Introduction

Voltage-gated sodium channels (VGSCs) are responsible for action potential (AP) initiation and propagation in the nervous system (Catterall 2012). VGSCs in brain are heterotrimers, composed of one pore-forming α subunit and two non-pore-forming β subunits (β1 or β3 and β2 or β4) (O'Malley and Isom 2015, Hull and Isom 2017). Mutations in several VGSC genes result in developmental and epileptic encephalopathies (DEE). The DEE Dravet syndrome (DS) is typically associated with heterozygous loss-of-function (LOF) variants in *SCN1A*, encoding the VGSC α subunit $Na_v1.1$ (Marini, Scheffer et al. 2011). Alternatively, gain-of-function (GOF) variants in *SCN8A*, encoding the VGSC

[1] Jacob Hull performed and analyzed all experiments with the following exceptions; Kachi Anumonwo and Chunling Chen performed mouse breeding, genotyping, and record keeping for Fig. 2.1 and 2.6. Yukun Yuan contributed a subset of recordings for Fig. 2.2. Alexandra Bouza and Nicholas Denomme generated samples and performed experiments for [^{3}H]-STX binding experiments

Nav1.6, result in early infantile epileptic encephalopathy type 13 (EIEE13) (Meisler, Helman et al. 2016). *A* subset of DEE patients, often diagnosed as DS, have homozygous LOF variants in *SCN1B*, encoding the VGSC β1 subunit and its splice variant, β1B (Patino, Claes et al. 2009, Ramadan, Patel et al. 2017) (EIEE52, OMIM 617350). Evidence from mouse models supports the hypothesis that haploinsufficiency of *Scn1a* drives cortical and hippocampal GABAergic interneuron hypoexcitability, leading to disinhibition (Yu, Mantegazza et al. 2006, Ogiwara, Miyamoto et al. 2007, Cheah, Yu et al. 2012) while GOF *Scn8a* mutations result in pyramidal neuron hyperexcitability. Importantly, evidence suggests that fast-spiking (FS) interneurons expressing parvalbumin (PV) are crucial components of DS pathology (Ogiwara, Miyamoto et al. 2007, Ogiwara, Iwasato et al. 2013, Tai, Abe et al. 2014, Rubinstein, Han et al. 2015). PV+ interneurons are hypoexcitable in *Scn1a*$^{+/-}$ mice, and sodium current (I_{Na}) density is reduced in dissociated non-pyramidal shaped neurons of the hippocampus (Yu, Mantegazza et al. 2006, Mistry, Thompson et al. 2014, Tai, Abe et al. 2014).

Scn1b$^{-/-}$ mice are a model of a severe DEE that is similar to DS, with spontaneous epilepsy, ataxia, and early lethality in 100% of animals (Chen, Westenbroek et al. 2004). β1 subunits are expressed ubiquitously in the brain, including in excitatory and inhibitory neurons of the cortex and hippocampus, where they associate with all major brain VGSC α subunits (Hull and Isom 2017). β1 modulates VGSC α subunit trafficking, expression, and gating in heterologous expression systems and in neurons (Hull and Isom 2017). β1 has also been shown to associate with and modulate some voltage-gated potassium channels (VGKCs) in heterologous cells (Deschenes and Tomaselli 2002, Nguyen,

Miyazaki et al. 2012). Importantly β1 subunits belong to the immunoglobulin superfamily of cell adhesion molecules (Ig-CAMS) (Isom and Catterall 1996). Their cell adhesive functions affect many aspects of neuronal development, including neurite outgrowth, axonal fasciculation and pathfinding, and neuronal migration (Brackenbury and Isom 2011). The observation of neuronal pathfinding defects in *Scn1b*$^{-/-}$ brain prior to the onset of epilepsy led to the proposal that altered development underlies epileptogenesis in this model (Brackenbury, Yuan et al. 2013). Subpopulations of pyramidal neurons in *Scn1b*$^{-/-}$ or in the related *Scn1b*-p.C121W homozygous knockin (*Scn1b*$^{CW/CW}$) mouse model have higher AP firing rates than *Scn1b*$^{+/+}$ (Brackenbury, Yuan et al. 2013, Reid, Leaw et al. 2014) suggesting a disease mechanism of increased excitability of pyramidal neurons, similar to EIEE13. Hyperexcitability was postulated to arise from reduced cell size and increased input resistance due to loss of β1-mediated CAM function. We recently tested this hypothesis, however, and reported that induced *Scn1b* deletion in adult animals, following normal development, is sufficient to result in severe epilepsy and 100% lethality, showing that altered brain development is not necessary for *Scn1b*-linked epilepsy and early mortality (O'Malley, Hull et al. 2019). This result raised the question of the mechanism of network and pyramidal neuron hyperexcitability in *Scn1b*-linked DEE. Here, we investigated the mechanism of DEE linked to *Scn1b* LOF using the *Scn1b*$^{-/-}$ mouse model. We show that, while *Scn1b* DEE mouse models share a disinhibition mechanism more similar to *Scn1a* models than *Scn8a* DEE models, *Scn1b*$^{-/-}$ mice have additional deficits that likely contribute to their more severe phenotype.

Results

Scn1b deletion in PV+ neurons results in seizures and death.

To examine whether PV+ FS interneurons contribute to seizures in *Scn1b*-linked DEE, we generated *Scn1b*$^{Fl/Fl}$/PV-Cre mice (Chen, Dickendesher et al. 2007) (JAX #017320) and compared their phenotype to *Scn1b*$^{-/-}$ mice. We found that selective *Scn1b* deletion in PV+ neurons results in epilepsy and 100% lethality, with disease onset displaced by one week relative to *Scn1b*$^{-/-}$ mice, likely due to the onset of PV promoter expression occurring after the first week of development in rodents (de Lecea, del Rio et al. 1995). Median survival was 18 days for *Scn1b*$^{-/-}$ mice and 25 days for *Scn1b*$^{Fl/Fl}$/PV-Cre mice (Fig. 2.1, $p<0.0001$, Mantel-Cox test). Movie S1 shows an example of a spontaneous convulsive seizure in a P17 *Scn1b*$^{Fl/Fl}$/PV-Cre mouse. Next, we generated *Scn1b*$^{Fl/FL}$/CAMK2a-Cre mice (Tsien, Chen et al. 1996, Chen, Dickendesher et al. 2007) (JAX # 005359) to ask if *Scn1b* deletion in excitatory neurons would also lead to spontaneous epilepsy and death. In contrast to *Scn1b*$^{Fl/Fl}$/PV-Cre mice, *Scn1b*$^{Fl/Fl}$/CAMK2a-Cre mice did not result in behavioral seizures or premature death.

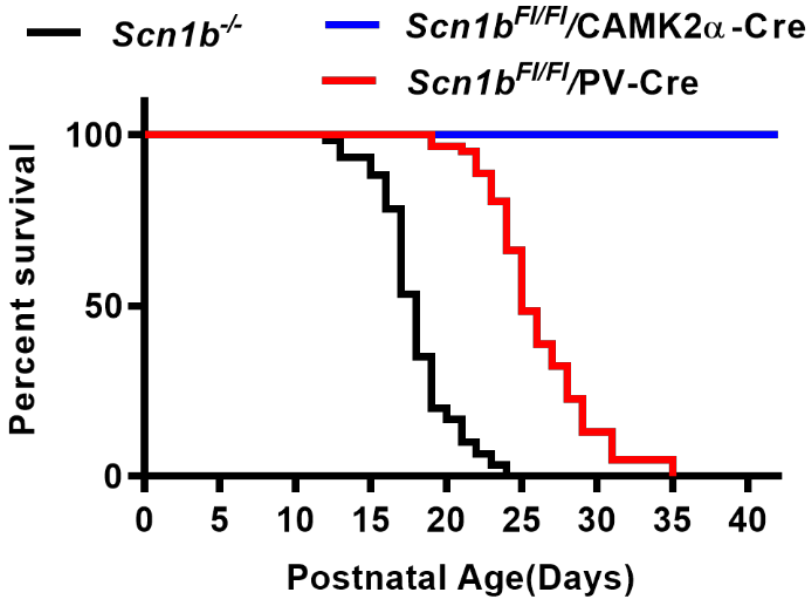


Fig. 2.1 PV-, but not CAMK2α-, dependent Cre deletion of *Scn1b* results in early lethality. A. Kaplan-Meier survival curve of *Scn1b*$^{Fl/Fl}$/PV-Cre mice (median 25 days, N=62) compared to *Scn1b*$^{-/-}$ mice (median of 18 days, N=60, p<0.0001, Mantel-Cox test) and *Scn1b*$^{Fl/FL}$/CAMK2α mice (no deaths, N=21) (p<0.0001, Mantel-Cox test).

Scn1b deletion results in PV+ cortical interneuron hypoexcitability

To test whether the excitability of FS interneurons is altered by *Scn1b* deletion, we intercrossed *Scn1b*$^{+/-}$ mice with a strain expressing the tdTomato/Ai14 fluorescent reporter (JAX #007908) under control of the PV promoter, generating *Scn1b*$^{+/+}$/PV-Cre/tdTom and *Scn1b*$^{-/-}$/PV-Cre/tdTom mice, to facilitate the identification of PV+ FS interneurons in brain slices by epifluorescence. We recorded APs from *Scn1b*$^{-/-}$/ PV-Cre/tdTom and *Scn1b*$^{+/+}$/PV-Cre/tdTom cortical layer 5 PV+ neurons in acute brain slices with 1s long current injections ranging from -20 to 300 pA (Fig. 2.2A). All recorded cells showed features of FS interneurons, including sharp after-hyperpolarizations and non-

accommodating APs. The maximal firing frequency was significantly reduced in *Scn1b*$^{-/-}$/PV-Cre/tdTom interneurons relative to interneurons from *Scn1b*$^{+/+}$/PV-Cre/tdTom littermates. (Fig. 2.2C). Fig. 2.2B shows representative traces comparing *Scn1b*$^{-/-}$/PV-Cre/tdTom and *Scn1b*$^{+/+}$/PV-Cre/tdTom firing patterns at 10, 100, 200, and 300 pA. We found no change in input resistance (Fig. 2.2E, Table 1), whole cell capacitance (Table 1), or resting membrane potential (RMP) between genotypes (Fig. 2.2D, Table 1). We compared AP peak voltage, peak dv/dt, and AP voltage threshold in AP trains elicited by 1-s long 100 pA current injections from the recordings in Fig. 2.2B and Table 1. Neither the first AP nor subsequent APs in the train were different between genotypes.

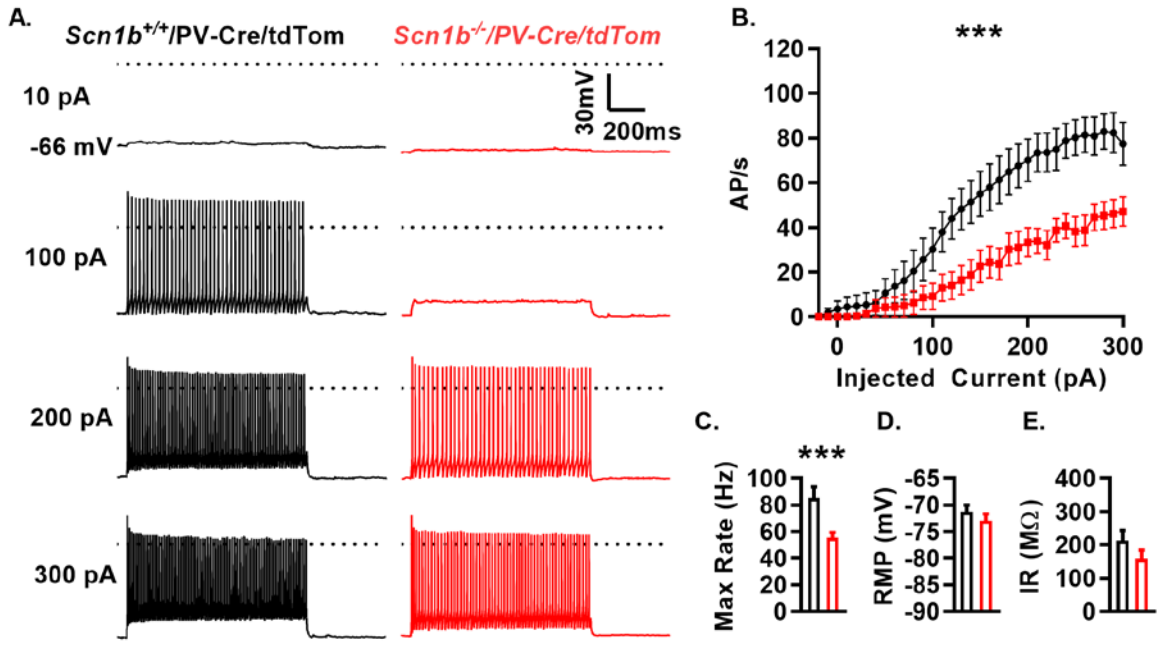


Fig. 2.2. *Scn1b* deletion results in cortical PV+ neuron hypoexcitability. A. Representative voltage traces from whole cell recordings of neurons positive for red fluorescence from brain slices of *Scn1b*$^{+/+}$/PV-Cre/tdTom (black) or *Scn1b*$^{-/-}$/PV-Cre/tdTom mice (red) at P14-20 **B.** Current injection vs. APs fired in 1-s of recordings above. Asterisks indicate p value for area under the curve (***p<0.005, n/N=11/4 *Scn1b*$^{+/+}$/PV-Cre/tdTom 11/4 *Scn1b*$^{-/-}$ /PV-Cre/tdTom . **C.** Maximum firing rate for neurons in B (***p<0.005). **D-E.**

Average resting membrane potential (D) and input resistance (E) from recordings in B. See Table 1 for numerical data and biophysical properties.

	Scn1b $^{+/+}$ vs *Scn1b*$^{-/-}$ (/PV-Cre/tdTom)
Resting V_m (mV)	-71.2±1.3 / -73.0±1.3
Input Resistance (MΩ)	214.2±29.8 / 159.1±26.6
Capacitance (pF)	21.7±3.0 / 22.0±1.4
Max Firing Rate (Hz)	85.5±8.1 / 55.6±3.7(***)
Depolarization Block (%)	10.5±6.9 / 15.7±10.3
1st AP Peak Voltage (mV)	14.8±3.4 / 14.1.3±0.9
AP Train Peak Voltage (mV)	6.4±3.2 / 6.2±3.2
1st AP Peak dv/dt (mV/ms)	231.8±24.4 / 198.3±21.4
AP Peak dv/dt Train (mV/ms)	152.0±19.6 / 131.2±18.3
1st AP Threshold (mV)	-63.3±1.7 / -56.3±3.4
AP Threshold Train (mV)	-54.1±0.9 / -50.5±1.8

Table 2.1 Scn1b deletion impairs excitability of PV+ neurons. Data shown graphically in Fig. 2.2 Values are mean +/- SEM. ***p<0.005

I_{Na} is reduced in dissociated *Scn1b*$^{-/-}$ cortical PV+ interneurons

We next recorded I_{Na} in acutely dissociated PV+ FS cortical interneurons of *Scn1b*$^{-/-}$/PV-Cre/tdTom and *Scn1b*$^{+/+}$/PV-Cre/tdTom mice in cells identified by red epifluorescence. Representative traces are shown in Fig 2.3A and the current-voltage relationship is shown in Fig 2.3 B. I_{Na} density at the mean peak current density (-25 mV) was reduced by approximately 30% in *Scn1b*$^{-/-}$ neurons compared to *Scn1b*$^{+/+}$ (Fig. 2.3C

and Table 2.2). The $V_{1/2}$ and slope factors for voltage dependent permeability and inactivation were unaffected by *Scn1b* deletion (Fig. 2.3D and Table 2.2).

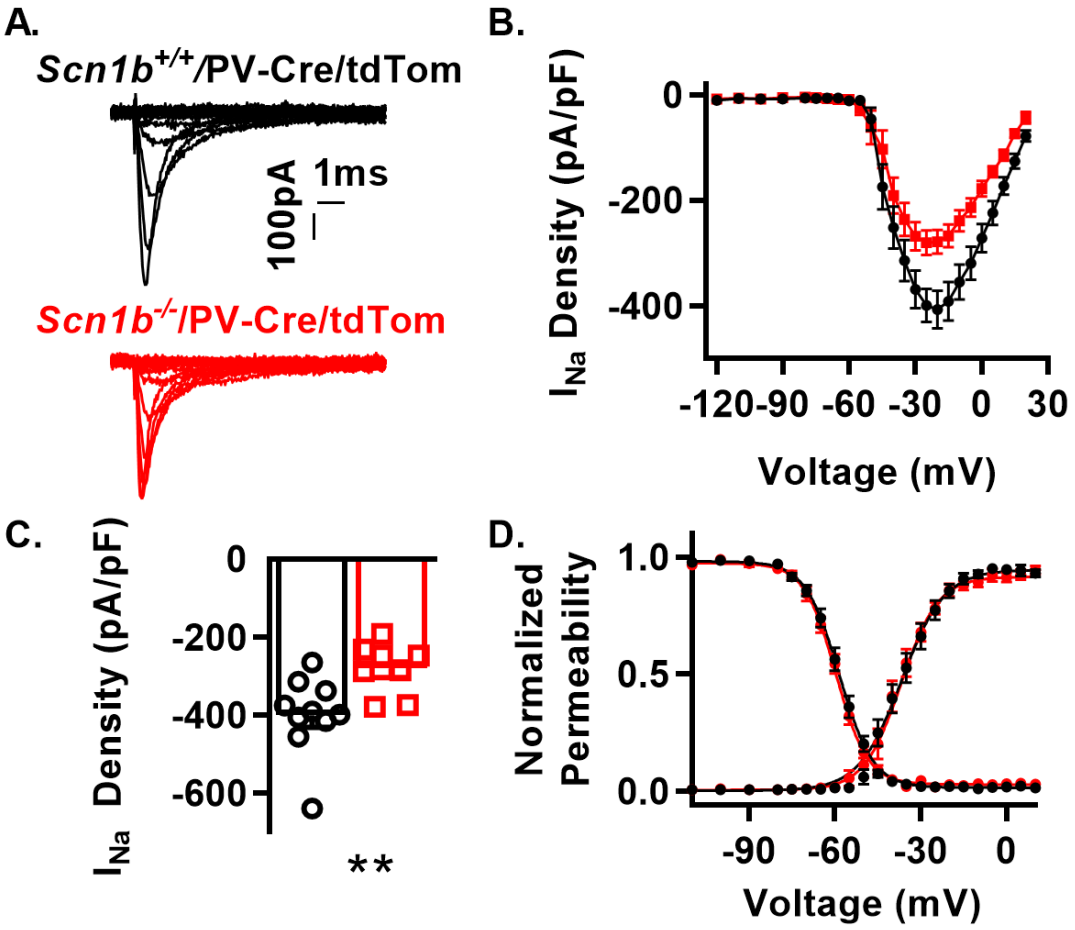


Fig. 2.3. Scn1b deletion reduces INa density in dissociated cortical PV+ neurons. A. Representative I_{Na} traces from whole cell recordings from cortical PV+ neurons of *Scn1b*$^{+/+}$/PV-Cre/tdTom and *Scn1b*$^{-/-}$/PV-Cre/tdTom mice. Current elicited by depolarizing steps from -120 mV to 30 mV from a holding potential of -120 mV (traces up to peak are shown for visualization of smaller nested currents). **B.** Current-voltage relationship for recordings as in A (n/N=10/3 *Scn1b*$^{+/+}$/PV-Cre/tdTom, 8/3 *Scn1b*$^{-/-}$/PV-Cre/tdTom). **C**. Peak I_{Na} density at -25 mV from recordings in B**.** Asterisks indicate p value (**p<0.01). **D.** Normalized voltage dependence of steady state activation and inactivation of recordings in B. See Table 2 for numerical values.

	Scn1b$^{+/+}$/PV-Cre/tdTom	*Scn1b*$^{-/-}$/PV-Cre/tdTom
Peak Current Density (pA/pF)		
Mean±SEM	-399±32(**)	-280±24
Variance	10,102	4,418
Peak Current (pA)		
Mean±SEM	-2,916±162	-2,349±264
Variance	558,457	262,502
Capacitance (pF)		
Mean±SEM	7.52±0.47	8.36±0.55
Activation $V_{1/2}$ (mV)		
Mean+/- SEM	-35.45+/- 1.70	-37.83+/- 2.27
Activation k (mV)$^{-1}$		
Mean+/- SEM	6.47+/- 0.52	5.86+/- 0.29
Inactivation $V_{1/2}$ (mv)		
Mean+/- SEM	-58.56+/- 1.22	-59.36+/- 0.97
Inactivation k (mV)$^{-1}$		
Mean+/- SEM	5.30+/- 0.11	5.28+/- 0.10
n/N	10/3	8/3

Table 2.2. Effects of Scn1b deletion on INa density and voltage-dependence in PV+ cortical neurons. Data shown graphically in Fig. 2.3 Values are mean +/- SEM, n/N indicate cells/mice, respectively. **p<0.01

Subpopulations of *Scn1b*$^{-/-}$ pyramidal neurons show hyperexcitable phenotypes that are dependent on acute network activity

Previous work showed that specific subpopulations of *Scn1b*$^{-/-}$ and *Scn1b*$^{CW/CW}$ pyramidal neurons are hyperexcitable (Brackenbury, Yuan et al. 2013, Reid, Leaw et al. 2014). Here, we recorded from several pyramidal neuron populations to determine whether *Scn1b* deletion resulted in excitability defects. APs were recorded in 1-s long current injections ranging from -20 to 200 pA, from pyramidal neurons in cortical layers 5

and 6 and the subiculum in acute brain slices from *Scn1b*$^{-/-}$ and *Scn1b*$^{+/+}$ littermate mice. We found no differences in evoked firing rates between genotypes in layer 5 pyramidal neurons (Fig. 2.4, panels A and B). In contrast, we observed altered excitability in *Scn1b*$^{-/-}$ subiculum (Fig. 2.4, panels E and F) and layer 6 (Fig. 2.4, panels I and J) neurons compared to *Scn1b*$^{+/+}$.

Fig. 2.4, panels A, E, and I show representative traces comparing P14-20 *Scn1b*$^{-/-}$ and *Scn1b*$^{+/+}$ cortical layer 5, subiculum, and layer 6 pyramidal neuron firing patterns at 10, 50, 100, and 150 pA. In layer 5, neurons showed no change in RMP, capacitance, or input resistance, while in subiculum and layer 6, *Scn1b*$^{-/-}$ neurons showed depolarized RMP, increased input resistance, and decreased capacitance in layer 6 (Fig. 2.4, panels C, D, G, H, K, and L and Table 2.3).

Increased firing in *Scn1b*$^{-/-}$ subicular and layer 6 neurons was limited to low current injections (Fig. 2.4F and J, respectively), quantified as area under the curve up to 50 pA of injected current. To quantify differential sensitivity of neurons to depolarization block at higher current injections, firing rate at the highest current injection was divided by the maximum firing rate for that cell. *Scn1b*$^{-/-}$ layer 6 neurons showed a greater degree of attenuation compared to *Scn1b*$^{+/+}$, with subiculum showing similar results (Table 3). We compared AP peak voltage, peak dv/dt, and AP voltage threshold between genotypes for neurons in layers 5, 6 and subiculum in AP trains elicited by 1-s long current injections from the recordings shown above. We analyzed layer 6 at 100 pA and subiculum and layer 5 at 150 pA due to near total depolarization block at 150 pA in layer 6 and the lower

firing rate at 100 pA in layer 5 and subiculum. In layer 6, the first AP in the train was not different between genotypes in peak voltage, firing threshold, or peak dv/dt, but subsequent APs showed decreased peak voltage, elevated threshold, and decreased peak dv/dt in *Scn1b*$^{-/-}$ neurons compared to *Scn1b*$^{+/+}$ (Table 3). In subiculum, the results were similar, but with the first AP in the train exhibiting a decreased peak dv/dt and subsequent APs showing decreased averaged peak voltage, elevated threshold, and decreased peak dv/dt in *Scn1b*$^{-/-}$ neurons compared to *Scn1b*$^{+/+}$ (Table 3). Pyramidal neurons in *Scn1b*$^{-/-}$ cortical layer 5 were the least affected population examined, with no difference between genotypes in the above AP properties (Table 3).

Scn1b is widely expressed across the CNS (Hull and Isom 2017), however our results show that its deletion results in network location specific alterations to pyramidal neuron excitability. To investigate this result in greater detail, we asked whether network activity underlies pyramidal neuron hyperexcitability in *Scn1b*$^{-/-}$ neurons. We recorded APs in cortical layer 6 pyramidal neurons from P14-20 *Scn1b*$^{-/-}$ or *Scn1b*$^{+/+}$ mice in the presence of CNQX (10 µM), APV (50 µM), and bicuculine (10 µM) to block fast synaptic transmission. Under these conditions, we found that, in contrast to recordings in brain slices with intact synaptic transmission, values for RMP were not different between genotypes (Fig. 2.4O, Table 2.3) and the increased firing of *Scn1b*$^{-/-}$ neurons that was observed previously at low current injections was not observed (Fig. 2.4N). However, early depolarization block at high current injections, increased input resistance, decreased cell capacitance, and the impaired AP properties observed above in *Scn1b*$^{-/-}$ vs. *Scn1b*$^{+/+}$ neurons remained (Fig. 2.4, panels N and P, Table 2.3), showing that these

properties are independent of ongoing network activity. Importantly, these data show that pyramidal neuron hyperexcitability alone cannot account for epileptogenesis in *Scn1b*$^{-/-}$ mice because it is the result of, rather than the cause of, increased network activity.

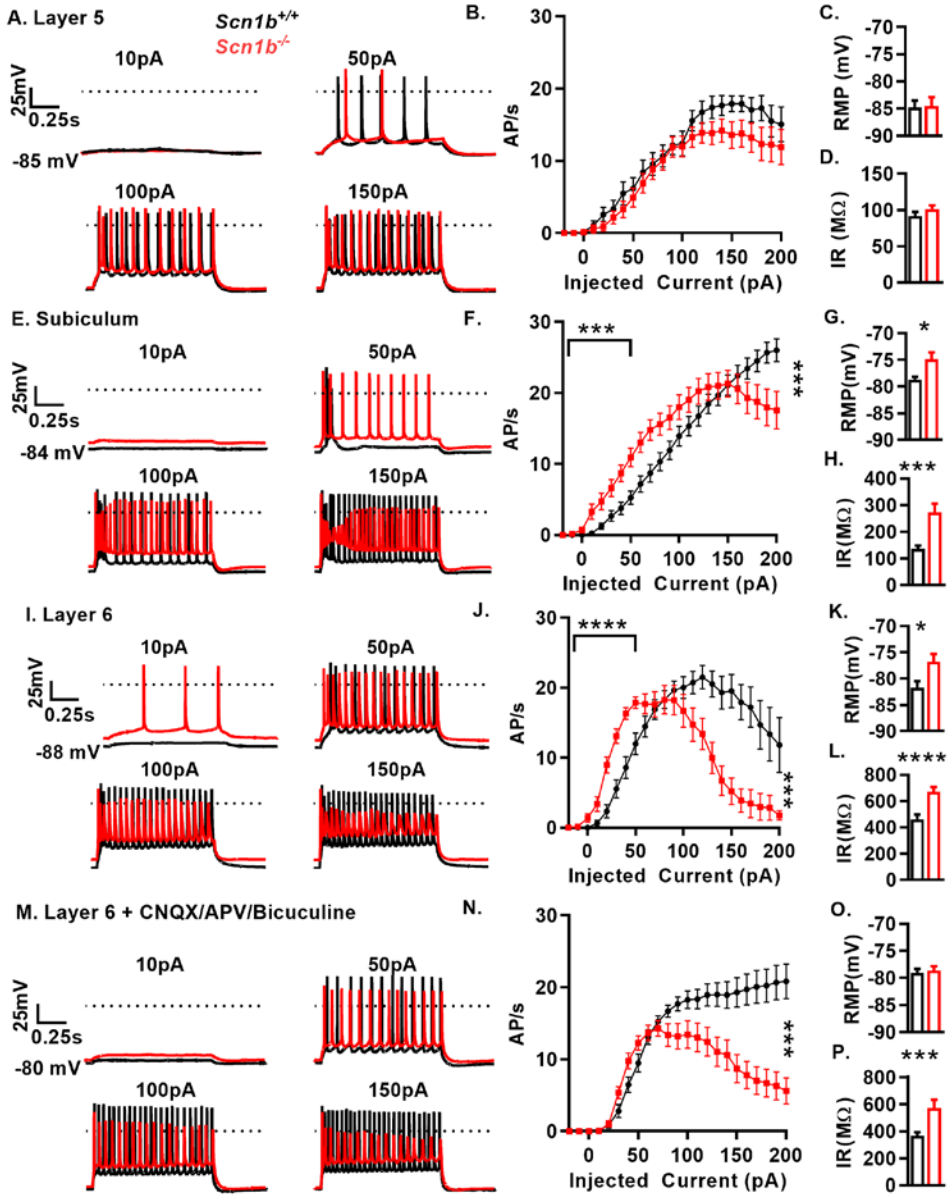


Fig. 2.4. Scn1b deletion results in network location and network activity dependent pyramidal neuron hyperexcitability. A., E, and I. Representative voltage traces from whole cell recordings of layer 5 (A), subiculum (E), layer 6 (I), and CNQX/APV/Bicuculine treated layer 6 pyramidal neurons (M) in acute brain slices of *Scn1b*$^{+/+}$ (black) or *Scn1b*$^{-/-}$ mice (red) **B., F., J., N.,** Current injection vs. APs fired in 1-s of

recordings above. Firing at low current injection quantified as area under the curve up to 50 pA. Depolarization block is quantified as AP count at highest current injection divided by max AP count (with AP failure defined as max voltage<0 mV). Layer 5 (B) pyramidal neurons show no change in firing at low current injections or degree of depolarization block (n/N=12/7 *Scn1b*$^{+/+}$, 14/7 *Scn1b*$^{-/-}$). Subicular (F) and Layer 6 pyramidal neurons (J) and show increased firing at low current amplitudes (left asterisks indicate p-value) in *Scn1b*$^{+/+}$ vs. *Scn1b*$^{-/-}$ mice (n/N=25/12 *Scn1b*$^{+/+}$, 24/13 *Scn1b*$^{-/-}$ subiculum; n/N= 20/10 *Scn1b*$^{+/+}$, 21/9 *Scn1b*$^{-/-}$ layer 6, Welch's t-test). **N.** Layer 6 pyramidal neurons treated with CNQX/APV/Bicuculine show no increase in firing at low current injections (left asterisks indicate p-value) and have early depolarization block (right asterisks indicate p-value, n/N= 21/7 *Scn1b*$^{+/+}$, 21/7 *Scn1b*$^{-/-}$). **C., G., K., O.,** RMP is not affected by *Scn1b* deletion in layer 5 (C) but is depolarized in subicular (G) and layer 6 pyramidal neurons (K) which is abolished by CNQX/APV/Bicuculine (O). **D., H., L., P.** Input resistance is unaffected by *Scn1b* deletion in layer 5 (D) but is increased in subicular (H) and layer 6 pyramidal neurons (L) which is not affected by treatment with CNQX/APV/Bicuculine (P). See Table 3 for quantification of biophysical properties. Asterisks indicate p-values (*p<0.05, *** p<0.005, and ****p<0.0001).

		Layer 5	**Subiculum**	**Layer 6**	**Layer 6+ CNQX/APV/Bicuculine**
	Scn1b:				
Resting V_m	**+/+**	-84.7±1.2	-78.5±0.5(*)	-81.7±1.2(*)	-79.09±0.81
(mV)	**-/-**	-84.6±1.7	-75.5±1.0	-76.8±1.5	-78.61±0.82
Input Resistance	**+/+**	91.7±5.6	135.7±53.5(***)	461.6±±36.4(****)	366.29±25.1(***†)
(MΩ)	**-/-**	101.5±4.9	247.0±29.7	669.4±37.4	570.68±59.63
Capacitance	**+/+**	52.2±3.4	32.8±2.3	19.5±2.1(***)	15.87±0.77(**†)
	-/-	43.2±2.2	27.5±1.7	14.3±1.0	13.33±0.34
Max Firing Rate	**+/+**	22.2±1.3	26.9±1.4	24.8±1.2	24.2±1.4(***)
	-/-	19.6±1.0	26.6±1.1	22.9±1.0	17.7±1.1
Depolarization Block	**+/+**	49.6±12.2	22.4±7.0(*)	63.7±9.3 (***†)	18.5±8.0(***)
(%)	**-/-**	47.8±12.9	46.5±9.2	92.8±1.1	70.4±8.9
1st AP Peak Voltage	**+/+**	22.0±1.3	30.7±1.2	24.8±1.0	32.7±1.4(****)
(mV)	**-/-**	23.2±1.2	27.6±1.5	22.9±0.9	23.1±1.7
AP Train Peak Voltage	**+/+**	12.1±2.1	24.6±1.4(**)	18.0±1.3(****)	26.7±2.2(***)
(mV)	**-/-**	15.2±1.8	18.0±1.9	9.1±1.1	13.2±1.9
1st AP Peak dv/dt	**+/+**	176.3±8.4	286.7±11.4(***)	170.1±6.5	226.1±11.6(***)
(mV/ms)	**-/-**	187.3±5.9	231.3±13.3	158.0±6.5	158.0±11.1
AP Peak dv/dt Train	**+/+**	111.0±10.4	203.0±14.6(***)	116.2.2±8.2(***)	152.6±14.3(***†)

(mV/ms)	**-/-**	134.7±8.5	131.5±13.3	73.4.3±7.3	69.9±6.7
1st AP Threshold	**+/+**	-68.7±0.9	-68.7±0.8	-65.2±0.7	-59.0±1.0(*)
(mV)	**-/-**	-68.4±1.0	-67.8±1.1	-64.3±0.8	-55.8±1.2
AP Threshold Train	**+/+**	-60.9±0.9	-60.8±0.9(**)	-56.5±0.9(***)	-51.6(****)
(mV)	**-/-**	62.2±1.5	-56.9±1.1	-51.6±1.2	-42.8±1.3

Table 2.3. *Scn1b* deletion alters excitability in subpopulations of pyramidal neurons in a network activity dependent manner. Data shown graphically in Fig. 2.4. Values are mean +/- SEM. † indicates t-test with Welch's Correction. *p<0.05, **p<0.01, ***p<0.005, ****p<0.0001

Scn1b$^{-/-}$ pyramidal neurons exhibit layer specific disinhibition

Because *Scn1b*$^{-/-}$ pyramidal neurons lose their hyperexcitability when isolated from network activity, we hypothesized that *Scn1b* deletion may differentially affect inhibitory transmission based on network location. To test this idea, we recorded spontaneous inhibitory post synaptic currents (sIPSCs) in cortical pyramidal neurons of layer 5 vs. layer 6, which we show above are unaffected vs. hyperexcitable populations in *Scn1b*$^{-/-}$ brain, respectively. Neither the mean amplitude (28.71 ± 2.55 pA in *Scn1b*$^{-/-}$, n/N=11/4 vs. 37.59 ± 3.99 pA in *Scn1b*$^{+/+}$, N=11/4) nor the mean frequency (6.21 ± 1.13 Hz in *Scn1b*$^{-/-}$, n/N=11/4 vs. 6.23 ± 0.99 Hz in *Scn1b*$^{+/+}$, N=11/4) of sIPSCs in layer 5 pyramidal neurons were different between genotypes (Fig. 2.5, panels B and C insets, respectively). The cumulative probability distributions of event amplitudes were significantly different between genotypes (Fig. 2.5B), suggesting that inhibitory transmission in layer 5 is affected by *Scn1b* deletion, but with non-significant effects on mean amplitude and event frequency. In contrast, *Scn1b*$^{-/-}$ layer 6 pyramidal neurons showed no change in the average (34.54 ± 1.28 pA in *Scn1b*$^{-/-}$, n/N=12/4 vs. 36.90 ± 5.28 pA in *Scn1b*$^{+/+}$, N=12/4,

Welch's t-test, F=16.98, p<0.0001, F-test) or cumulative probability distribution of current amplitudes compared to *Scn1b*$^{+/+}$, but received a 2.76 fold lower average frequency (1.38 ± 0.21 Hz in *Scn1b*$^{-/-}$, n/N=12/4 vs. 3.81 ± 0.66 Hz in *Scn1b*$^{+/+}$, N=12/4, p<0.005, Welch's t-test, F=9.98, p<0.005, F-test) of sIPSCs (Fig. 2.5F) accompanied by an altered cumulative probability distribution. These data show that global *Scn1b* deletion results in network location dependent effects on inhibitory neural transmission, the relative magnitude of which correlates with the network activity dependent pyramidal neuron hyperexcitability shown in Fig. 2.4.

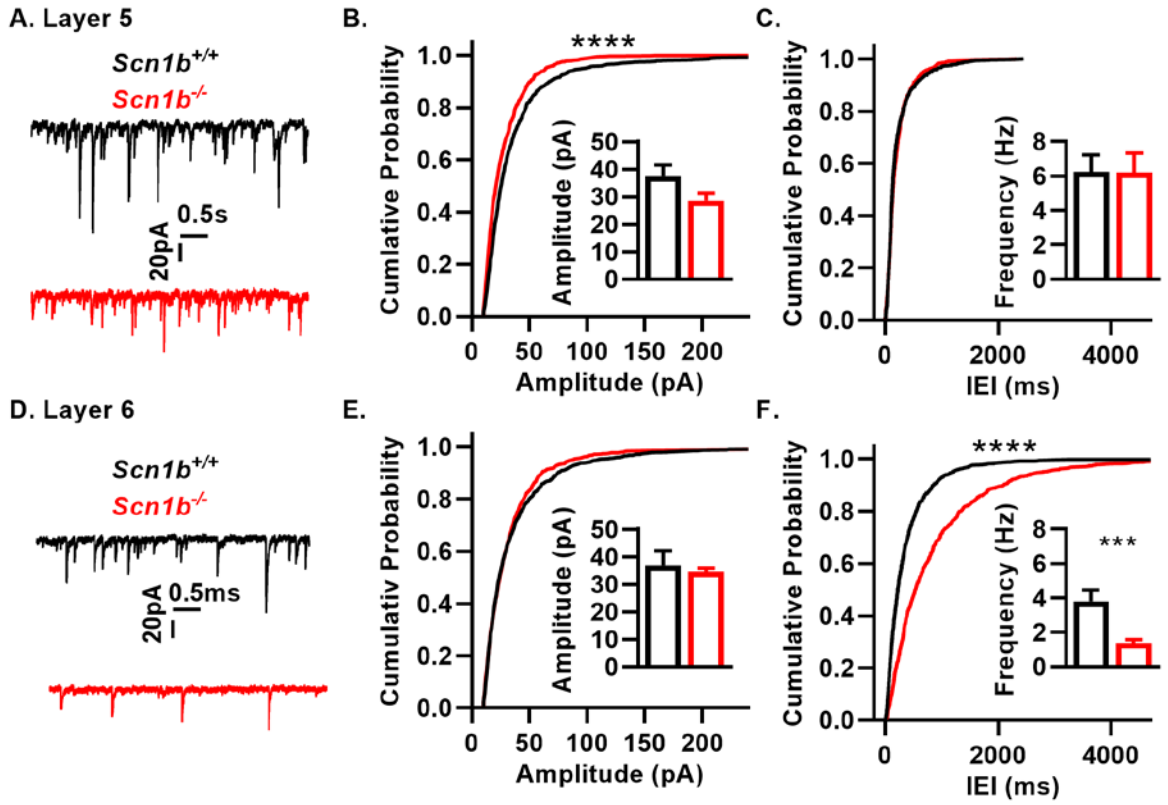


Fig. 2.5. *Scn1b* deletion differentially impacts spontaneous inhibitory post synaptic currents in layer 5 and layer 6 pyramidal neurons. A. and D. Representative sIPSC traces from whole cell recordings from layer 5 (A) and layer 6 (D) pyramidal neurons of *Scn1b*$^{+/+}$ (black) and *Scn1b*$^{-/-}$ (red) mice. **B. and E.** Cumulative probability plots of sIPSC amplitude in layer 5 (B, n/N=11/4 *Scn1b*$^{+/+}$, 11/4 *Scn1b*$^{-/-}$) and layer 6 (E, n/N=12/4 *Scn1b*$^{+/+}$, 12/4 *Scn1b*$^{-/-}$) pyramidal neurons as in A and D. Asterisks indicate p-value

comparing cumulative probabilities (****p<0.0001, Kolmogorov-Smirnov test). Inset bar graphs show mean sIPSC amplitudes. **C. and F.** Cumulative probability plot of interevent intervals in layer 5 (C) and layer 6 (F) pyramidal neurons as in A and D. Top asterisks indicate p-value for comparing cumulative probabilities (****p<0.0001, Kolmogorov-Smirnov test). Inset bar graphs shown mean sIPSC frequency (1/IEI). Asterisk indicates p-value (***p<0.005, Welch's t-test).

Reducing *Scn8a* expression does not impact the *Scn1b* DS phenotype

Our data showing that *Scn1b* deletion impairs the excitability of FS interneurons and that *Scn1b*$^{-/-}$ pyramidal neuron hyperexcitability is the product of rather than caused by altered network activity suggests that *Scn1b*-DEE pathogenesis and *Scn1a*-DS pathogenesis may share common elements. Importantly, however, there remain a variety of differences in the two models. *Scn1b*$^{-/-}$ mice have a more severe phenotype than *Scn1a*$^{+/-}$ mice, with earlier age of seizure onset and 100% lethality by the third postnatal week. In *Scn1a*-DS mice, heterozygous deletion of *Scn8a* prolongs lifespan (Martin, Tang et al. 2007). It was proposed that reduction of *Scn8a* expression in DS pyramidal neurons dampens their excitability and normalizes excitatory/inhibitory balance, leading to reduced seizures and increased survival. We asked whether *Scn8a* haploinsufficiency in *Scn1b*$^{-/-}$ mice had a similar effect on disease severity. We found that intercrossing *Scn1b*$^{+/-}$ mice with *Scn8a*$^{med/+}$ mice (Burgess, Kohrman et al. 1995) to generate *Scn1b*$^{-/-}$/*Scn8a*$^{+/+}$ and *Scn1b*$^{-/-}$/*Scn8a*$^{med/+}$ progeny had no impact on the survival of *Scn1b*$^{-/-}$ mice (Fig. 2.6). In other work, deletion of *Mapt*, the gene encoding the microtubule-binding protein Tau, was shown to attenuate hyperexcitability and prevent disease in the *Scn1a*^{R1407X} mouse model of DS (Gheyara, Ponnusamy et al. 2014). We reported that intercrossing *Scn1b*$^{+/-}$ mice with *Mapt*$^{+/-}$ mice to generate *Scn1b*$^{-/-}$/*Mapt*$^{+/+}$ *and Scn1b*$^{-/-}$ /*Mapt*$^{-/-}$ progeny had no impact on seizures or survival of *Scn1b*$^{-/-}$ mice (Chen, Holth et al.

2018). Taken together, these results show that there remain critical differences in the mechanisms of *Scn1a*- and *Scn1b*-linked DEE.

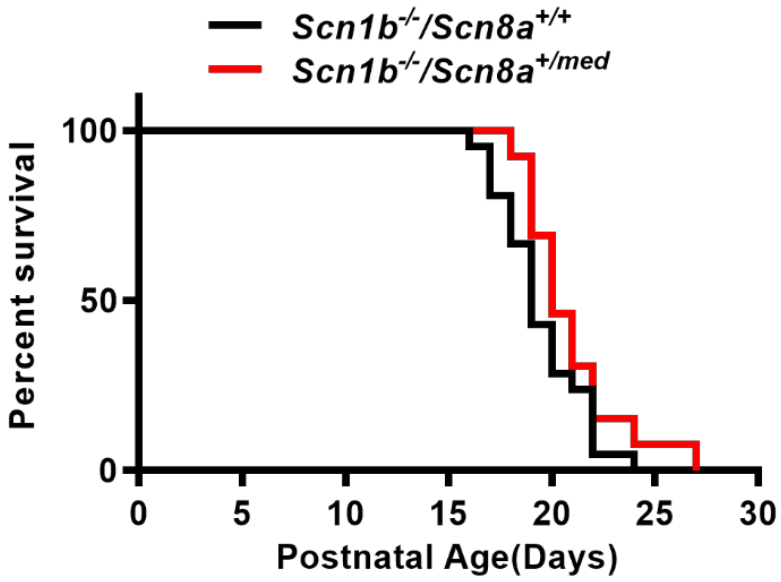


Fig 2.6. *Scn8a* haploinsufficiency does not rescue *Scn1b*$^{-/-}$ mice. Kaplan-Meier survival curve of *Scn1b*$^{-/-}$/*Scn8a*$^{+/+}$ mice (median 19 days, N=21) compared to *Scn1b*$^{-/-}$/Scn8a$^{med/+}$ mice (median 20 days, N=13, Mantel-Cox test).

Scn1b deletion impairs I_{Na} density and density diversity in cortical layer 6 and subicular pyramidal neurons.

Fig. 2.4 shows that *Scn1b*$^{-/-}$ cortical layer 6 and subicular pyramidal neurons are hyperexcitable at low current injections but have early depolarization block at higher current injections compared to *Scn1b*$^{+/+}$ mice. Both neuronal populations show increased input resistance, which is predicted to promote hyperexcitability, but hyperexcitability in layer 6 is absent following blockade of network activity. These results suggest that there may be additional effects of *Scn1b* deletion on excitability that offset the effects of

increased input resistance. We hypothesized that I_{Na} may be altered in *Scn1b*$^{-/-}$ layer 6 and subicular pyramidal neurons and that these changes may account for the observed AP defects and hypoexcitability. To test this idea, we recorded I_{Na} using nucleated patches from cortical layer 6 and subicular pyramidal neurons in acute brain slices (Fig. 2.7). I_{Na} density at the mean peak current density (-20 mV) was reduced by approximately 40% in *Scn1b*$^{-/-}$ neurons compared to *Scn1b*$^{+/+}$ (Fig. 2.7, panels A and B, and Table 4). Similar results were found in subiculum (Fig. 2.7, panels F and G, and Table 4). There was also a dramatic reduction in the variance of I_{Na} density values between genotypes (Fig. 2.7C and Table 4, $p<0.0001$, layer 6; Fig. 2.7G and Table 2.4, $p<0.05$, Subiculum). Previous work showed no change in I_{Na} density in hippocampal pyramidal neurons in *Scn1a*$^{+/-}$ DS mice at P14, with a subsequent increase in I_{Na} density at P21. Thus, the present results in *Scn1b*$^{-/-}$ mice showing decreased I_{Na} density provide further evidence that there remain critical differences in the mechanisms of *Scn1a*- and *Scn1b*-linked DEE.

We found that the effect of *Scn1b* deletion on I_{Na} density dispersion shown in Fig. 2.7 was predominantly due to a decreased measurement of high I_{Na} density patches. In layer 6, I_{Na} density values in the lowest quartile were similar between genotypes (-111.68 pA for *Scn1b*$^{+/+}$ vs. -120.8 pA for *Scn1b*$^{-/-}$), while values for the highest quartile were 2.37-fold larger in *Scn1b*$^{+/+}$ patches than in *Scn1b*$^{-/-}$ (-341.55 pA for *Scn1b*$^{+/+}$ vs -144.38 pA for *Scn1b*$^{-/-}$). The interquartile range was 9.39-fold higher in *Scn1b*$^{+/+}$ patches than in *Scn1b*$^{-/-}$ (-71.22 pA for *Scn1b*$^{+/+}$ vs -7.58 pA for *Scn1b*$^{-/-}$). The results were similar in the subiculum with a comparable first quartile between genotypes (-116.59 pA for *Scn1b*$^{+/+}$ vs -103.49 pA for *Scn1b*$^{-/-}$) while the highest quartile was 1.97-fold higher in *Scn1b*$^{+/+}$

patches (-288.01 pA for *Scn1b*$^{+/+}$ vs -145.95 pA for *Scn1b*$^{-/-}$). The interquartile range was 3.52-fold higher in *Scn1b*$^{+/+}$ than in *Scn1b*$^{-/-}$ patches (-34.33 pA for *Scn1b*$^{+/+}$ vs -9.75 pA for *Scn1b*$^{-/-}$). The $V_{1/2}$ values for I_{Na} activation and inactivation, as well as for the slope factor of activation, were unaffected by *Scn1b* deletion in both layer 6 and subiculum (Fig. 2.7D and Table 4 and Fig. 2.7H and Table 2.4 respectively). The slope factor of availability was increased in *Scn1b*$^{-/-}$ patches compared to *Scn1b*$^{+/+}$ in both layer 6 and subiculum (Fig. 2.7D and Table 2.4 and Fig. 2.7H. and Table 2.4 respectively).

To determine whether reduced I_{Na} density in *Scn1b*$^{-/-}$ neurons compared to *Scn1b*$^{+/+}$ was due to reductions in total cellular VGSC expression, we performed equilibrium [^{3}H]-saxitoxin (STX) binding to membranes prepared from forebrain homogenates of *Scn1b*$^{-/-}$ and *Scn1b*$^{+/+}$ mice. We found no difference between genotypes in total levels of VGSC expression (134 ± 26 fmoles/mg protein in *Scn1b*$^{-/-}$, N=7 vs. 127 ± 21 fmoles/mg protein in *Scn1b*$^{+/+}$, N=5), suggesting that alterations in I_{Na} density in *Scn1b*$^{-/-}$ brain may be the result of the known function of β1 subunits to chaperone VGSC α subunits to the plasma membrane (Isom, Scheuer et al. 1995).

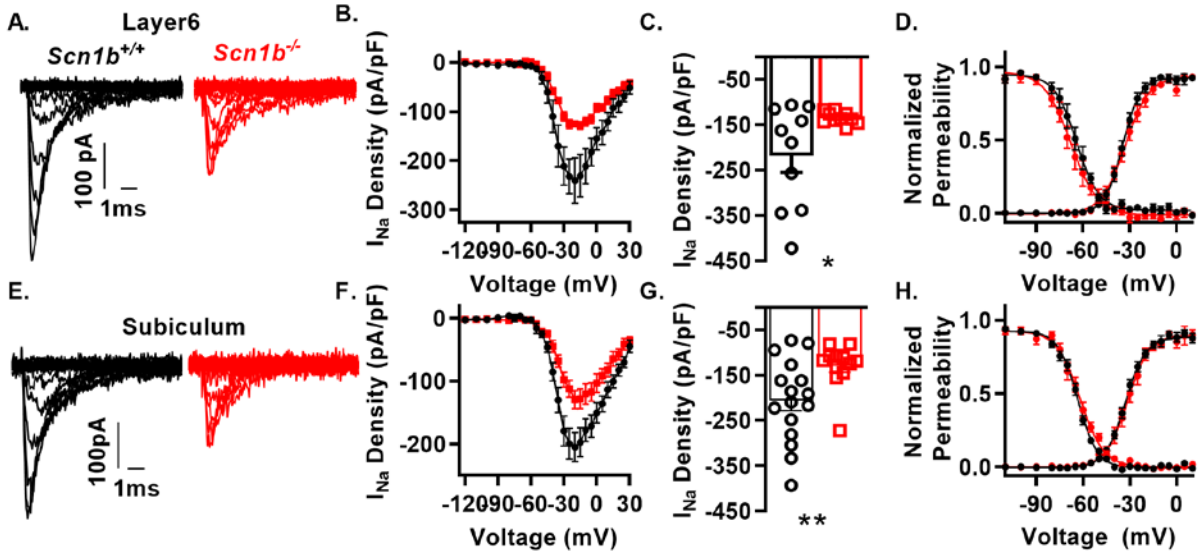


Fig. 2.7. Scn1b deletion reduces INa density and density diversity in nucleated patches from cortical layer 6 and subicular pyramidal neurons. A. and E. Representative I_{Na} traces from nucleated patches from cortical layer 6 (A) and subicular (E) pyramidal neurons of *Scn1b*$^{+/+}$ and *Scn1b*$^{-/-}$ mice in acute brain slices. Current elicited by depolarizing steps from -120 mV to 30 mV from a holding potential of -120 mV (traces up to peak are shown for visualization of smaller nested currents). **B. and F.** Current-voltage relationship for nucleated patches as in A and E (n/N=10/10 *Scn1b*$^{+/+}$, 10/9 *Scn1b*$^{-/-}$ layer 6; n/N=16/8 *Scn1b*$^{+/+}$, 12/8 *Scn1b*$^{-/-}$ subiculum). **C**. **and G.** Peak I_{Na} density at -20 mV from recordings in B and F**.** Asterisks indicate p value (*p<0.05, **p<0.01, Welch's t-test). **D. and H.** Normalized voltage dependence of steady state activation and inactivation of recordings in B and F. See Table 4 for numerical values.

	Scn1b$^{+/+}$ Layer 6	*Scn1b*$^{-/-}$ Layer 6	*Scn1b*$^{+/+}$ Subiculum	*Scn1b*$^{-/-}$ Subiculum
Peak Current Density (pA/pF)				
Mean±SEM	-218.33±36.33(*†)	-134.36±4.30	-204.82±22.89(**†)	-129.07±14.46
Variance	13,199.94(****)	184.62	8385.8(*)	2408.43
Peak Current (pA)				
Mean±SEM	-256.34±35.82(*†)	-154.88±5.71	-311.51±37.77	-214.41±26.90
Variance	12,830(****)	294.12	22,825.67	8683.9
Capacitance (pF)				
Mean±SEM	1.23±0.07	1.16±0.05	1.57±0.11	1.67±0.12
Activation $V_{1/2}$ (mV)				
Mean+/- SEM	-38.75+/- 1.69	-36.52+/- 1.94	-35.84±1.07	-34.36±2.03
Activation k $(mV)^{-1}$				
Mean+/- SEM	6.03+/- 0.57	6.51+/- 0.45	6.34±0.31	6.32±0.36
Inactivation $V_{1/2}$ (mv)				
Mean+/- SEM	-67.10+/- 1.43	-71.11+/- 2.43	-67.08±1.19	-65.81±1.70
Inactivation k $(mV)^{-1}$				
Mean+/- SEM	5.28+/- 0.37(*)	6.86+/- 0.49	5.78±0.19(*)	7.00±0.53
n/N	10/10	10/9	16/8	12/8

Table 2.4. Effects of Scn1b deletion on INa density and voltage-dependence in layer 6 and subicular pyramidal neurons. Data shown graphically in Fig. 2.7. Values are mean +/- SEM, n/N indicate cells/mice, respectively. † indicates t-test with Welch's Correction *p<0.05, **p<0.01, ****p<0.0001.

Scn1b deletion does not affect potassium current density in layer 6 pyramidal neurons.

VGSC β1 subunits associate with VGKCs in heterologous systems (Deschenes and Tomaselli 2002, Nguyen, Miyazaki et al. 2012) and have been postulated to modulate voltage-dependent potassium currents (I_K) *in vivo* (Marionneau, Carrasquillo et al. 2012). To test if changes in I_K contribute to altered excitability in *Scn1b*$^{-/-}$ cortical layer 6 pyramidal neurons, we recorded two classes of I_K in acute brain slices from this neuronal population in *Scn1b*$^{-/-}$ and *Scn1b*$^{+/+}$ mice. Transient and non-inactivating I_K were isolated

using 300 ms long voltage prepulses to -110 mV or -40 mV, respectively, in the presence of 100 nM TTX and 200 µM Cd^{2+}. We found no differences in the density or voltage dependence of activation or inactivation for either I_K component (Fig. 2.8, panels A-I, Table 5), suggesting that I_K is not affected by *Scn1b* deletion in this neuronal population.

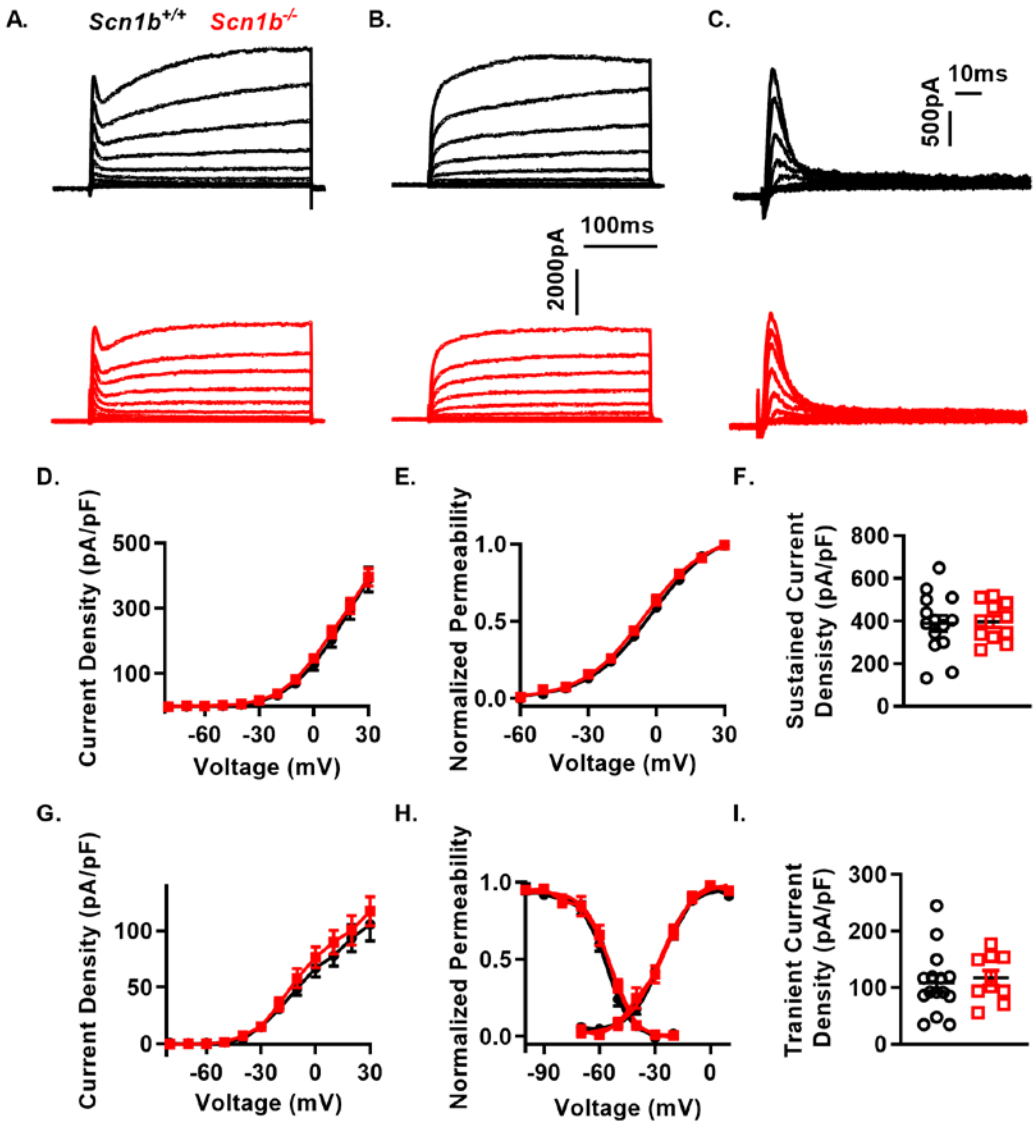


Fig. 2.8. Scn1b deletion does not impact VGKC density or voltage dependence in layer 6 pyramidal neurons. A. Currents elicited by voltage steps between -120 to 30 mV in *Scn1b*$^{+/+}$ (top) or *Scn1b*$^{-/-}$ neurons (bottom) after a 300 ms long prepulse to -120 mV. **B.** Currents elicited by voltage steps as in A. after a 300 ms long prepulse to -40 mV. **C.** Subtraction of currents in B from A show currents sensitive to voltage

dependent inactivation at -40 mV. **D.** IV relationship of non-inactivating current as in B. **E.** Voltage dependence of permeability from data in D. **F.** Current density from data in D at 30 mV. **G.** IV relationship of currents sensitive to inactivation at -40 mV as in C. **H.** Voltage dependence of permeability and inactivation from data in G. **I.** Peak Current density from data in G. at 30 mV. See Table 5 for numerical values.

	***Scn1b*$^{+/+}$**	***Scn1b*$^{-/-}$**
Non-Inactivating IK		
Current Density (pA/pF)	388.7±38.06	396.4±27.13
Current (pA)	5020±437.8	4260±281.5
Activation $V_{1/2}$ (mV)	-0.20±3.61	-3.11±2.26
Activation k (mV)	13.18±0.90	14.15±1.10
Transient IK		
Current Density (pA/pF)	108.4±14.6	117.3±12.79
Current (pA)	1431±193.5	1152±147.4
Activation V1/2 (mV)	-26.80±1.76	-28.74±2.60
Activation k (mV)	8.07±0.48	8.17±0.75
Inactivation $V_{1/2}$ (mv)	-52.16±2.27	-48.28±1.86
Inactivation k (mV)	-9.54±0.91	-9.52±0.84
Capacitance (pF)	13.77±0.80 (*)	10.94±0.68
n/N	15/5	11/5

Table 2.5 Effects of *Scn1b* deletion on current density and voltage dependence of transient and non-inactivating IK. Data shown graphically in Fig. 2.8. Values are mean +/- SEM, n/N indicate cells/mice, respectively. *p<0.05.

Discussion

While pediatric patients with homozygous *SCN1B* LOF variants have been diagnosed with DS (Patino, Claes et al. 2009, Ogiwara, Nakayama et al. 2012, Ramadan, Patel et al. 2017), increasing evidence suggests *SCN1B*-linked DEE is distinct and more severe than DS. Here, we used *Scn1b*$^{-/-}$ mice to model the homozygous LOF phenotype of *SCN1B*-linked DEE. We show that global *Scn1b* deletion in mice results in FS interneuron hypoexcitability, similar to *Scn1a*-DS mice (Yu, Mantegazza et al. 2006, Ogiwara, Miyamoto et al. 2007, Cheah, Yu et al. 2012). PV+ neuron specific deletion of

Scn1b using a Cre-lox strategy is sufficient to cause severe epilepsy and death, while excitatory neuron deletion, using CAMK2a-Cre, is not. Subpopulations of *Scn1b*$^{-/-}$ pyramidal neurons are hyperexcitable at low current injections but are hypoexcitable at high current injections, with hyperexcitability dependent on network activity and correlated with disinhibition. We show *Scn1b*$^{-/-}$ pyramidal neuron hyperexcitability results from a combination of altered network activity and increased input resistance that mask underlying impairments of I_{Na} density, with preferential loss of higher I_{Na} density measurements. Finally, we show that, unlike *Scn1a*-DS mice (Martin, Tang et al. 2007), intercrossing *Scn1b*$^{-/-}$ mice with *Scn8a*$^{med/+}$ mice does not prolong survival. Taken together, our work shows, while *Scn1a*-DS and *Scn1b*$^{-/-}$ mice share a common mechanism of neuronal disinhibition and PV+ interneuron hypoexcitability, *Scn1b*$^{-/-}$ mice have additional deficits, including loss of pyramidal I_{Na} density and density diversity, which may contribute to their increased phenotypic severity alongside developmental defects reported previously.

Scn1b$^{-/-}$ mice have FS interneuron defects and disinhibition

Our results show selective *Scn1b* deletion in PV+ neurons is sufficient to generate spontaneous convulsive seizures and early lethality, while *Scn1b* deletion in CAMK2a+ neurons is not. We also show *Scn1b*$^{-/-}$ cortical FS interneurons have impaired AP firing. Thus, disinhibition is common to the *Scn1a* and *Scn1b* models of DEE. Importantly, our work provides the first measurement of impaired I_{Na} density in FS interneurons, as well as of impaired I_{Na} density in any type of cortical interneuron, in a VGSC gene linked DEE

model. Excitatory/inhibitory imbalance has been described in a variety of epilepsy models, with *Scn1a*-DS mice being a prototypical example of impaired inhibitory neurotransmission driving epileptogenesis (Catterall 2018). Evidence of comparatively higher levels of *Scn1a* expression in GABAergic interneurons over pyramidal neurons, data from cell type selective *Scn1a* deletion studies, and demonstration of interneuron hypoexcitability have provided a framework for disinhibition as an underlying mechanism of DS. Alternatively, gain-of-function (GOF) variants in *SCN8A*, encoding the VGSC Nav1.6, result in early infantile epileptic encephalopathy type 13 (EIEE13) (Meisler, Helman et al. 2016), a disease with a similar phenotype to DS and to *SCN1B*-linked DEE posited to arise from pyramidal neuron hyperexcitability (Lopez-Santiago, Yuan et al. 2017). Here, in *Scn1b*$^{-/-}$ mice, we observed reduced I_{Na} density in both PV+ neurons and pyramidal neurons, reflecting the expression of VGSC β1 subunits in both cell populations. Finally, we show inhibitory neurotransmission is altered in a layer specific manner, reflecting the network location dependent pyramidal neuron hyperexcitability.

Multifaceted origins of altered excitability in *Scn1b*$^{-/-}$ pyramidal neurons

Our previous observation of neuronal pathfinding defects in *Scn1b*$^{-/-}$ brain prior to the onset of epilepsy led to the proposal that altered development underlies epileptogenesis in the *Scn1b* model of DEE (Brackenbury, Yuan et al. 2013). In addition, a developmental increase in input resistance in pyramidal neurons at specific circuit points was proposed to lead to epilepsy in *Scn1b*$^{CW/CW}$ mutant mice (Reid, Leaw et al. 2014). Recent work from our laboratory, however, demonstrated that inducible deletion

of *Scn1b* in adult mice, following normal development, resulted in severe epilepsy and 100% lethality within 3 weeks (O'Malley, Hull et al. 2019). This result, combined with FS interneuron hypoexcitability, shown here, has led us to re-examine the role and origins of pyramidal neuron hyperexcitability resulting from *Scn1b* deletion. We report several alterations to pyramidal neuron excitability, including increased input resistance, depolarized RMP, and reduced I_{Na} density. Because we found inhibition of network activity blocked pyramidal neuron hyperexcitability and the depolarized RMP, we concluded that increased input resistance alone is insufficient to overcome reduced pyramidal neuron I_{Na} to result in pyramidal neuron intrinsic hyperexcitability. We also found the network location and network activity dependent hyperexcitability of *Scn1b*$^{-/-}$ pyramidal neurons correlates with a reduction in the rate of sIPSCs in layer 6 but not layer 5 pyramidal neurons. The increased input resistance may, reduce the effectiveness of the hyperexcitability-mitigating reduction in I_{Na} in layer 6 and subicular pyramidal neurons but pyramidal neuron hyperexcitability cannot account for epilepsy in *Scn1b*$^{-/-}$ mice as it does in the EIEE13 mouse model. Finally, the developmental brain defects we reported previously in *Scn1b*$^{-/-}$ mice may be critical to the mechanism of other aspects of DEE in human patients, such as intellectual disability or autism spectrum disorders.

Impaired I_{Na} but not I_K in *Scn1b*$^{-/-}$ neurons

β1 was first identified as a VGSC subunit in brain (Hartshorne, Messner et al. 1982). Subsequent work showed that β1 co-expression enhances the cell surface expression of VGSC α subunits in heterologous cells, although in a cell type specific

manner (Calhoun and Isom 2014). In spite of these results, early characterization of acutely dissociated *Scn1b*$^{-/-}$ hippocampal pyramidal and bipolar shaped neurons suggested β1 had no effect on I_{Na} density in either class of neuron (Chen, Westenbroek et al. 2004, Patino, Claes et al. 2009). The inability to clearly identify neuronal subtypes and their previous network location in dissociated preparations may have explained these results in light of the present data showing that β1 subunits alter neuronal excitability depending on cell type and network location. Here we show clearly that *Scn1b* deletion does reduce I_{Na} density in cortical FS interneurons and in pyramidal neurons of cortical layer 6 and the subiculum. The impact of impaired I_{Na} on *Scn1b*$^{-/-}$ pyramidal neurons is reduced by the accompanying decrease in cell size and increase in input resistance, which mask the effects of reduced I_{Na} on excitability except at extreme current injections. Neuronal networks have the capacity to achieve activity patterns with a broad range of mean conductances through ion channel diversity with compensatory mechanisms to balance firing rates. The net average effect of increased input resistance and impaired I_{Na} density on firing rates in *Scn1b*$^{-/-}$ mice appears to directly cancel at the lower stimulation intensities that are likely relevant *in vivo*. This raises the question of how altered I_{Na} in pyramidal neurons may contribute to network dysfunction outside of effects on mean firing rate. Our data in *Scn1b*$^{-/-}$ pyramidal neurons suggest β1 normally enhances I_{Na} density in a highly variable manner. While we found mean I_{Na} density to be reduced in *Scn1b*$^{-/-}$ cortical layer 6 and subiculum, the comparatively larger effect was observed in the loss of high I_{Na} density measurements in both regions. The importance of intrinsic neuronal diversity has received growing attention in the literature (Gjorgjieva, Drion et al. 2016). Evidence suggests that biophysical heterogeneity within neuronal class is integral to

nervous system function, with the capacity for enhancing information content, contributing to low spike correlation, and allowing for parallel information processing (Padmanabhan and Urban 2010, Soltesz and Losonczy 2018). Thus, in future work, the differential roles of input resistance and I_{Na} density heterogeneity on network activity and spike coordination need to be further examined to understand the role of β1 and its effects on information processing in the nervous system.

In addition to modulating VGSCs, β1 subunits have also been shown to enhance the cell surface expression of various VGKCs in heterologous systems. While we did not detect an effect of *Scn1b* deletion on either transient or non-inactivating I_K components in layer 6 pyramidal neurons in this study, it is possible β1 may modulate I_K in other cell types or in other brain regions. The effects of β1 on I_K may also be limited to channels in more distal cellular compartments, such as A-type potassium currents in distal dendrites, which may be obscured in whole cell recordings.

Circuit Location Specific Dysfunction

Cortical Layer 6 pyramidal neurons form connections locally as well as project between cortical layers, cortical columns, and to the thalamus (Briggs 2010) which makes it of interest in DEEs, disorders exhibiting generalized seizures and thalamocortical dysfunction. Key roles of layer 6 include suppression or desynchronization of superficial cortical layers, gain control of cortical activity, and thalamic feedback (Olsen, Bortone et al. 2012, Bortone, Olsen et al. 2014, Kim, Matney et al. 2014). FS interneuron

hypoexcitability and disinhibition have been implicated in a wide variety of neurological disorders in addition to epilepsy (Marin 2012). While some of these disorders, e.g. bipolar disorder, may overlap with epilepsy diagnoses, it is unclear why similar effects of global excitatory/inhibitory imbalance result in such disparities in pathology. Potentially important to this phenotypic divergence are specific points in neuronal networks at which inhibition fails, which we find to be critical in understanding hyperexcitability in the *Scn1b*$^{-/-}$ model of DEE. In conclusion, our work may guide the future understanding of specific network dysfunction in DEE patients, leading to the identification of novel targets for antiepileptic drug development. Targeted manipulation of network function may offer more effective treatments for DEE than current therapies that alter global excitatory/inhibitory imbalance.

Methods

Animals

All experiments were performed according to NIH guidelines. Animal protocols were approved by the University of Michigan Institutional Animal Care and Use Committee (IACUC). *Scn1b*$^{-/-}$ and *Scn1b*$^{+/+}$ mice were generated as described previously (Chen, Westenbroek et al. 2004) and were congenic on the C57Bl/6J background for over 20 N generations. *Scn1b*$^{Fl/Fl}$ mice, congenic on the C57BL/6J background, were generated as described (Chen, Dickendesher et al. 2007). To generate mice with specific *Scn1b* deletion in labeled PV+ neurons, *Scn1b*$^{Fl/Fl}$ mice were crossed with td tomato

(B6;129S6-*Gt(ROSA)26Sor*$^{tm14(CAG-tdTomato)Hze}$/J, JAX #007908) and PV Cre (B6.129P2-*Pvalb*$^{tm1(cre)Arbr}$/J, JAX #017320) mice, both received from Dr. E. Goldberg at the University of Pennsylvania on the (C57BL/6J x CBA)F1 background and then backcrossed to C57Bl/6J, to generate *Scn1b*$^{Fl/Fl}$/*PV-Cre/tdTom* and *Scn1b*$^{E/E}$/*PV-Cre/tdTom* mice. To label PV+ FS neurons in *Scn1b*$^{-/-}$ brains, *Scn1b*$^{+/-}$ mice were crossed with PV-Cre/tdTom mice, described above, to generate *Scn1b*$^{+/+}$/PV-Cre/tdTom and *Scn1b*$^{-/-}$/PV-Cre/tdTom mice. *Scn1b* deletion in pyramidal neurons was achieved by crossing *Scn1b*$^{Fl/Fl}$ mice with CAMK2a-Cre mice (B6.Cg-Tg(Camk2a-cre)T29-1Stl/J, JAX# 005359). All electrophysiological measurements were performed between P14-20.

Brain Slice Preparation

Acute brain slices were prepared as described (Brackenbury, Yuan et al. 2013). Briefly, mice were anesthetized with isoflurane anesthesia and decapitated. Brains were removed and placed in 95:5% O_2:CO_2 continuously aerated ice-cold slice solution containing in mM: (110 sucrose; 62.5 NaCl; 2.5 KCl; 6 $MgCl_2$; 1.25 KH_2PO_4; 26 $NaHCO_3$; 0.5 $CaCl_2$; and 20 D-glucose (pH 7.35-7.40 when aerated at RT). Brains were then blocked and slices were obtained in 300 μm thick coronal sections from primary sensory cortical areas (visual cortex for pyramidal neuron data for comparability to previous *Scn1b* model publications) or somatosensory cortex (PV+ neuron data for comparison to previous *Scn1a*-DS publications). Slices were incubated in an aerated holding chamber containing slice solution for 30 min at RT and then incubated in 1:1 slice:artificial cerebrospinal solution (ACSF) for 30 min. ACSF contained in mM (125 NaCl; 2.5 KCl; 1

$MgCl_2$; 1.25 KH_2PO_4; 26 $NaHCO_3$; 2 $CaCl_2$; and 20 D-glucose (pH 7.35-7.40 with aeration). Slices were then transferred to an aerated holding chamber containing 100% ACSF for at least 30 min before use.

Action Potential Recording and Analysis

Individual brain slices were placed in a recording chamber and superfused with 2-3 ml/min aerated ACSF. Pyramidal neurons were identified based on their size, shape, and location using a Nikon A1R upright confocal microscope equipped with IR-DIC optics with a 40X water immersion objective. Layer 5 was identified by the large soma size and location, and layer 6 was identified as the small pyramidal neurons between layer 5 and the boundary of the slice. Only vertically oriented pyramidal cells were selected for recording. FS interneurons were identified via red fluorescence using PV-Cre/tdTom mice. Recording electrodes had a resistance of 3-6 MΩ with solutions containing in mM (140 K-Gluconate, 4 NaCl, 0.5 $CaCl_2$, 10 HEPES, 5 EGTA, 5 phosphocreatine, 2 Mg-ATP, and 0.4 GTP (pH adjusted to 7.2-7.3 with KOH). The junction potential was calculated to be 14.3 mV using the P-clamp junction potential calculator and all values were corrected offline, with all values presented in the study as corrected values. Following break in at -94.3 mV in voltage clamp mode, the resting membrane potential was defined as the membrane potential in current clamp <10 s after initial break in. Repetitive firing was elicited in the whole cell current clamp configuration from the resting membrane potential in 1-s long current injections in 10 pA steps. There was a 1-s long 0 current injection period between each sweep. Data were acquired at 20 kHz and were

filtered at 10 kHz. Cells with an access resistance measured in voltage clamp >20 MΩ or RMP more depolarized than -64.3 mV were discarded. Access resistance and pipette capacitance were compensated using bridge balance. Whole cell capacitance was measured using P-clamp whole cell capacitance compensation in voltage clamp with 10 mV depolarizing steps from -94.3 mV. Automated action potential (AP) quantification was performed using custom MATLAB (MathWorks) software. APs were defined as the voltage crossing 0 mV subsequent to a dv/dt>10 mV/ms, defined here as the AP threshold. Input resistance was calculated using Ohm's law with -10 pA current injection from the resting membrane potential after 250 ms.

Nucleated Patch Clamp

Nucleated patches were pulled from acute brain slices of layer 6 cortical and subicular pyramidal neurons. Internal solution contained in mM (115 CsCl, 0.5 $CaCl_2$, 5 EGTA:CsOH, 10 HEPES, 5 Na_2Phosphocreatine, 20 TEA, 2 Mg-ATP, and 0.4 GTP (pH adjusted to 7.2-7.3 with CsOH). The junction potential was calculated to be 3.5 mV and all values presented are corrected. Patches were pulled by applying light suction in the whole cell configuration while slowly (5-10 min) withdrawing the pipette until the nucleus-containing patch cleared the surface of the brain slice. Suction was then reduced before recording. External recording solution consisted of aerated ACSF with 200 μM Cd^{2+} added after establishment of the whole cell configuration. To maintain slice health, slices were discarded if perfused with Cd^{2+} >60s. Patches with access resistance >20 MΩ or

with input resistance < 1 GΩ were discarded. Intersweep holding potentials were -80 mV with a preceding 500 ms long step to -120 mV before current steps.

Neuronal Dissociation and Whole Cell I_{Na} *Recording*

Brain slices were prepared as described above but were maintained in 100% slice solution at RT until dissociation. Somatosensory cortex was isolated via microdissection using a 26.5-gauge needle under a dissection microscope. Tissue was then incubated at 35°C in oxygen saturated HBSS supplemented with 10 mM HEPES with 1.5 mg/ml protease type XIV (Sigma) for 23 min. Tissue was then washed 3 times with oxygen saturated ice cold low-calcium HBSS (1:10 HBSS with calcium and magnesium: HBSS calcium and magnesium Free) containing 10 mM HEPES. Finally, HBSS was replaced with ice cold, oxygen saturated Na-isethionate solution (in mM; 140 Na-isethionate, 23 glucose, 15 HEPES, 2KCl, 4MgCl2, 0.1 CaCl2) and tritiated with fire polished glass Pasteur pipettes to suspend cells. Cells were then allowed to settle on a class coverslip for 10 min prior to recording. All recordings were acquired < 1.5 h post dissociation. PV+ cells were identified by red fluorescence and cells lacking neurites were not selected for recording. Voltage clamp recording was then performed in the standard whole cell configuration with conditions described previously (Lopez-Santiago, Yuan et al. 2017). Cells were superfused with external sodium channel recording solution containing in mM (30 NaCl, 1BaCl2, 2MgCl2, 45 CsCl, 0.2 CdCl2, 1CaCl2, 10 HEPES, 20 TEA-Cl, and 100 D-glucose (pH 7.35 with CsOH, Osmolarity 300-305 mOsm). Fire-polished pipettes were

filled with sodium channel internal recording solution described above. The junction potential was calculated to be 2.7 mV with all reported voltages uncorrected.

[^{3}H]-STX Binding

[^{3}H]-STX binding to *Scn1b*$^{+/+}$ and *Scn1b*$^{-/-}$ forebrain membrane preparations was performed to assess total VGSC expression. Brains were isolated following decapitation from anesthetized P16-18 mice. The brainstem and cerebellum were removed from each sample to isolate the forebrain. Membrane preparations and [^{3}H]-STX binding were performed as described previously (Isom, Scheuer et al. 1995, Kazarinova-Noyes, Malhotra et al. 2001) with 5 nM C-11 labeled [^{3}H]-STX (20 Ci/mmol, American Radiolabeled Chemicals Inc) in the presence and absence of 10 μM TTX (Alomone Labs) for 1 h at 4C to measure specific binding at equilibrium. Fmol of VGSC were normalized to protein measured by the BCA assay.

Whole Cell I_K Recording

Transient and sustained I_K were recorded in layer 6 cortical pyramidal neurons in acute brain slices. Internal solution was identical to that used to record APs described above. External recording solution consisted of aerated ACSF supplemented with 200 μM Cd^{2+} and 100 nM TTX. Cells with access resistance >20 MΩ or RMP > -64.3 mV were discarded. Intersweep holding potentials were –80 mV. Currents were evoked by stepping to different test voltages after a 700 ms step to -120 mV followed by a 300 ms long step

to either -120 mV or -40 mV. The peak difference between currents elicited by the two different prepulses gave transient I_K and the current at the end of the voltage steps after the -40 mV prepulse gave the non-inactivating I_K currents. Voltage dependence of steady state inactivation protocols were performed as above with different conditioning test pulses followed by stepping to 0 mV or after a preceding step for 300 ms to -40 mV. The difference between currents elicited by the two prepulses gave the voltage dependence of inactivation for transient I_K.

Calculation of Permeability

To estimate the voltage dependence of activation for I_{Na} and I_K recordings, we calculated permeability using the Goldman-Hodgkin-Katz (GHK) current equation.

Equation 2.1:

$$I_s = \mathrm{P}_s \mathrm{z}_s^2 \frac{\mathrm{EF}^2}{\mathrm{RT}} \frac{[\mathrm{S}]_i - [\mathrm{S}]_o \exp(-\frac{\mathrm{z}_s \mathrm{FE}}{\mathrm{RT}})}{1 - \exp(-\frac{\mathrm{z}_s \mathrm{FE}}{\mathrm{RT}})}$$

where I_s is the measured current density, z_s is the ion valence, E is the membrane potential, F is Faraday's constant, $[S]_i$ and $[S]_o$ are the internal and external ion concentrations respectively, and P_s is the calculated permeability. Use of permeability for the estimation of voltage dependent properties was selected over the more common conductance due to prominent rectification that occurs with large ionic gradients (Hille 2001). Data were calculated by fitting with a Boltzmann equation for the calculation of the voltage-dependence of activation and inactivation.

sIPSC Recording

sIPSCs were recorded under similar slice conditions as AP recording described above, altered to allow for recording of sIPSCs. Intracellular solution contained (in mM): CsCl (135), NaCl (4), GTP (0.4), Mg-ATP (2), CaCl2 (0.5), EGTA (5), and HEPES (10). Currents were recorded in voltage clamp at a holding potential of -80 mV after >5 min in the whole cell configuration. CNQX (10 µM) and APV (50 µM) were applied for >5 min to block excitatory synaptic currents. sIPSCS were recorded for 5 min at a sampling rate of 20 kHz and filtered at 2kHz. sIPSCs were autonomously analyzed using MiniAnalysis software with a 10 pA amplitude threshold and visual exclusion/inclusion of events. Mean frequency and amplitude were calculated from the averages all events for each cell recorded over the 5 min period. Cumulative probability distributions were calculated by sampling 100 random events from each cell and combining across cells to compare conditions.

Statistics

No more than 1 cell from a brain region was acquired per slice, no more than 4 cells per region were acquired per animal, and each experiment was performed with at least 3 animals. Each cell is reported as n=1 and each animal is reported as N=1.

Significance was set at $p<0.05$. Comparisons were made with an unpaired two-tailed student's t-test unless stated otherwise in the text. All listed p-values are tested for significance after multiple comparisons and reported as non-significant if $q>0.05$ using the Benjamini, Krieger, and Yekutieli two stage step-up method with a 5% false discovery rate correction. Values were tested for a non-Gaussian distribution using D'Agostino-Pearson omnibus normality test. Differences in variance were tested using an F-Test.

Chapter III. Voltage Gated Sodium Current Heterogeneity Reduces Synchrony While Preserving Spike Timing Reliability in Pyramidal Neurons

Introduction

Voltage gated sodium channels (VGSCs) are fundamental to action potential (AP) generation and propagation in neurons (Hille 2001). VGSCs in brain are composed of one pore-forming α subunit and two β subunits (β1 or β3 and β2 or β4), which do not conduct ions directly but influence channel trafficking, gating, and kinetics (Hull and Isom 2018). Ion channel density varies between neurons, resulting in heterogeneity even within clearly defined neuronal types (Schulz, Goaillard et al. 2006). Recent work has begun to characterize the role that ion channel heterogeneity plays in neuronal network function, including in spiking decorrelation, firing rate heterogeneity, and information handling within neuronal networks (Gawne, Kjaer et al. 1996, Padmanabhan and Urban 2010, Soltesz and Losonczy 2018). Despite the pivotal role of VGSCs in AP generation, little work has been directed at understanding how differences in sodium current (I_{Na}) density between neurons is involved in normal brain function or how these differences may contribute to pathology. VGSC availability is the target of several neurotransmitters and

alterations to mean I_{Na} density within neuronal populations are implicated in brain disease (Ahern, Payandeh et al. 2016). While previous studies have focused on the control of mean I_{Na} density between neuronal populations, the role of I_{Na} density heterogeneity between individual neurons has not been addressed.

We reported in chapter 2 that mice null for *Scn1b*, encoding VGSC β1 subunits, have impaired I_{Na} heterogeneity between cortical pyramidal neurons, suggesting that I_{Na} density variability is subject to dysregulation. *Scn1b*$^{-/-}$ mice are a model of the developmental and epileptic encephalopathy (DEE) Dravet syndrome (DS) (Chen, Westenbroek et al. 2004). In other work investigating a related DEE mouse model with a gain of function mutation in the VGSC gene *Scn8a*, *Scn8a*$^{N1768D/+}$, we found that I_{Na} density heterogeneity is impaired to a similar degree (Lopez-Santiago, Yuan et al. 2017). Impaired I_{Na} variability in two different DEE models suggests that loss of I_{Na} density diversity may contribute to network dysfunction in brain disease.

It has been shown previously that fluctuating inputs can generate spike trains with high temporal precision in cortical pyramidal neurons, while non-fluctuating inputs generate spike trains with drifting spike times between trials (Mainen and Sejnowski 1995). Furthermore, while this high temporal precession has been shown to hold within the same neuron, an identical fluctuating input was shown to generate dissimilar spike trains between neurons of the same class, an effect that was attributed to intrinsic biophysical differences (Padmanabhan and Urban 2010). In the neocortex, membrane potential fluctuations within neighboring neurons is high but the neurons generate low

correlation in spike times, with intrinsic biophysical variability being a potential contributor (Crochet and Petersen 2006, Poulet and Petersen 2008, Gentet, Avermann et al. 2010). The role of biophysical heterogeneity in spike synchrony to fluctuating inputs is therefore important to understanding epilepsy, a disorder of both neuronal hyperexcitability and hypersynchrony. Here, we examine the effects of I_{Na} density variability between neurons on spike synchrony and firing rate heterogeneity in cortical pyramidal neurons using genetic, pharmacological, and computational approaches.

Results

Scn1b$^{-/-}$ pyramidal neurons have increased spike synchrony between neurons

Our above work in *Scn1b*$^{-/-}$ mouse layer 6 pyramidal neurons of the visual cortex in chapter 2 showed reduced variability in I_{Na} density, as measured in nucleated patches, compared to *Scn1b*$^{+/+}$. A similar result was observed in subicular pyramidal neurons between genotypes. *Scn1b*$^{-/-}$ mice have retarded growth, with decreased neuronal cell size, resulting in increased input resistance. This property maintains mean firing rate at a level similar to *Scn1b*$^{+/+}$ neurons. Thus, this situation provided an opportunity to study neurons with impaired I_{Na} heterogeneity but with a compensatory developmental mechanism to keep mean firing rates similar to *Scn1b*$^{+/+}$. We recorded from acute brain slices to ask whether spike time correlation, firing phase synchrony, or firing rate heterogeneity are impaired in *Scn1b*$^{-/-}$ mice relative to *Scn1b*$^{+/+}$ in response to fluctuating

inputs. To isolate cell intrinsic differences in firing, fast synaptic transmission was blocked

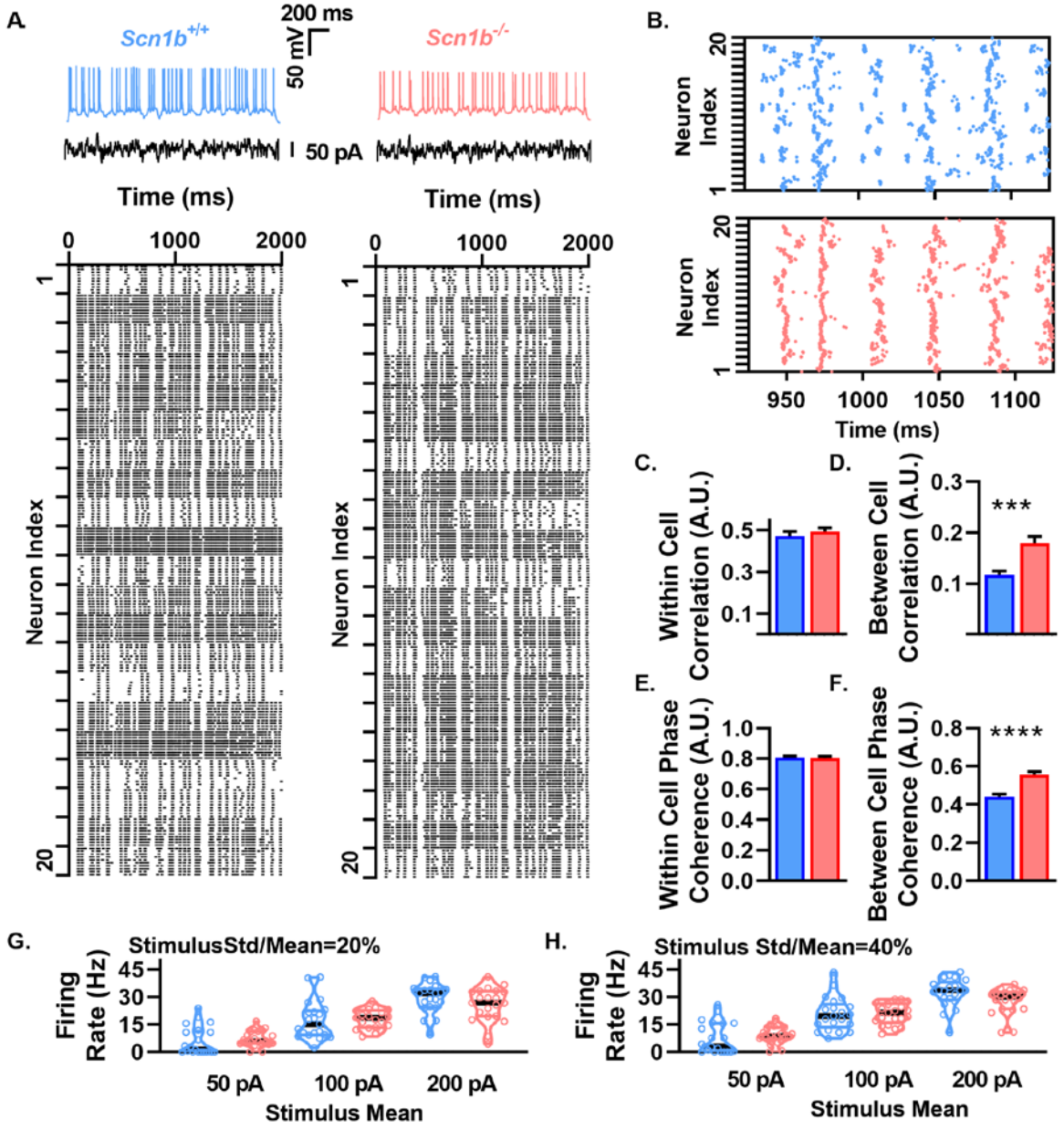


Fig. 3.1. *Scn1b* deletion causes increased spike synchrony and impaired firing rate heterogeneity to fluctuating input. A. (Top) Spike trains in a Scn1b+/+ and Scn1b-/- neuron in response to a time varying stimulus below with μ=100 and σ=40 pA. Rasters below show the resulting spike pattern of the stimulus above given to 20 cells over ten trials for both *Scn1b*$^{+/+}$ and *Scn1b*$^{-/-}$ mice. (n=20,N=5 for both genotypes). **B.** Expanded view of rasters in A. **C.** Average pairwise correlation between the repeated trials within each cell. **D.** Average pairwise correlation of trains compared between different cells. **E.** Average phase coherence between the repeated trials within each cell. **F.** Average phase coherence of trains compared

with CNQX (10 µm), APV (50 µm), and bicuculine (10 µm). Fluctuating currents were generated by convolving uncorrelated Gaussian white noise with an alpha function with a τ of 3 ms. This τ was shown previously to be effective in generating reliable spike trains within cortical pyramidal neurons (Galán, Ermentrout et al. 2008). Various combinations of mean (µ=50 to 200 pA) and standard deviations (σ=10 to 80 pA) were tested. Fig. 3.1A shows spike trains generated from a µ=100 pA and σ=40 pA current injection in neurons from *Scn1b*$^{+/+}$ and *Scn1b*$^{-/-}$ mice. Raster plots included below the voltage traces show the corresponding spike times over ten trials of this stimulus in 20 *Scn1b*$^{+/+}$ and 20 *Scn1b*$^{-/-}$ neurons. Fig. 3.1B shows an expanded time view of the raster plots in Fig. 3.1A at the midpoint of the recording. Ten trials per neuron are also plotted in Fig. 3.1B, however, this is obscured by high within-cell spike train similarity.

To compare spiking synchrony between neurons and between trials within the same neuron, we used two measures: spike train correlation and spike phase coherence (equation 3.28). To compare spike correlation between cells, we converted spike times to vectors of 1 s and 0 s at 1 ms resolution and compared their cross correlation with a time lag of 0. To account for spike time jitter, we set values 1ms before and after the spike to 1. We then performed pairwise cross-correlation between trials within the same cell (Fig. 3.1C) and between trials from different cells (Fig. 3.1D). We averaged values between trials to generate two values per cell, within-cell spike correlation (average of pairwise correlation in trials within the same cell) and between-cell spike correlation (average of pairwise correlation between trials and all other cells). The mean correlation within neurons was not significantly different between *Scn1b*$^{-/-}$ and *Scn1b*$^{+/+}$ mice (Fig.

3.1C), showing that *Scn1b* deletion does not alter an individual neuron's capacity to generate reliable spike trains. Spike trains between cells, however, were more highly correlated in *Scn1b*$^{-/-}$ mice compared to *Scn1b*$^{+/+}$ mice (Fig. 3.1D). We next measured the phase coherence of spike trains within and between cells. This value quantifies the coherence of spike intervals between neurons, i.e. a spike could be displaced in time between trials but have high phase coherence through shifting of neighboring spikes. This value varies between 0 and 1, with 1 indicating perfect spike coherence and 0 indicating no coherence. We found no difference in phase coherence of trials within neurons between genotypes (Fig. 3.1E). However, phase coherence between neurons was higher in *Scn1b*$^{-/-}$ neurons than *Scn1b*$^{+/+}$ neurons.

Altering I_{Na} density desynchronizes spike times between conditions without affecting spike train reliability

Fig. 3.1 shows that in *Scn1b*$^{-/-}$ layer 6 pyramidal neurons, which have impaired I_{Na} density heterogeneity, that spike train correlation and phase coherence are increased relative to *Scn1b*$^{+/+}$ neurons. We next asked whether altering I_{Na} density is sufficient to suppress spike synchrony in response to fluctuating input. We tested this pharmacologically by repeatedly recording a spike train in *Scn1b*$^{+/+}$ neurons in the absence and presence of 3 nM TTX, thereby modeling neurons that serve as their own controls. We injected current with μ=100 pA and σ= 40 pA, as in Fig. 3.1. To insure constancy of recording conditions across these relatively long experiments, we used the perforated patch clamp technique, which allows for preservation of intracellular

constituents and signaling that can be affected by washout in whole cell experiments. We swept continuously every 8 sec, giving the same stimulus to compare the effect of 3 nM TTX on spiking patterns. Fig. 3.2A shows a representative spike train before the addition of TTX (top), followed by the spike train in the presence of TTX (middle), and the spike train after washout (bottom). The raster plot at the bottom of Fig. 3.2A shows each sweep throughout the recording. Fig. 3.2B presents an expanded time view of these data, showing several representative effects on spike times observed in the recordings. Effects included variable amounts of spike timing shift, missed spikes, novel spikes, unreliable spikes that were replaced by reliable ones, and spikes which were unaffected. We observed a minor decrease in the mean firing rate in the presence of TTX relative to baseline and wash conditions (Fig. 3.2C). The correlation between trains in the presence vs. absence of TTX was not reduced relative to that observed by comparing trains before the addition of TTX to themselves or comparing trains after wash out of TTX to themselves, showing that blocking a fraction of I_{Na} does not reduce the capacity of a neuron to generate reliable spike trains (Fig. 3.2D). The pairwise correlation between baseline and TTX administration (and TTX vs. wash) conditions was reduced to levels similar to that observed between different neurons shown in Fig. 3.1 (Fig. 3.2E). Spike train correlation between the before TTX condition and the washout condition did not entirely return to baseline levels, likely due to the high sensitivity in this measure making it sensitive to long recording times (~45 minutes). Phase coherence between trains within conditions was not affected by administration of TTX, showing again that altering I_{Na} density does not impair the capacity of a neuron to generate reliable spike trains (Fig. 3.2G). The phase coherence between the before and during TTX conditions was reduced

to levels similar to those measured between neurons and this effect was removed by washout (Fig. 3.2H). These results show that heterogeneous I_{Na} densities between pyramidal neurons is sufficient to desynchronize firing of otherwise identical cells in response to fluctuating input without compromising neuronal reliability.

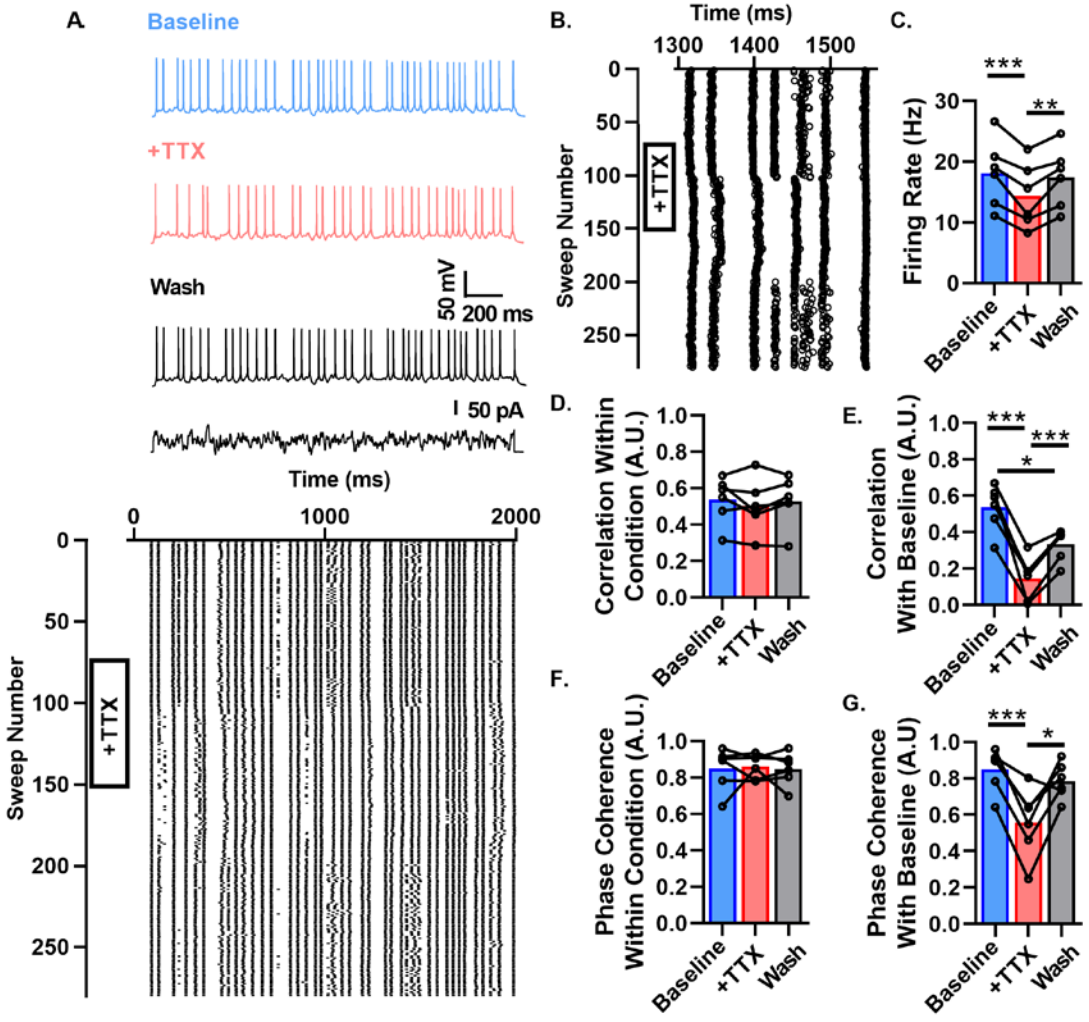


Fig. 3.2. Altering INa desynchronizes spiking without affecting spike reliability. A. Spike trains in a WT neuron (Top), the same neuron in the presence of 3nM TTX (Middle), and washout (Bottom) in response to a time varying stimulus below with μ=100 and σ=40 pA. Raster below shows the resulting spike pattern of the stimulus above given over repeated trials during addition and wash off of TTX (n=,6, N=5). **B.** Expanded view of raster in A. **C.** Average firing rate before, during, and after wash of TTX. **D.** Average pairwise correlation between the repeated trials within each condition. **E.** Average pairwise correlation of trains compared between different cells. **F.** Average phase coherence between the repeated trials within

each cell. **G.** Average phase coherence of trains compared between different cells.($p<0.05$*, $p<0.01$**,$p<0.005$***)

Spike time correlation is sensitive to sodium conductance density in a computational model

To systematically investigate the effect of I_{Na} variation on firing rate heterogeneity and spike synchrony between neurons, we examined firing rates and spike synchrony as described above to fluctuating input in a simple single compartment Hodgkin-Huxley style model neuron. To facilitate comparison with mouse layer 6 cortical pyramidal neurons, we first generated a model neuron to heuristically recapitulate the single neuron properties we measured previously. We started with a minimalistic neuron, limited to 4 ionic currents: a sodium current with maximal conductance (g_{Na}) (Hu, Tian et al. 2009), an A-type potassium current with maximal conductance (g_{Ka}), (Bogaard, Parent et al. 2009) a delayed rectifier potassium current with maximal conductance (g_{KDR})(Bogaard, Parent et al. 2009), and a leak conductance(Bogaard, Parent et al. 2009). Throughout the modeling, results had cell diameter and E_{leak} values to approximate the conditions of *Scn1b*$^{+/+}$ layer 6 pyramidal neurons, as detailed in Materials and Methods section.

We examined firing in response to a fluctuating conductance, which was designed previously to replicate the features of somatically recorded membrane potential fluctuations that occur *in vivo (Destexhe, Rudolph et al. 2001)*. Briefly, the conductance was generated by an Ornstein-Uhlenbeck like process with mean excitatory and inhibitory synaptic conductance μ_E and μ_I with standard deviation σ_E and σ_I. We initially set these

values to achieve a mean membrane potential of -55 mV and membrane potential standard deviation of 8 mV (μe=0.00216 μS, μi= 0.00216 μS, σe=0.000126 μS, and σi=0.000504 μS). Fig. 3.3A shows representative firing of the model neuron with g_{Na} set to several mean values within the range of *Scn1b*$^{+/+}$ neurons recorded in chapter 2. Fig. 3.3B examines the effect of increasing g_{Na} on the resulting spike pattern to an identical fluctuating synaptic conductance, showing a high dynamic range of altering g_{Na} to alter spiking patterns over a broad range of g_{Na} conductance densities. Fig. 3.3, panels C-E, examines the effect of impairing the coefficient of variation (standard deviation/mean) of g_{Na} (CV-g_{Na}) as we measured in *Scn1b*$^{+/+}$ and *Scn1b*$^{-/-}$ neurons in chapter 2 (0.53 and 0.10, respectively). The g_{Na} in each neuron was determined by sampling a lognormal distribution with a mean of 67.3 pS/μm^2 with a CV-g_{Na} of 0.53 or 0.10. A lognormal distribution was used to circumvent negative and near-zero conductances resulting from sampling a normal distribution. Histograms of g_{Na} distributions for the above groups of neurons are shown in Fig. 3.3, panels C and F. While these values were taken for layer 6 *Scn1b*$^{+/+}$ and *Scn1b*$^{-/-}$ pyramidal neurons, comparing these CVs to those in dissociated hippocampal CA3 pyramidal neurons in the *Scn8a*$^{N1768D/+}$ model of EIEE13 measured previously shows similar values of impaired I_{Na} variability (CV-g_{Na}= 0.53 and 0.13 respectively).

The 0.53 CV-g_{Na} group of neurons generated highly variable array of spikes (Fig. 3.3D), while lowering the CV-g_{Na} to levels observed in *Scn1b*$^{-/-}$ and *Scn8a*$^{N1768D/+}$ mice, resulted in spike trains that were highly stereotyped (Fig. 3.3G). To compare spike trains resulting from these two distributions, we quantified the spike train correlation, phase

coherence, firing rate, and firing rate heterogeneity. The spike train correlation was 0.12 in the 0.53 CV-g_{Na} group and 0.34 in the 0.10 CV-g_{Na} group. The phase coherence was 0.66 in the 0.53 CV-g_{Na} group and 0.84 in the 0.10 CV-g_{Na} group. The mean firing rate was 9.27 Hz and the firing rate CV was 1.12 in the CV-g_{Na} group and 8.20 Hz and 0.47 in the 0.10 CV-g_{Na} group. To quantify the effect of increasing the magnitude of input fluctuations in the high and low CV-g_{Na} groups, we measured the above parameters after multiplying the σi and σe by factors between 0.5 and 3 (resulting in ranges of 0.000252 to 0.001512 µS for σi and 0.000063 to 0.000378 µS for σe, Fig. 3.3E). With increasing input fluctuations, both the 0.53 CV-g_{Na} and 0.10 CV-g_{Na} groups increased in spike correlation, with the 0.10 CV-g_{Na} group matching the 0.53 CV-g_{Na} group at a 5-fold higher synaptic conductance σ. The phase coherence was relatively insensitive to altering the magnitude of input fluctuations (Fig. 3.3E). Firing rates were increased by increasing input fluctuations, with similar rates in both groups across the measured range. The CV-Firing Rates dropped with increasing input fluctuations, with the 0.53 CV-g_{Na} reaching equal values at a 2.5-fold higher synaptic conductance σ. These results show, using a simple computational model, the strong influence of g_{Na} heterogeneity on spike synchrony and firing rate heterogeneity under fluctuating synaptic conductances.

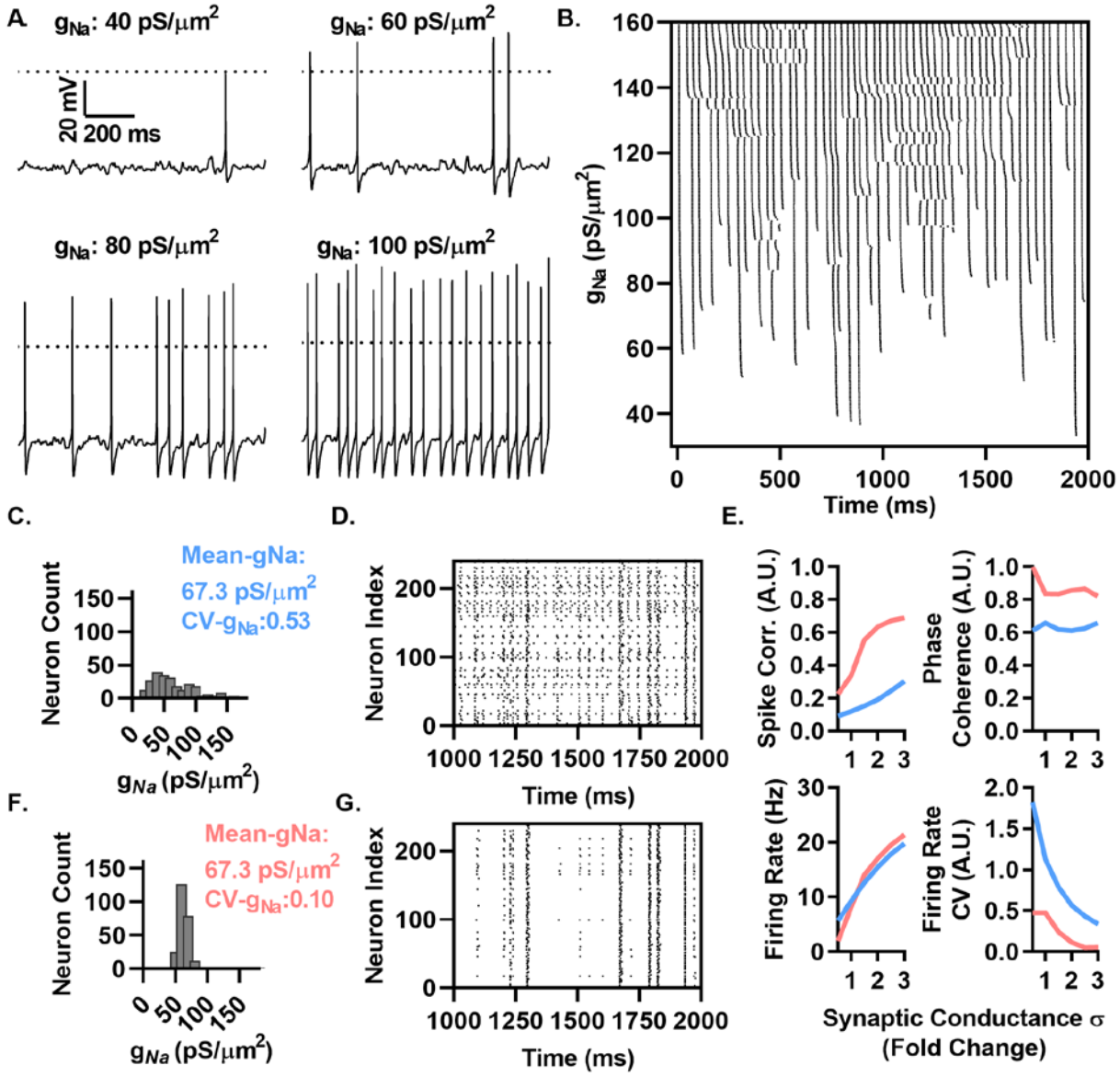


Fig. 3.3. g_{Na} variability desynchronizes spiking in response to fluctuating synaptic conductances in a computational model. A. Spike patterns of neurons with several levels of maximal sodium conductance (g_{Na}) in response to a time varying synaptic conductance with μ_e=0.00216 μS, μ_i= 0.00216 μS, σ_e=0.000126 μS, and σ_i=0.000504 μS. **B.** Raster plot of 240 neurons to an identical stimulus as in A. where g_{Na} increases uniformly in neurons between 30 pS/μm^2 (bottom) to 160 pS/μm2. **C** and **F.** Histograms of the g_{Na} assigned to neurons used in the simulations in D and G. CV-g_{Na} denotes the coefficient of variation in g_{Na}. Distribution includes 3 values >180 pS/μm^2 not shown on the histogram for visibility. **D** and **G.** Raster plots of spike patterns of the groups of neurons in C. and F. respectively in response to stimulation as in A. **E.** The effect

of increasing input fluctuations by multiplying the synaptic conductances σ between 0.5 and 3 fold in 0.53 and 0.1 CV-g_{Na} neurons on firing rate, spike correlation, phase coherence and firing rate heterogeneity.

g_{Na} heterogeneity shifts the network connectivity requirements for network synchronization

In the above results showing the effects of g_{Na} heterogeneity in neurons firing synchronous spikes in response to fluctuating inputs, it was assumed that neurons receive highly correlated (in the above cases identical) inputs from an external source that is independent of the neurons targeted. In actual neural networks however, external input correlations between neurons are likely not identical and external inputs may vary dynamically in response to the activity of target neurons. An alternative source of correlated membrane potential fluctuations observed *in vivo* is recurrent local network connectivity, where individual neurons have a high likelihood of having the same or neighboring target neurons and are likely to receive reciprocal connections.

Thus, we sought to systematically investigate the relationship between g_{Na} heterogeneity and network connectivity on synchronization of small networks of neurons as in local network processing. A directed Watts-Strogratz small world model (WS) was chosen as a convenient connectivity scheme for which we could investigate these properties under defined network contexts (Bogaard, Parent et al. 2009). The WS network provides an architecture characterized by the small path length and high clustering observed in neuronal networks *in vivo* (Watts and Strogatz 1998, Sporns and Zwi 2004). Networks were formed by starting with N neurons placed in a circle, connected in a

directed manner to their neighbors with radius (R) on each side. Then, with an associated probability (P), connections were rewired randomly to any other neuron in the network. We used a network with P = 30 and connection radius R = 6 for simulations (Fig. 3.4), and investigated other P and R values below. We also added 40 inhibitory neurons (1:5, excitatory:inhibitory neurons) with properties as above, with local reciprocating connections to excitatory neurons with radius = 6 neurons. Excitatory and inhibitory synaptic currents were generated as detailed in Materials and Methods. Importantly, this network modeling strategy was designed for interpretability and was focused on investigating the relationship between g_{Na} heterogeneity and network coupling while still capturing the low connection probability and small world characteristics of local neuronal networks.

We quantified network function using three different measures averaged over each neuron in the network, including the CV-IEI (Equation 3.26, Arb. Units) to examine divergence from randomly distributed activity of presynaptic neurons, the phase coherence PC to measure firing phase synchrony, and the mean firing rate (F, Methods, Equation 3.29, Hz). Each neuron was stimulated to sustain a background level of activity by an uncorrelated Gaussian distributed noise current injection (mean and standard deviation = 80 pA unless stated otherwise) with random (uniform distribution) time of onset over 50 ms to avoid synchronous stimulation onset artifacts. In the absence of synaptic connections, this approach supports asynchronous background activity in both high and low g_{Na} variability networks (CV-IEI=0.99 ± 0.00, PC=0.28 ± 0.00, F=20.79 ±

0.26 Hz for CV-g_{Na}=0.53; CV-IEI=0.97 ± 0.01, Fig. 3.4B Top and CV-IEI=1.01 ± 0.00, PC= 0.46 ± 0.00, and F=27.14 ± 0.01 Hz for CV-g_{Na}=0.10, Fig. 3.4D Top).

We next investigated the effects of coupling the neurons in a small world network as described above. To start, we connected the neurons with connection probability of 6% (radius=6 neurons) and rewiring probability of 30%. We found that synchrony was markedly increased in the 0.10 CV-g_{Na} network (CV-IEI=2.88 ± 0.10 and PC=0.91 ± 0.02) compared to the highly desynchronized 0.53 CV-g_{Na} network (CV-IEI=1.09 ±0.04 Arb. Units, PC = 0.30 ± 0.00 Arb. Units) (Fig. 3.4, panels B and D, Middle). Fig. 3.4D, Bottom, shows the onset of synchrony from the random activity at the start of the simulation in the CV-g_{Na}=0.10 network, while synchrony failed to develop in the CV-g_{Na}=0.53 network (Fig 3.4 B Bottom).

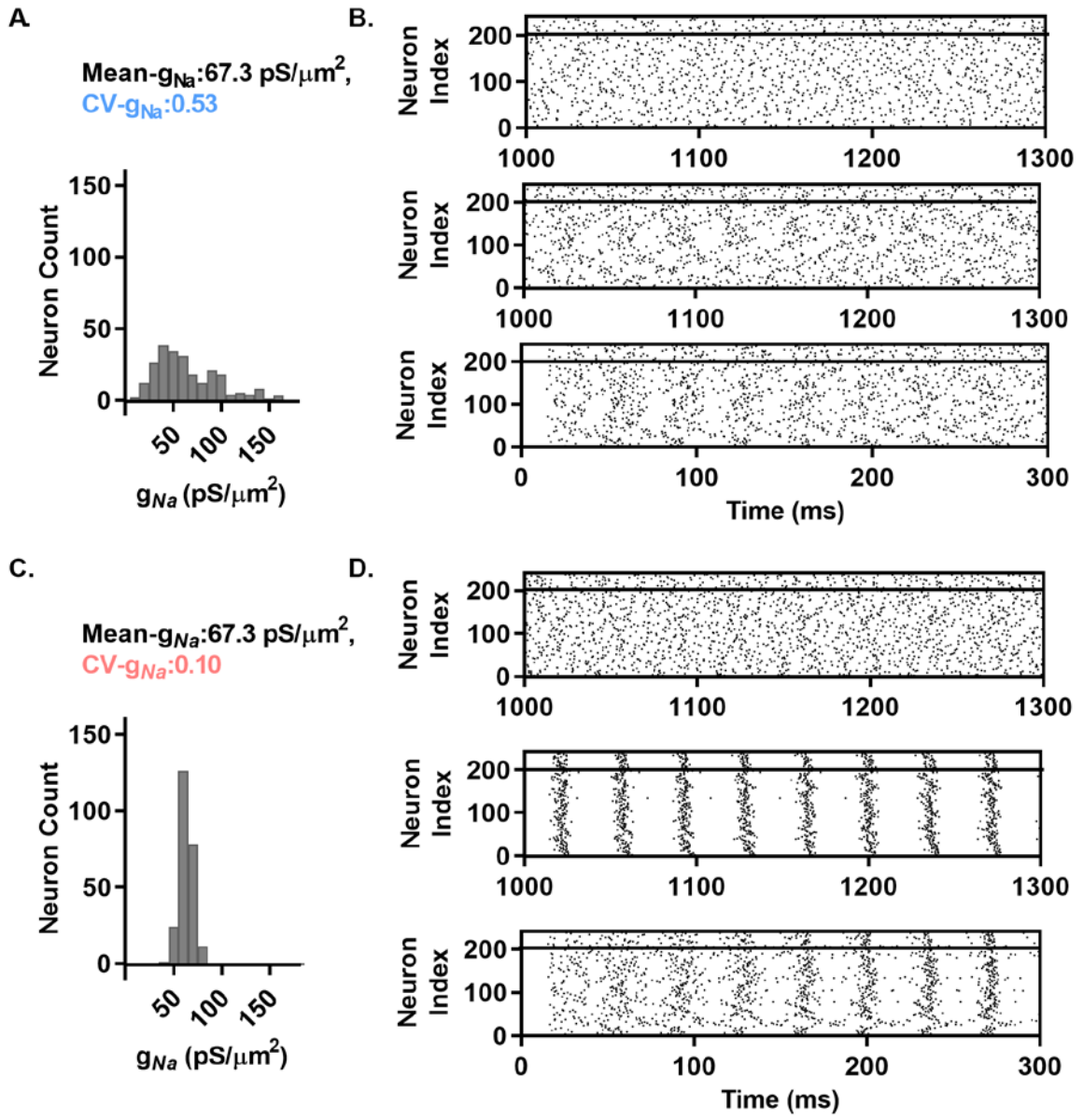


Fig. 3.4. g_{Na} diversity suppresses spontaneous network synchrony. A. and **C**. Histogram of the g_{Na} assigned to neurons used in the simulations shown in B. and D. CV-g_{Na} denotes the coefficient of variation in g_{Na}. Distribution includes 3 values >180 pS/μm^2 not shown on the histogram for visibility. **B. and D.** (Top graphs) Rasters of the activity of the neurons in A. and C. with no synaptic connections between them, supported in firing by independent noise to each neuron. (Middle) Raster plots of networks activity after 1000 ms with a connection radius of 6 neurons and rewiring probability of 30%. (Bottom) Rasters of activity at the beginning of the simulations, showing synchrony onset in the CV-gNa=0.10 network but not in the CV-g_{Na}=0.50 network. Values of F, IEI, and PC can be found in the text.

We next investigated the effects of mean g_{Na} and CV-g_{Na} on network activity over a range of values (Fig. 3.5, panels A and B). Representative raster plots of activity at mean g_{Na}=70 pS/µm^2 with CV-g_{Na} increasing in increments of 0.10 from 0.0 to 0.60 are shown in Fig. 3.5A, demonstrating the correspondence between increasing CV-g_{Na} and decreasing synchrony, quantified in Fig. 3.5B. This effect occurred over various levels of mean g_{Na}, quantified in Fig. 3.5B. Increasing mean g_{Na} resulted in increased F across different CV-g_{Na} values (Fig. 3.5B). Increased synchrony resulting from reduced CV-g_{Na} persisted in spite of the inclusion of alternative densities for g_{KA} and g_{KDR}. Halving or doubling the values for g_{KA} and g_{KDR} failed to overcome the effects of CV-g_{Na} on CV-IEI and PC, while strongly affecting F (Table 3.1). We tested for the ability of CV-g_{Na} to suppress CV-IEI and PC with g_{Na} values sampled from either gamma or Gaussian distributions, respectively (mean=67.3, CV-g_{Na}=0.53 or 0.10). In the Gaussian case, resampling of values <25 pS/um^2 resulted in distortions to the mean g_{Na} (77.3 ± 0.60 pS/µm^2) and CV-g_{Na} (0.38 ± 0.01). With both alternative distributions, the effect of

lowered CV-g_{Na} was similar to results found using a lognormal distribution (Table 3.1).

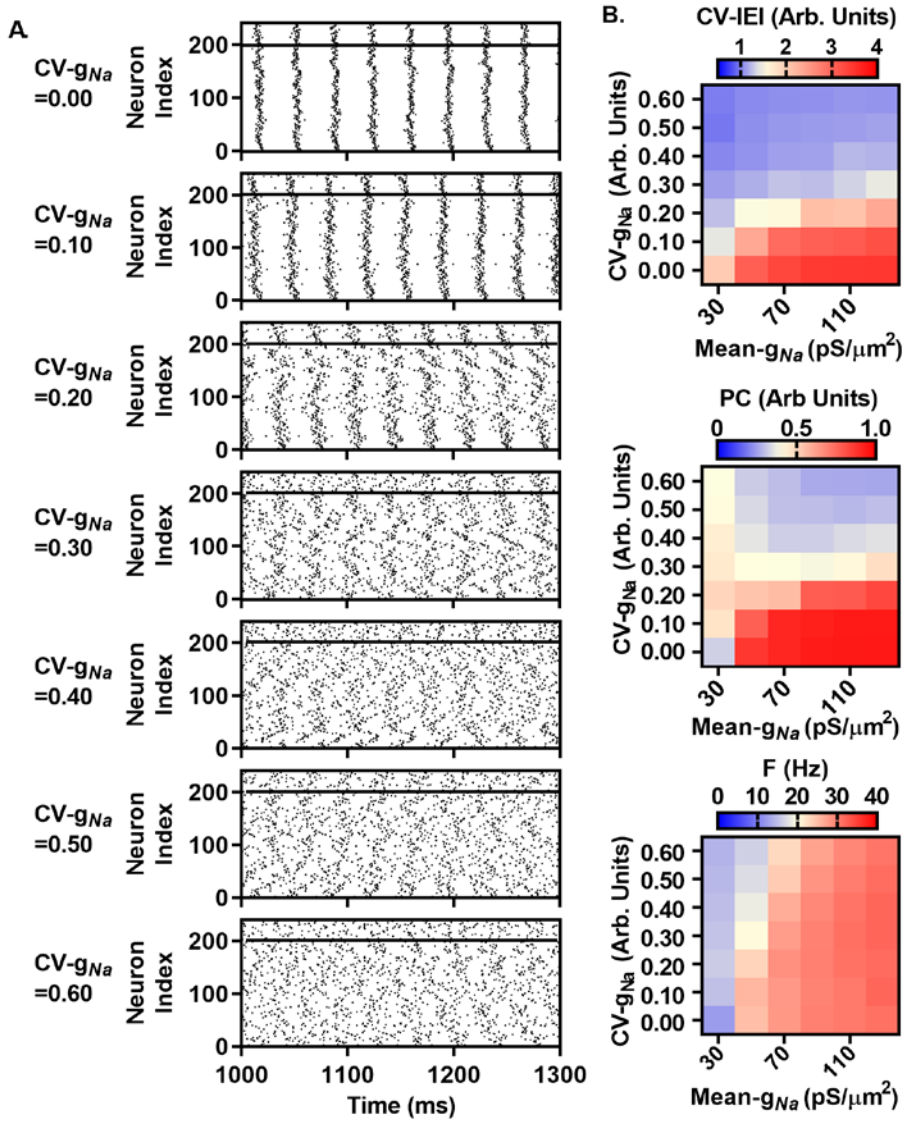


Fig. 3.5. Asynchrony increases with increasing CV-g_{Na}, with weak dependence on mean g_{Na}. A. Representative raster plots of activity in *Scn1b*-WT networks, as in Fig. 3.4A, but with mean g_{Na} set at 70 pS/μm^2 (from parameter sweep in B) and CV-g_{Na} increasing from top to bottom in 0.1 increments from 0 to 0.60. **B.** Quantification of network activity as in A, with sweeps over mean g_{Na} (30 to 130 pS/μm^2) and CV-g_{Na} (0 to 0.60), showing weak dependence of CV-IEI (left) and PC (middle) on mean g_{Na} but strong dependence on CV-g_{Na}, while F (right) shows weak dependence on CV-g_{Na} and strong dependence on mean g_{Na}. Note, the mean g_{Na} = 30 pS/μm^2 group exhibited no activity when I_{Noise} = 80 pA, thus I_{Noise} was increased to 100 pA to support network activity.

	CV-g_{Na}=0.53	CV-g_{Na}=0.10
Scn1b$^{-/-}$ Cell Diameter		
CV-IEI (Arb. Units)	1.14 ± 0.00	3.23 ± 0.00
PC (Arb. Units)	0.33 ± 0.00	0.92 ± 0.00
F (Hz)	31.22 ± 0.07	33.00 ± 0.02
Scn1b$^{-/-}$ g_{Na} (I_{Noise}=80 pA)		
CV-IEI (Arb. Units)	0.98 ± 0.01	1.26 ± 0.01
PC (Arb. Units)	0.36 ± 0.01	0.48 ± 0.01
F (Hz)	11.67±0.11	13.85 ± 0.11
Scn1b$^{-/-}$ g_{Na} (I_{Noise}=100 pA)		
CV-IEI (Arb. Units)	1.06 ± 0.02	3.04 ± 0.06
PC (Arb. Units)	0.37 ± 0.00	0.92 ± 0.00
F (Hz)	22.85±0.07	33.91 ± 0.08
g_{KDR}=20 pS/µm^2		
CV-IEI (Arb. Units)	1.09 ± 0.01	3.09 ±0.01
PC (Arb. Units)	0.30±0.00	0.93 ± 0.00
F (Hz)	28.34 ± 0.01	31.00±0.03
g_{KDR}=80 pS/µm^2		
CV-IEI (Arb. Units)	1.09±0.02	2.87 ± 0.02
PC (Arb. Units)	0.35 ± 0.01	0.88 ± 0.01
F (Hz)	22.82 ± 0.07	31.92± 0.02
Gamma Distributed g_{Na}		
CV-IEI (Arb. Units)	1.11 ± 0.02	2.89 ± 0.02
PC (Arb. Units)	0.32 ± 0.01	0.90 ± 0.00
F (Hz)	21.89 ± 0.83	28.00± 0.00
Gaussian Distributed g_{Na} (Resampled if g_{Na}<25 pS/µm^2)		
CV-IEI (Arb. Units)	1.14 ± 0.01	2.84 ± 0.10
PC (Arb. Units)	0.34 ± 0.01	0.90 ± 0.01
F	26.10 ± 0.11	30.00 ± 0.00

Table 3.1. High CV-gNa suppresses synchrony across multiple cellular conditions. Right two columns segregate results comparing 0.53 CV-g_{Na} and 0.10 CV-g_{Na} networks (excepting specific altered condition noted in left-most column). Here cell diameter is 26.2 µm in all simulations except those labeled *Scn1b*$^{-/-}$ where diameter is 22.5 µm. Mean g_{Na} is 67.3 pS/µm^2 except those labeled *Scn1b*$^{-/-}$, where g_{Na} is 41.4 pS/µm^2 g_{KDR} and g_{KA} are 40 and 10 pS/µm^2 respectively except those labeled with alternative densities where g_{KA} is fixed relative to g_{KDR} at 1:4. Gamma distribution denotes the alternative distribution used for sampling of g_{Na}. Gaussian distribution denotes the alternative distribution used for sampling of g_{Na}, with the added inaccuracy of required resampling of g_{Na} for low and negative values. Values were resampled if g_{Na} was < 25 pS/µm^2, which shifts the CV-g_{Na} distribution from nominal mean 67.3 to 77.3 pS/µm^2 and the

nominal CV-g_{Na} 0.53 to 0.38. In all simulations, I_{Noise} was 80 pA (mean and standard deviation) unless noted, where it is increased to 100 pA.

We next tested the capacity of CV-g_{Na} to suppress network synchrony across different network conditions by comparing a network with mean g_{Na}=67.3 pS/μm^2 and CV-g_{Na}=0.53 to the same network with CV-g_{Na}=0.10. Across all simulations with various P and R, the 0.1 CV-g_{Na} network exhibited higher CV-IEI and PC (Fig. 3.6, panels A and B). At low R however, the 0.1 CV-g_{Na} networks approached CV-IEI and PC levels similar to CV-gNa=0.53 network. While the 0.53 CV-g_{Na} networks exhibited increasing F with increasing R (up to 27% increase), the 0.10 CV-g_{Na} networks exhibited only minor changes in F with increasing R (up to a 3% increase) (Fig. 3.6C). To quantify the relative network requirements to support synchrony under high and low CV-g_{Na} conditions, we performed simulations with increasing R and with P fixed at 30%. The 0.53 CV-g_{Na} networks required R to be increased to 12 to reach levels of CV-IEI and PC found in the 0.10 CV-g_{Na} network model at R=6 (Fig. 3.6D). Similarly, varying the synaptic weights showed that the 0.53 CV-g_{Na} networks required synaptic weights to be increased by ~2 fold to approach the CV-IEI and PC values observed in the 0.10 CV-g_{Na} network (Fig. 3.6E). F was again relatively insensitive to increasing R and synaptic weights in the 0.10 CV-g_{Na} networks but increased with increasing R or synaptic weights in the 0.53 CV-g_{Na} networks, converging with the 0.1 CV-g_{Na} networks at higher values (Fig. 3.6E). To examine the dependence of high CV-g_{Na} suppression of network synchrony on firing rate, we tested various amplitudes of external drive. We found that increasing I_{Noise} had minor effects on CV-IEI and PC but resulted in large increases in F (Fig. 3.6F). I_{Noise} below 80 pA failed to support any spiking in the 0.10 CV-g_{Na} network and supported only a small

number of neurons in the 0.53 CV-g_{Na} network. We performed simulations sweeping across network size with P=30 and R=6 and found that CV-IEI and PC remained higher in 0.10 CV-g_{Na} networks compared to 0.53 CV-g_{Na} networks at all network sizes tested (Fig. 3.6G).

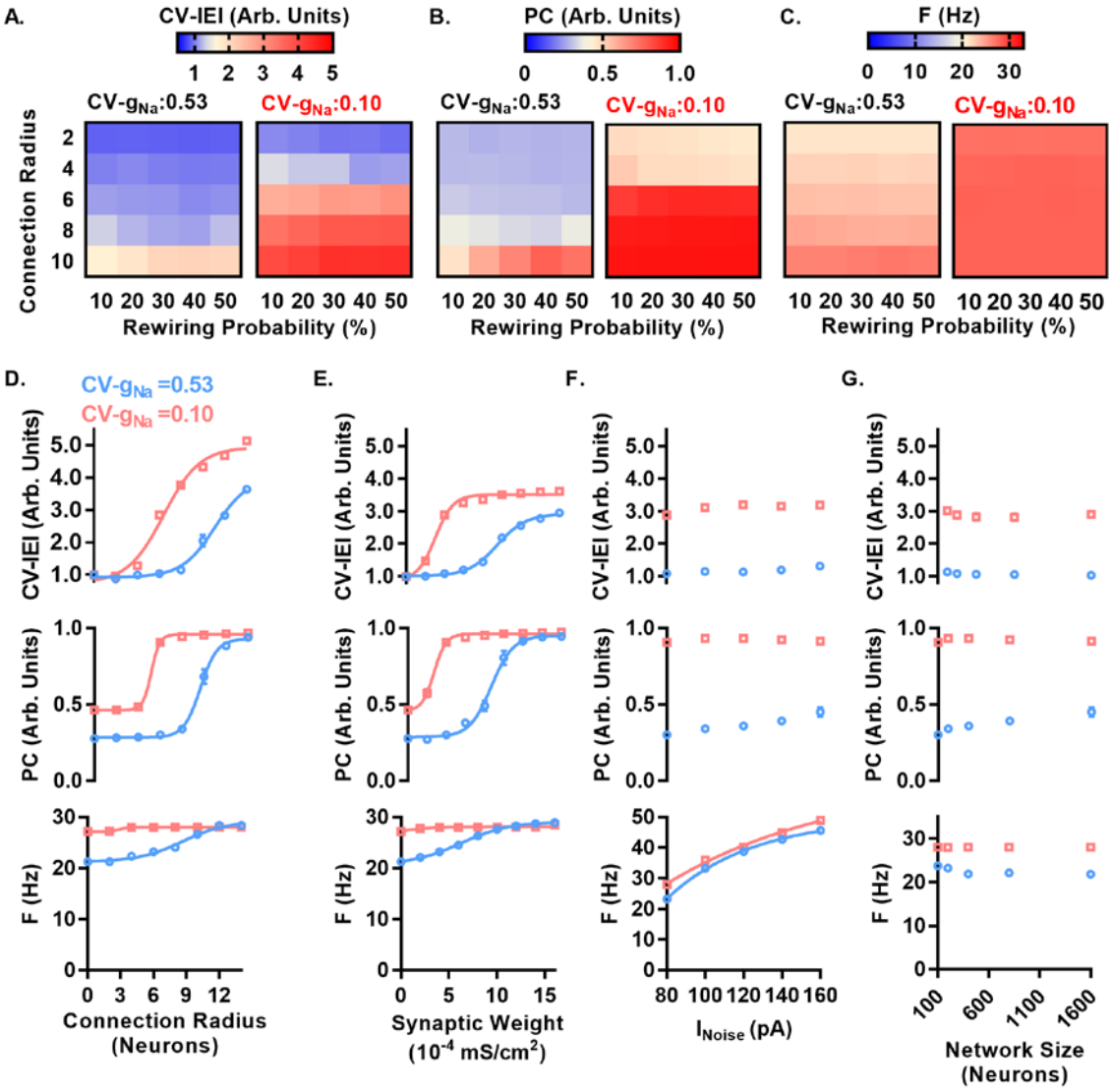


Fig. 3.6 High CV-g_{Na} displaces the network coupling requirements to support synchrony. A. CV-IEI, **B.** PC, and **C.** F, across connectivity radius (R) and rewiring probability (P) in WS networks with parameters 0.53 CV-g_{Na} (left) and 0.10 CV-g_{Na} (right). Mean g_{Na} was set at (67.3 pS/µm^2) for all simulations. Note similar CV-IEI between groups at low R and increasing CV-IEI and PC with increasing R but weak dependence on

P. F (right) increases with increasing R in the CV-g_{Na}=0.53 case while F remains similar across all R in the 0.10 CV-g_{Na} cases, showing insensitivity of low CV-g_{Na} networks to respond to changing network conditions. **D.** Sweep over R with P fixed at 30% from 0 to 14 neurons showing high CV-g_{Na} displaces the dependence of CV-IEI (top) and PC (middle) on R to higher levels. F (bottom) shows high CV-g_{Na} networks change F with increasing R, while low CV-g_{Na} networks maintain similar F across R. Line represents fit with Boltzmann equation throughout figure. **E.** Dependence of CV-IEI (top), PC (middle), and F (bottom) as in D, but sweeping over weight of synaptic connections from 0.0000 to 0.0016 mS/cm^2 while R is fixed at 6, showing similar displacement of CV-IEI (top) and PC (middle) as in D. F (bottom) shows similar insensitivity to changing network conditions in 0.10 CV-g_{Na} networks while 0.53 CV-g_{Na} networks increase frequency with increasing synaptic weight. **F.** Dependence of CV-IEI and PC on I_{Noise}, sweeping (mean and standard deviation) from 80 to 160 pA. In contrast to altering internal network conditions as in D and E, increasing the amount of external stimulation does not strongly affect CV-IEI (top) and PC (middle) while F (bottom) in both 0.53 and 0.10 CV-g_{Na} groups is strongly affected, suggesting that the alterations shown in D and E are effects of network coupling, rather than increased excitation. **G.** Dependence of CV-IEI (top), PC (middle) and F (bottom) on network size with fixed P (30 %) and R (6 neurons) sweeping from 100 to 1600 neurons, showing relative insensitivity to network size.

The simulations above model several different network types by varying R between high and low values including regular, small-world, and random networks. While *in vivo* neuronal networks exhibit small world like characteristics like those investigated above, there is also evidence that they exhibit heterogeneous distributions in the number of synaptic connections. In particular, there is evidence of power-law or “scale-free” like distributions in connection probability, i.e. there exist neuronal “hubs” with a low number of highly connected neurons and a high number of neurons with much fewer (Bui, Kim et al. 2015) connections which may be of particularly high relevance in epilepsy. Thus, we asked whether CV-g_{Na} also impacts the network requirements for synchronization in networks with these characteristics. We generated directed scale-free like networks as detailed in (Prettejohn, Berryman et al. 2011). Briefly, directed networks of size N with power-law like distribution in synaptic connection probability were generated by starting

with a seed network of m neurons with all-to-all connectivity. Then iteratively, N-m neurons were added to the network with each new neuron j receiving m connections from m different pre-existing k_i neurons in the network. Selection of neurons for k_i was random, with probability proportional to the existing number of target neurons post-synaptic to neuron k_i. This resulted in a heterogeneous connection probability, with few neurons having a high connection probability and a greater number with fewer connections as the network grew in size. A graphical representation of a network with N=200 and m=12 is shown in Fig 3.7A. The accompanying distribution in out-degree is shown in Fig. 3.7B. 40 inhibitory neurons were added as above for WS networks, with local (from neuron index) connection radius of 6 neurons. To examine the relative requirements for synchronization in 0.10 and 0.53 CV-g_{Na} networks, we swept across m from 0 to 28 neurons. Similar to our findings for WS networks, we found that 0.10 CV-g_{Na} networks exhibit higher CV-IEI and PC across a variety of network conditions, with 0.53 CV-g_{Na} networks requiring ~2 fold higher m to achieve similar degrees of CV-IEI and PC as the 0.10 CV-g_{Na} network (Fig 3.7D Top and Middle). Similar to the WS networks, firing rate in the 0.1 CV-g_{Na} network remained relatively unaffected by changing network connectivity, while in the 0.53 CV-g_{Na} network, F increased with increasing m (Fig 3.7D Bottom). These results show that high g_{Na} diversity raises the network connectivity requirements to support neuronal synchrony in networks with heterogeneous degree distribution.

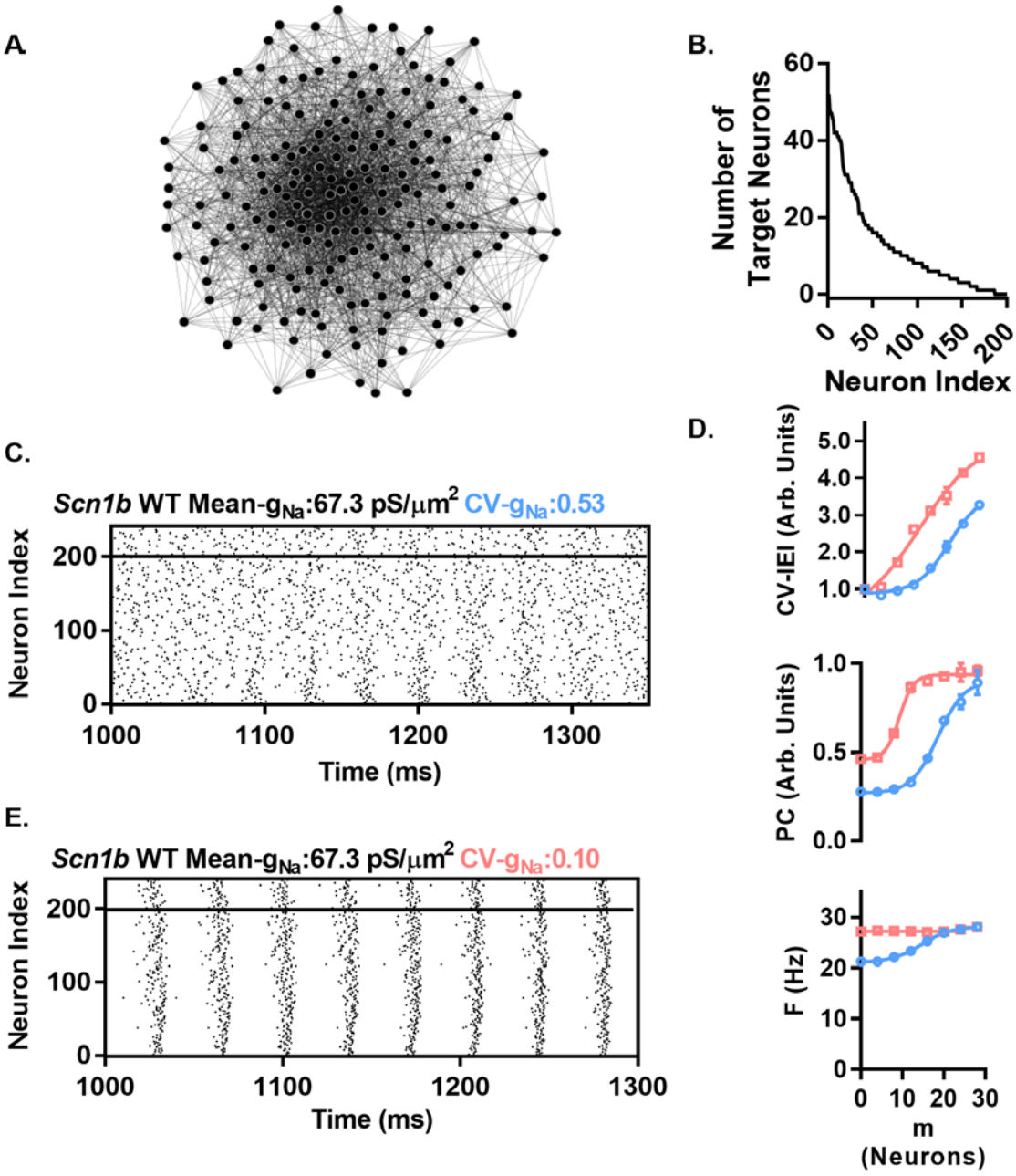


Fig. 3.7 High CV-g_{Na} displaces the network coupling requirements to support synchrony in networks with heterogeneous connection probability. A. Graphical representation of a representative Scale-Free like network structure of N=200 excitatory neurons. **B.** Histogram of the number of target excitatory neurons for each excitatory neuron in the network shown in A, exhibiting the heavy tailed distribution characterizing scale free networks. **C.** Representative raster plots of m=12 networks with CV-g_{Na}=0.53 (top) or 0.10 (bottom) and mean 67.3 pS/μm^2. Note in 0.53 CV-g_{Na} network, transient synchrony observable in neurons

with low index (high out-degree neurons) which grows over ~100 ms but is dissipated shortly after reaching peak while the 0.10 CV-g_{Na} network maintains network wide synchrony. **D.** CV-IEI (Top), PC (Middle) and F (Bottom) resulting from sweeping from m=0 to 30 neurons, showing similar to WS networks investigated in 3.6 CV-g_{Na}=0.10 networks have lower network requirements (here m) required to support neuronal synchrony. Again similar to WS networks, F in the 0.53 CV-g_{Na} networks is sensitive to altering network connectivity while the F in the 0.10 CV-g_{Na} networks are insensitive.

Discussion

Here we show, using pharmacological, genetic, and computational approaches that variability in I_{Na} density between neurons contributes to firing rate heterogeneity, low spike correlation, and suppresses network synchronization. *Scn1b*$^{-/-}$ pyramidal neurons, which we showed in chapter 2 to have impaired I_{Na} density heterogeneity, have higher spike time correlation and phase coherence between neurons in response to fluctuating input than the more I_{Na} density diverse *Scn1b*$^{+/+}$ neurons. Furthermore, firing rate heterogeneity at smaller fluctuation intensities is impaired in *Scn1b*$^{-/-}$ neurons. Application of a low concentration of TTX does not impair the capacity of WT neurons to fire repeatable and reliable spike trains but reduces spike train correlation and phase coherence between concentrations to levels similar to that seen between different neurons. Next we showed using a computational modeling approach, that I_{Na} density heterogeneity contributes to low spike synchrony in response to externally generated fluctuating synaptic conductances and that g_{Na} heterogeneity can displace network connectivity requirements to support spontaneous network synchronization in a variety of networks. This work provides critical new information on the importance of I_{Na} density

heterogeneity in neural coding, network synchronization, and on pathophysiological contexts for impaired ion channel heterogeneity impacting network function.

I_{Na} Heterogeneity Suppresses Spike Synchrony Resulting from External or Autonomously Generated Activity

Our work shows that g_{Na} heterogeneity desynchronizes activity generated from fluctuating somatic input from external identical inputs and suppresses the generation of spontaneous network synchrony within small networks. In our network simulations, neurons had a low connection probability, were stimulated by independent noise processes, and fired asynchronously in the absence of network connections. Thus, local network connectivity interacting with neuronal heterogeneity can serve to generate synchronous firing even in cells that are not directly connected. The degree of heterogeneity in g_{Na} alters the degree to which neurons need to be connected to undergo synchronization, whether through increasing synaptic weight or in increasing the number of network connections. g_{Na} heterogeneity is therefore an import component of network synchronization that interacts with the effects of network activity, network architecture, and synaptic weights.

Conductance, Morphological, and Input Heterogeneity

In contrast to voltage-gated potassium channels, the repertoire of VGSC genes expressed in the brain is relatively limited and VGSCs do not vary as dramatically in their

voltage dependent or kinetic properties (Jan and Jan 2012). While the repertoire of voltage-gated potassium channel gene expression is high in brain, suggesting a high combinatorial capacity to promote spike pattern diversity, the role of VGSCs in spike initiation in response to a given membrane potential fluctuation gives them a special role in translating fluctuations into outputs. The possibility of diverse dendritic morphologies and synapse locations limiting input correlations are also important considerations. *In vivo* paired whole cell recordings however have shown that neighboring neurons exhibit high membrane potential correlation (Crochet and Petersen 2006, Poulet and Petersen 2008, Eggermann, Kremer et al. 2014). This shows that in spite of the fact that no two neurons have identical dendritic morphology or the same location or strength of synapses that input in vivo is capable of converging to similar fluctuations in somatic membrane potential in neighboring neurons. Despite these high membrane correlations, spiking is largely asynchronous in layer 2/3 (Petersen 2017) pyramidal neurons and in the cortex in general (Ecker, Berens et al. 2010). It then follows that how neurons fire in response to similar membrane potential fluctuations at the soma may in large part be due to their variable density of VGSCs. We have shown here that a mouse model with impaired VGSC density heterogeneity exhibits increased spike synchrony, that blocking a fraction of VGSCs channels alters spike synchrony to levels comparable between different neurons, and show computationally that VGSC density confers a broad spectrum of spike patterns, affects spike pattern to identical inputs, and suppresses spontaneous network synchronization. We therefore posit that the density heterogeneity of VGSCs between neurons is a crucial mediator for converting similar input fluctuations into dissimilar AP outputs whether generated by local or afferent activity.

VGSC density heterogeneity at the AIS may be an important means of controlling heterogeneous firing, as it is known that the length and location of the AIS variable in pyramidal neurons and utilized to alter excitability (Leterrier 2018). Variability in the subcellular distribution of channels has been proposed previously to contribute to neuronal diversity (Nusser 2009). The variable length and distance of the AIS from the soma also however presents difficulties in assessing variability in AIS VGSC density as recording techniques would need to be directed to insure recording from the same relative location within the AIS since channel density within the AIS itself varies with distance. Interestingly, within dopaminergic neurons of the rat substantia nigra which have high AIS structural variability, that somatodendritic influences normalize these effects, with AP shape and pacemaking being independent of AIS morphology (Moubarak, Engel et al. 2019). It has been shown previously that spiking pattern is affected by dendritic morphology (Mainen and Sejnowski 1996). While we do not investigate this property here, the *C121W* mutation in *Scn1b* is known to impair dendritic arborization and this affect may be important in the higher spike synchrony in *Scn1b* null mice (Reid, Leaw et al. 2014). This furthermore highlights the concept of the co-regulation of mechanisms that affect excitability. Ion channel degeneracy has received growing attention as a means of neurons converging to similar outputs despite having different levels of ionic conductances. *Scn1b* is both a VGSC modulator and a cell adhesion molecule which affects neurite outgrowth (Hull and Isom 2018). The dual roles of both enhancing cell size and enhancing I_{Na} suggests that *Scn1b* is directly related to the degeneracy of VGSC density and input resistance. Ion channel degeneracy has received an increasing amount

of attention, as it is a means of achieving similar outputs with different combinations of channels (Drion, O'Leary et al. 2015). We show here however that while the degeneracy of I_{Na} and input resistance balance mean firing rates in Scn1b$^{-/-}$ mice, it does not extend to resulting in degeneracy of spike rate heterogeneity, spike pattern, and neuronal synchronization in response to fluctuating input. This result is important as it highlights that degeneracy mechanisms may be effective in balancing some aspects of excitability while failing in others.

Epilepsy, Hyperexcitability, and Hypersynchrony

An underlying motivation in this work was to understand the consequences of pyramidal neurons having variable levels of I_{Na} between neurons, a question brought to our attention by its impairment in pyramidal neurons of *Scn1b*$^{-/-}$ mice. *Scn1b*$^{-/-}$ mice are model of a DEE. As we showed in chapter 2, severe epilepsy and death occurs with *Scn1b* deletion in parvalbumin positive neurons but not in CAMK2a positive neurons, suggesting that pyramidal neuron intrinsic loss of *Scn1b* is the primary cause of epilepsy in this model. This suggests that impaired I_{Na} in pyramidal neurons may be secondary to seizures or involved in the increased severity of this model relative to other DEE models. The effect of reduced mean I_{Na} in *Scn1b*$^{-/-}$ mice has no effect on mean firing rate, but has a large effect on spike synchrony in response to input fluctuations. Seizures are detected electrographically as large fluctuations in the field potential, which requires that activity be synchronous. However, the relationship between hyperexcitability and neuronal synchrony in epilepsy is unclear and the relative importance of either effect in epilepsy

mechanisms is a topic of active debate. The work presented here suggests that enhanced neuronal synchronization in the *Scn1b* and *Scn8a* models of DEE could be a consequence of impaired neuronal heterogeneity. Furthermore, heterogeneous spike timing between neurons during synchronous fluctuating input such as occurs during seizures, may serve as a break to the propagation of synchronous network activity. Importantly the similar effect of impaired heterogeneity in *Scn1b* and *Scn8a*$^{N1768D/+}$ DEE models, two related VGSC-linked DEEs, underscores the pathophysiological relevance of understanding I_{Na} heterogeneity in the relationship between neuronal synchrony and hyperexcitability in epilepsy.

Methods

Brain Slice Preparation

Acute brain slices were prepared as described in chapter 2. Mice were anesthetized with isoflurane anesthesia, decapitated, and brains were removed and placed in 95:5% O_2:CO_2 continuously aerated ice-cold slice solution containing in mM: (110 sucrose; 62.5 NaCl; 2.5 KCl; 6 $MgCl_2$; 1.25 KH_2PO_4; 26 $NaHCO_3$; 0.5 $CaCl_2$; and 20 D-glucose (pH 7.35-7.40 when aerated at RT). 300 μm thick coronal sections from the visual cortex region. Slices were incubated in an aerated holding chamber containing slice solution for 30 min at 34°C and then incubated in a mixture of artificial cerebrospinal fluid (ACSF) and slice solution (1:1) for 30 min at room temperature. ACSF contained in mM

(125 NaCl; 2.5 KCl; 1 $MgCl_2$; 1.25 KH_2PO_4; 26 $NaHCO_3$; 2 $CaCl_2$; and 20 D-glucose (pH 7.35-7.40 with aeration). Slices were then aerated with 100% ACSF for at least 30 min before use.

Whole Cell Action Potential Recording and Analysis

During recording, slices were superfused with 2-3 ml/min aerated ACSF at 34°C. Neurons were visualized using a Nikon A1R upright confocal microscope equipped with IR-DIC optics with a 40X water immersion objective. Only vertically oriented pyramidal cells were selected for recording. Recording electrodes had a resistance of 3-6 MΩ with solutions containing in mM (140 K-Gluconate, 4 NaCl, 0.5 $CaCl_2$, 10 HEPES, 5 EGTA, 5 phosphocreatine, 2 Mg-ATP, and 0.4 GTP (pH adjusted to 7.2-7.3 with KOH). The junction potential was calculated to be 14.3 mV using the P-clamp junction potential calculator in the whole cell mode and all values were corrected offline, with all values presented in the study as corrected values. The resting membrane potential was defined as the membrane potential in current clamp <10 s after initial break in. Data were acquired at 20 kHz and were filtered at 10 kHz. Cells with an access resistance measured in voltage clamp >20 MΩ or RMP>-64.3 mV were discarded. Access resistance and pipette capacitance were compensated using bridge balance. APs were defined as the voltage crossing -20 mV subsequent to a dv/dt>10 mV/ms, defined here as the AP threshold. Input resistance was calculated using Ohm's law with 10 pA current injection from the resting membrane potential after 250 ms. Cell which had changes in access resistance >20% of the value between the start and end of recordings were discarded.

Perforated Patch Clamp

Perforated patch clamp was performed in the same recoding conditions as whole cell recordings above. Amphotericin B stock solution was made by dissolving in DMSO at a concentration of 50 mg/ml and sonicating. Stock solution was then added to the whole cell recording internal solution above to give a final concentration of 100 µg/ml and sonicating. Recording pipettes tips were then filled with recoding solution above and pipettes were backfilled with solution Amphotericin B containing internal solution. After the establishment of a gigaohm seal, cells were allowed to perforate for between 15-30 minutes until access resistance <30 Mohms was stable (<10% change) for 5 minutes. Input resistance was monitored by a -10 pA hyperpolarizing current injection between sweeps and cells were discarded if input resistance changed by more than 20%. Cells with access resistance changes >20% throughout the recording were discarded.

Statistics

No more than 1 cell was acquired per slice, no more than 4 cells were acquired per animal, and each experiment was performed with at least 4 animals. Each cell is reported as n=1 and each animal is reported as N=1. For measures of spike train correlation or phase coherence between trials within the same cell, the pairwise cross correlation and phase coherence was measured between all trials and averaged to generate a single value (phase coherence or correlation) for each cell (n=1). Then

between groups comparisons (e.g. *Scn1b*$^{+/+}$ vs *Scn1b*$^{-/-}$) were calculated by comparing the average phase coherence or average correlation values between groups. For measures of between cell correlation or phase coherence, pairwise comparisons between trials of cell A were compared to all trials of cell B, C, etc. and the average was taken to generate a single value of phase coherence and correlation for cell A. Then between groups comparisons (e.g. *Scn1b*$^{+/+}$ vs *Scn1b*$^{-/-}$) were calculated by comparing the average phase coherence or correlation between groups. Significance was set at $p<0.05$. Comparisons were made with an unpaired two-tailed student's t-test in experiments comparing between *Scn1b*$^{+/+}$ and *Scn1b*$^{-/-}$ mice. Comparisons with application of TTX were made using a paired t-test. All listed p-values are tested for significance after multiple comparisons and reported as non-significant if $q>0.05$ using the Benjamini, Krieger, and Yekutieli two stage step-up method with a 5% false discovery rate correction. Values were tested for a non-Gaussian distribution using D'Agostino-Pearson omnibus normality test. Differences in variance were tested using an F-Test.

Computational Modeling

All simulations were performed in the NEURON, version 7.4, simulation environment. The model equations were based on a previous model used in the investigation of the interplay between heterogeneous intrinsic neuronal properties and network structure. We modified this model to take into account (but not to explicitly model) adolescent layer 6 pyramidal neurons gNa, input resistance and resting membrane potential, and to examine the impact of g_{Na} diversity in the relative context of *Scn1b*$^{+/+}$ and

Scn1b$^{-/-}$ differences. Simulations were performed using the following current balance equation:

Equation 3.1:

$$C_m \frac{dV_m}{dt} = -g_{Na} m^3 h (V_m - E_{Na}) - g_{K_{DR}} n^4 (V_m - E_K) - g_{K_A} qr (V_m - E_K) - g_L (V_m - E_{leak}) - I_{Syn} + I_{Noise}$$

where V_m is the membrane voltage; C_m is the cell capacitance calculated using specific capacitance of 0.9 µF/cm^2 and surface area from morphologies as detailed below; g_x are the maximum conductances of the respective ionic currents; E_x are the equilibrium potentials for respective ions; and m, h, n, q, and r are gating functions detailed below. E_{Na} was set at 75 mV, E_k, -90 mV, and E_{leak} at -81.7 or -76.8 mV for *Scn1b*$^{+/+}$ or Scn1b$^{-/-}$ simulations respectively. Gating functions followed the general form

Equation 3.2:

$$\frac{dx}{dt} = \frac{x_{inf}(V_m) - x}{\tau_x(V_m)}$$

where x_{inf} and τ_x are given by gating variables detailed below. Here, F is Faraday's constant, R is the gas constant, and T is temperature in K. Simulations were performed at a nominal temperature of 37°C with rates defined at 23°C with temperature dependent rates adjusted according to q10= 2.3 (I_{Na}), 5 (I_{KA}), and 1 (I_{KDR}). Note voltage dependent rates in I_{Na} were adjusted as in source model with an input voltage shift of -10 mV (Hu, Tian et al. 2009). For I_{Na}, values were adjusted such that the h_{inf} curves in a 10 µm diameter and length model cell at 23°C were within 0.1 of their respective units of the slope factor and $V_{1/2}$ recorded in nucleated patches in chapter 2.

Na+ current was calculated according to:

Equation 3.3:

$$I_{Na} = g_{Na} m^3 h (V_m - E_{Na})$$

With steady state activation function:

Equation 3.4:

$$m_{inf}(V_m) = \frac{\alpha_m(V_m)}{\alpha_m(V_m) + \beta_m(V_m)}$$

and activation time constant:

Equation 3.5:

$$\tau_m(V_m) = \frac{1}{\alpha_m + \beta_m}$$

Equation 3.6:

$$\alpha_m(V_m) = 0.182(V_m + 36.42)/(1 - e^{-\frac{V_m+36.42}{6.8}})$$

Equation 3.7:

$$\beta_m(V_m) = 0.124(V_m + 36.42)/(e^{\frac{V_m+36.42}{6.8}} - 1)$$

With Steady State Inactivation Function:

Equation 3.8:

$$h_{inf}(V_m) = \frac{1}{1 + e^{(V_m+65.7)/5.25}}$$

Where

Equation 3.9:

$$\alpha_h(V_m) = \frac{0.024(V_m + 50)}{1 - e^{-\frac{V_m+50}{5}}}$$

Equation 3.10:

$$\beta_h(V_m) = 0.0091(V_m + 75)/(e^{\frac{V_m+75}{5}} - 1)$$

Inactivation time constant function:

Equation 3.11:

$$\tau_h(V_m) = \frac{1}{\alpha_h(V_m) + \beta_h(V_m)}$$

Delayed rectifier type K+ current was calculated according to:

Equation 3.12:

$$I_{K_{DR}} = g_{K_{DR}} n^4 (V_m - E_K)$$

With Steady state activation function:

Equation 3.13:

$$n_{inf}(V_m) = \frac{1}{1 + \gamma_n(V_m)}$$

And Activation time constant function:

Equation 3.14:

$$\tau_n(V_m) = \max\left[\frac{50\delta_n(V_m)}{1 + \gamma_n(V_m)}, 2\right]$$

Where

Equation 3.15:

$$\gamma_n(V_m) = e^{10^{-3} * -3 * \left(V_m - (-10) * \frac{F}{RT}\right)}$$

Equation 3.16:

$$\delta_n(V_j) = e^{10^{-3} * -2.1 * (V_m - (-10) * \frac{F}{RT})}$$

A-type K+ current was generated according to:

Equation 3.17:

$$I_{K_A} = g_{K_A} qr(V_m - E_K)$$

With Steady state activation function:

Equation 3.18:

$$q_{inf}(V_m) = \frac{1}{1 + \gamma_q(V_m)}$$

Equation 3.19:

and activation time constant function:

Equation 3.20:

$$\tau_q(V_m) = \max\left[\frac{4\delta_q(V_m)}{1 + \gamma_q(V_m)}, 0.1\right]$$

Where

Equation 3.21:

$$\gamma_q(V_m) = e^{10^{-3}(-1.5-(1+e^{(Vm+40)/5}))^{-1}(V_m-11)\frac{F}{RT}}$$

Equation 3.22:

$$\delta_q(V_m) = e^{10^{-3}*0.55(-1.5-(1+e^{(Vm+40)/5}))^{-1}(V_m-11)\frac{F}{RT}}$$

Steady state inactivation function:

Equation 3.23:

$$r_{inf}(V_m) = \frac{1}{1 + \gamma_r(V_m)}$$

And time constant function:

Equation 3.24:

$$\tau_r(V_m) = \max[0.26(V_m + 50), 2]$$

Where

Equation 3.25:

$$\gamma_r(V_m) = e^{10^{-3} * 3(V_m + 56)\frac{F}{RT}}$$

g_{Na} was set at the experimentally measured conductance densities in nucleated patches at -20 mV, corrected by 14% for incomplete activation at -20 mV (67.3 pS/µm^2 for *Scn1b*$^{+/+}$ and 41.4 pS/µm^2 for *Scn1b*$^{-/-}$) as calculated from nucleated patches in chapter 2. Note conductance is used in model for simplicity and continuity with the source models while permeability is used experimentally for the measurement of steady state activation due to prominent rectification at higher test potentials. Comparison of the experimental mean *Scn1b*$^{+/+}$ conductance density to values recorded in nucleated patches previously in layer 5 pyramidal neurons shows a similar density where the 50% open channel probability corrected density was 60 pS/µm^2 (here 67.3 pS/µm^2) and a similar range of 27 to 136 pS/µm^2 (here 32.7 to 130.2 pS/µm^2) (Hu, Tian et al. 2009).

Cell morphology consisted of a single isopotential cylindrical compartment with equal diameter and length. Cell diameter was determined such that C_m was equal to whole cell capacitance measured experimentally for layer 6 pyramidal neurons in chapter 2 in *Scn1b*$^{+/+}$ (diameter=26.2 µm yielding a capacitance of 19.5 pF) or *Scn1b*$^{-/-}$ (diameter =22.5 µm yielding a capacitance of 14.3 pF). R_m ($1/g_L$) was set at 10.1 kΩcm^2 such that the input resistance calculated by a -10 pA current injection at resting membrane potential in the *Scn1b*$^{+/+}$ neuron was equal to 460 MΩ (experimental IR = 462 MΩ), yielding an

Scn1b$^{-/-}$ neuron input resistance of 627 MΩ (experimental IR=669 MΩ). The ratio of g_{KDR} to g_{KA} was fixed in all simulations at 4 (the ratio of non-inactivating to transient I_K in I_K recordings in chapter 2). The density of g_{KDR} was determined by sweeping from 10 pS/μm^2 to a max of 200 pS/μm^2, setting the density at 40 pS/μm^2 for further simulations, as this value results in depolarization block in *Scn1b*$^{+/+}$ and *Scn1b*$^{-/-}$ models at similar current injection ranges recorded experimentally. Doubling or halving this density did not significantly change the effect of high or low CV-g_{Na} on network synchrony but altered F, with the g_{KDR}=80 pS/μm2 group requiring increased external stimulation to maintain network activity (Table 1).

Synaptic Currents were generated as in (Bogaard, Parent et al. 2009). When a presynaptic cell V_m crossed 0 mV an exponentially decaying synaptic current in the target cell was generated according to:

Equation 3.26:

$$I_{syn} = wexp\left(-\frac{(t-t_i)}{\tau}\right)(V_m - E_{syn})$$

where E_{syn} =0 or -80 mV for excitatory and inhibitory synapses respectively, τ = 0.5 or 1.5 ms for excitatory or inhibitory synapses respectively, t_i is the presynaptic spike time, and *w* is the synaptic weight set at a default 0.0004 mS/cm^2, selected such that excitatory synapses provide a ~2mV depolarization at the resting membrane potential in a *Scn1b*$^{+/+}$ style model neuron. The effect of different synaptic weights on network function are investigated in Fig. 6E. Neuronal activity was supported by a background Gaussian distributed current injection I_{Noise}, generated independently for each neuron with a new value sampled at each time step (0.0125 ms). Time of onset was generated randomly

(from a uniform distribution) over 50 ms at the start of network simulations for each neuron to avoid synchronous activation at simulation initialization. With the exception of simulations noted in text and figure legends, all simulations used a noise with an equal mean and standard deviation of 80 pA (the minimum required in the majority of simulations to maintain network activity), with the above special cases increased to 100 pA to maintain network activity.

Network Structure

Assembly of the neurons above into directed Watts-Strogatz small world model networks was performed as in (Bogaard, Parent et al. 2009). The network was formed with initial wiring starting from a circular network, with each excitatory neuron connected to its (R) nearest neighbors in both directions. Then, with an associated probability (P), a subset of connections was rewired to randomly (uniform probability) chosen excitatory neurons within the network. Inhibitory neurons were added to the network with local reciprocating connections to excitatory neurons with a radius of 6 excitatory neurons (with a 50% overlap between inhibitory neuron targets). Inhibitory neuron number was set at 1/5 the excitatory neuron number in all simulations. Inhibitory neuron structure and conductances were generated as for excitatory neurons for simplicity.

For heterogeneous synaptic degree simulations, neuron placement as shown graphically in Fig 3.7A is according to the Yifan Hu algorithm using Gephi network visualization software (Bastian, Heymann et al. 2009). Black circles represent excitatory

neurons with connectivity as described below. Network was grown from seed network of size m (here 12) with all to all connectivity, with iterative addition of N-m neurons receiving m (12) connections from m (12) different preexisting neurons in the network. Source neurons were selected randomly with a probability bias proportional to the number of connections already existing for the presynaptic neuron (i.e. if a random number drawn from a uniform probability distribution is less than the fraction of existing outgoing connections in the network belonging to the putative source neuron, the new connection is assigned to that neuron. If the random number is greater than the fraction of existing outgoing connections, the procedure is repeated with a new random source neuron, excluding neurons already connecting to the N-m neuron). 40 inhibitory neurons were added independently of the scale free network structure, with a connection radius of 6 neurons selected based on neuron index.

Model Network Quantification

Simulations were run for 2000 ms with activity during the final 1000 ms used to quantify network behavior with three different measures: the mean coefficient of variation in interevent interval (CV-IEI, Equation 3.27) (Cox 1966) to examine event clustering, mean phase coherence (PC, Equation 3.28) (Bogaard, Parent et al. 2009) to analyze spike phase synchrony, and the mean firing rate (F, Equation 3.29) (Bogaard, Parent et al. 2009). All measures presented are the average +/- SEM of 3 simulations.

The coefficient of variation in inter-event intervals for cell n (event defined as a spike in a cell presynaptic to cell n) was computed according to (Cox 1966):

Equation 3.27:

$$\boldsymbol{CV - IEI_n} = \frac{\sqrt{\frac{\mathbf{1}}{\boldsymbol{S-1}}\sum_{\boldsymbol{j=1}}^{\boldsymbol{S}}\left|\boldsymbol{\tau_{nj}} - \mu_{\boldsymbol{n}}\right|^2}}{\mu_{\boldsymbol{n}}}$$

where τ_n is the vector of inter event intervals j ($\tau_{nj} = t_{n(j+1)}$-t_{nj}) of the time ordered list of spike times t_{nj} of the cells presynaptic to cell n, with τ_n having length S and mean μ_n. The CV-IEI$_n$ for each cell was then averaged over all cells and referred to as CV-IEI in the text.

Phase coherence between cells n and m was computed as in (Bogaard, Parent et al. 2009) according to:

Equation 3.28:

$$\boldsymbol{PC_{nm}} = \left|\frac{\mathbf{1}}{\boldsymbol{S}}\sum_{\boldsymbol{j=0}}^{\boldsymbol{S-1}} \boldsymbol{e^{i\phi_{nm}}}\right|$$

where S is the number of samples for cell n's spike time vector and ϕ_{nm} is the phase between cells n and m during inter-spike interval j. ϕ_{nm} for interspike interval j ($\tau_{nj} = t_{n(j+1)}$-t_{nj}) of cell n was computed by taking the inter-event interval as 2π and taking the associated spike of cell m associated with τ_{nj}, to be $t_{nj} <= t_{mj} <= t_{n(j+1)}$. Phase between spikes is then defined as:

Equation 3.29:

$$\boldsymbol{\phi_{nm}} \equiv 2\pi\frac{t_{mj} - t_{nj}}{\tau_{nj}}$$

PC_{nm} across all neurons was then averaged and referred to as PC in the text.

Firing frequency for cell n was calculated as in (Bogaard, Parent et al. 2009) by the inverse of the average interspike interval according to:

Equation 3.29:

$$\boldsymbol{F_n = \frac{1}{\tau_n}, \tau_n = \sum_{k=1}^{S-1} \frac{t_{j+1} - t_j}{S-1}}$$

with S being the total number of spikes of cell n that occur at times t_j. Then each F_n was averaged over all neurons in the network and referred to as PC in the text.

Chapter IV. Conclusions

The work presented in this thesis expands upon knowledge in two areas of voltage-gated sodium channel (VGSC) biology; the role of sodium current (I_{Na}) and hyperexcitability in the *Scn1b*$^{-/-}$ model of developmental and epileptic encephalopathy (DEE), and in clarifying the role of VGSC density between neurons in the patterning of neuronal activity. These findings advance our understanding more broadly by uncovering common and unique mechanisms in a *Scn1b* DEE model and provide additional perspective on the role of VGSC density in the nervous system beyond effects on firing rate.

Hyperexcitability and Hypersychrony in Epilepsy

At the level of an individual cell in isolation, we can characterize firing activity in several ways. One such way is the rate at which action potentials (APs) occur. Such rate coding and its relevance to both neuronal communication and in epilepsy have clear foundations. Adrian and Zotterman showed in 1926 that the rate of firing in a sensory

neuron was directly proportional to the amount of weight attached to the muscle. (Adrian and Zotterman 1926) Alternatively, in the cortex temporal coding is of unknown significance but spiking is highly irregular and neurons have the capacity to respond with robust precision to fluctuating input, indicating there may be mechanisms at work utilizing the timing of spikes (Softky and Koch 1993, Mainen and Sejnowski 1995). At the level of multiple neurons, new modes of communication, and of dysfunction, become available that are combinatoric and relational. At a basic level, the differential roles of GABAergic and glutamatergic neurons in controlling firing rate of target neurons by their relative activity is established to be crucial to neuronal function in the CNS. The control of mean activity, based on the balance of excitatory and inhibitory drive, is certainly known to occur and has a clear relationship to rate coding (Yizhar, Fenno et al. 2011). Furthermore, many studies of disease mechanisms in epilepsy are directed at understanding excitatory vs. inhibitory imbalance as we reviewed in the introduction. Another mode of output, once multiple neurons are considered, is the relationship of the timing of APs, not only in the activity pattern within a single cell, but their relative timing or rate of APs to those of other neurons in a network. It is the role of VGSCs at the interface between individual neurons and network level excitability and in activity patterning that forms the primary focus of this thesis.

Epilepsy is directly related to neuronal excitability and the relational firing of neurons. A major underlying theme of the work presented in this thesis is the interface

between two approaches to understanding epilepsy, which relate intimately to the question above of the relational nature of communication between neurons. On one hand, epilepsy is often broadly described as a disorder of imbalance between excitation and inhibition. In *Scn1a* models of Dravet syndrome (DS) for example, our current understanding is that neuronal networks are hyperexcitable. This is largely thought to be the result of disinhibition, where GABAergic inhibitory neurons of the cortex and hippocampus have lowered excitability, resulting in overall network hyperexcitability. (Catterall 2016) Alternatively, there is also evidence that glutamatergic pyramidal neurons in DS become hyperexcitable and have increased I_{Na} at disease onset (Mistry, Thompson et al. 2014). In line with this excitatory and inhibitory imbalance scheme, the other side of the imbalance is known to occur in *Scn8a* models of epilepsy, where gain of function mutations in *Scn8a* drive excitatory neuron hyperexcitability (Meisler, Helman et al. 2016). Whether epilepsy results from impaired inhibitory interneuron firing or increased pyramidal neuron firing, these two mechanisms both focus on network hyperexcitability.

Another facet of epilepsy, however, is that of hypersynchronous activity. Indeed, the primary method of seizure detection and of epilepsy diagnoses is the presence of hypersynchronous EEG activity. Intrinsic to the technique of EEG is the measurement of changes in extracellular potential. Field potentials rely on the potential changes induced by ionic flux during neuronal activity (Mitzdorf 1985). This means that an individual neuron will act as both a voltage source and a sink at different times, as depolarization and repolarization occur. The consequence of this fact however, is that the sum of many neurons doing so asynchronously would dampen measured fluctuations and result in

small fluctuations in EEG signal. When such activity is synchronous, the effects of many neurons are additive, resulting in a larger signal deflection as more neurons act simultaneously. These large signal deflections are the defining characteristic of the different varieties of seizures detected by EEG. What then, are the differential roles of hyperexcitability, the basis of our mechanistic understandings in many epilepsy disorders, and of hypersynchrony, the fundamental basis by which we diagnose them? While the work here does not resolve the interface between neuronal hyperexcitability and hypersynchrony, we provide mechanistic information regarding both hyperexcitability and hypersychrony resulting from impairment of VGSC function. The first question we sought to ask in this thesis, explored in Chapter 2, focused on the origins of hyperexcitability in *Scn1b*$^{-/-}$ mice and the contributions of *Scn1b* in modulation of I_{Na} in different cell types. Our finding of impaired I_{Na} heterogeneity in that work also had implications for neuronal synchrony originating from a fundamental relation between heterogeneity and synchrony, which we explored in Chapter 3.

Origins of Neuronal Hyperexcitability in *Scn1b*$^{-/-}$ Mice

DEEs are devastating diseases that affect children in the first year of life and carry a high risk of SUDEP. The work in this thesis was largely performed in the context of understanding the mechanism of DEE linked to homozygous, loss-of-function variants in *SCN1B*, a particularly severe form of DEE. *Scn1b* null mice have neuronal pathfinding defects in brain that precede the onset of epileptiform activity (Brackenbury, Yuan et al. 2013). Subicular neurons of homozygous *Scn1b*-p.C121W mutant mice, have impaired

cell size, increased input resistance, and hyperexcitability (Reid, Leaw et al. 2014). Taken together, these results led to the hypothesis that epilepsy in *SCN1B*-linked DS patients may arise from pyramidal neuron hyperexcitability resulting from impaired neuronal development related to β1's CAM function. We recently reported, however, that deletion of *Scn1b* in adult animals, following normal development, results in seizures and 100% lethality(O'Malley, Hull et al. 2019). This led us to reexamine the origins and role of pyramidal neuron hyperexcitability and ask about the role of PV+ interneurons. We found that *Scn1b* deletion in PV+ neurons, but not in pyramidal neurons, results in seizures and 100% lethality. We also found that *Scn1b* deletion results in hypoexcitability and reduced I_{Na} in cortical PV+ neurons. This work established that, while there exist key remaining differences between *Scn1a* and *Scn1b* models of DEE, there is a shared commonality of impaired fast spiking interneuron excitability, supporting the view that these neurons underlie dysfunction in both models. A question remained however on the origin of hyperexcitability in pyramidal neurons. To investigate this problem, we measured AP firing rates in several groups of pyramidal neurons and found that *Scn1b* deletion differentially impacts the excitability of pyramidal neurons based on network location. This suggested to us that a potential origin of their increased excitability may be network activity. Correspondingly, we found that hyperexcitability in *Scn1b*$^{-/-}$ cortical pyramidal neurons is dependent on network activity and is correlated with network location specific disinhibition. This result provides important information regarding the network specificity of dysfunction and hyperexcitability due to disinhibition in a DEE model. Such information is invaluable, as many nervous system disorders are proposed to be the result of excitatory/inhibitory imbalance and impaired PV+ neuron function. One potential

resolution for why such similar differences in excitatory and inhibitory imbalance could result in differences in pathology is the network locations primarily affected. One important facet of understanding excitatory and inhibitory imbalance is the wide array of interneuron types. While PV+ neurons are thought to be of principle importance in DS, there is known dysfunction in other subtypes of interneurons including those that express somatostatin and VIP, with others potentially affected. The differential location and activity of these interneuron subtypes within the cortex may differentially contribute to inhibitiory tone and activity in different pyramidal neuron populations. Overall, the specificity in circuit dysfunction may guide the targeted treatment of specific networks in the treatment of epilepsy. Many of our current therapies rely on dampening excitability globally, a manipulation that has undesirable side effects.

Key differences between models of *Scn1a* and *Scn1b* DEE were also uncovered. In contrast to *Scn1a*-DS mice, we found that crossing *Scn1b*$^{-/-}$ mice with *Scn8a*$^{med/+}$ mice did not increase survival (Martin, Tang et al. 2007). We found that I_{Na} density is impaired in *Scn1b*$^{-/-}$ cortical layer 6 and subicular pyramidal neurons, showing that β1 normally enhances I_{Na} within multiple CNS neuronal subtypes. Thus, while the *Scn1a* and *Scn1b* models of DEE share a common mechanism of neuronal disinhibition, *Scn1b*$^{-/-}$ mice, which have the more severe phenotype of the two models, having additional deficits that contribute to disease.

Scn1b Deletion Impairs I_{Na} Heterogeneity

In addition to impaired density of VGSCs in pyramidal neurons of *Scn1b*$^{-/-}$ mice, we also detected a relatively larger impairment in the variability of I_{Na} densities between pyramidal neurons. We also observed a strikingly similar impairment in variability in a related *Scn8a* DEE model that we published previously(Lopez-Santiago, Yuan et al. 2017). Chapter 3 focuses on the impact of I_{Na} heterogeneity between neurons on physiology. Immunohistochemical detection of β1 protein expression in mouse cortex shows a wide variability within and between cortical layers, consistent with our functional data discussed above (Wimmer, Harty et al. 2015). This heterogeneity may be regulated through intrinsic developmental lineage factors or through cell signaling cascades regulating the post-translational processing of β1. VGSC β subunits are postulated to modulate gene transcription through sequential BACE1 and γ-secretase cleavage resulting in liberation of an intracellular domain peptide that may translocate to the nucleus (Farzan, Schnitzler et al. 2000). The liberated β1 extracellular domain may, as is the case for the *Scn1b* splice variant β1B, function as a soluble ligand to modulate VGSCs or other cell adhesion molecules in local microcircuits (Patino, Brackenbury et al. 2011). The cell type and VGSC α subunit specific effects of β1 in modulation of channel expression and modulation have confounded our understanding of the role of *Scn1b* in brain (Calhoun and Isom 2014). The remarkable diversity of context-dependent *Scn1b* expression and function correlates with our functional data whereby β1 may be performing a context dependent enhancement of I_{Na}. Furthermore, the difficulty of assigning a specific role to *Scn1b* in the regulation of brain excitability may be the result of a central role for β1 in promoting diversity in the nervous system. Alternatively, the impaired heterogeneity of I_{Na} could be the result of damage or altered development

caused by seizures. This too has interesting implications, as it would imply that neurons are able to down-regulate VGSCs specifically in high firing rate neurons as a means of controlling network excitability. While such mechanisms are likely to occur, this further raises the question of why down regulation of I_{Na} has not been detected in *Scn1a* models of DEE and why *Scn1b* DEE models are comparatively so severe.

Variability and Degeneracy

In the biological sciences we largely focus on measurements of central tendency. In most cases we report the mean with an accepted high level of "biological variability." The universal frustration with variable data in experimental biology, however, is at odds with the broader scope of biology where variation provides the substrate for evolution. The focus on central tendency in neuroscience may be especially misplaced. A characteristic feature of neuroscience is the elaborate and often incomprehensibly complex array of cell morphologies in the brain (RAMON 1952). Much like snowflakes, two neighboring neurons may be similar but obviously unique. Increasingly, neuronal diversity is being investigated in its own right. In neurons, even when the exact location and identity within a circuit is known, variation in specific conductances and function is known to be highly variable between animals, and between circuits within the same animal (Schulz, Goaillard et al. 2006, Haley, Hampton et al. 2018). A related notion is the degeneracy of ion channels. When a neuron has a specific role in a circuit, different combinations of conductances can be utilized for fulfillment of the same activity patterns (Drion, O'Leary et al. 2015). Why then, does the nervous system fail in pathological states,

such as epilepsy, to achieve the appropriate circuit function? In Chapter two of this work, we found that, if network activity is blocked, layer 6 pyramidal neurons of *Scn1b*$^{-/-}$ mice fire at similar rates as *Scn1b*$^{+/+}$ mice at the current injection intensities relevant *in vivo*. This occurs because there is a balance achieved between the decreased mean I_{Na} and the increased mean input resistance, which directly cancel. This is an example of degeneracy in excitability mechanisms that balance to maintain similar mean firing rates. There remains however, a reduction in the variability of I_{Na} between neurons, the effects of which form the basis of Chapter 3 of this work and shows that, while excitability degeneracy mechanisms take place to balance mean firing rates in *Scn1b*$^{-/-}$ mice, other excitability effects remain uncompensated. One such important effect outside of the mean firing rate is neuronal heterogeneity and its effects on synchrony. Importantly, there exists an intimate connection between heterogeneity and synchrony that can both guide and inform our understanding of the role of VGSCs in the nervous system.

Heterogeneity and Response Synchrony

Synchrony is a broad phenomenon that pervades many branches of science and everyday experience. Anyone who has coordinated a group of people meeting at a restaurant has an expectation of synchronous arrival. This kind of synchrony appears trivial, as the event was coordinated beforehand and often has a centralized coordinator. In another form of synchrony, such as a synchronous response of a group of people in reaction to balloon popping, the result is similarly unsurprising due to the large perturbation. A more interesting example of everyday synchrony is two close friends

laughing at a situation with a shared joke, often leaving others baffled by the shared laughter. Here, the two who are in on the joke exhibit synchronous behavior due to a unique shared response. Those who not in on the joke have no basis for a similar response and thus may have no reaction or may even respond differently. In Chapter 3 of this work we investigated the role of VGSCs in response variability to a fluctuating stimulus. *In vivo*, the primary cause of neuronal firing is synaptic activity, resulting in fluctuations in membrane potential. In whole cell recordings of neighboring layer 2/3 pyramidal neurons of the cortex recorded *in vivo*, it has been found that membrane potential fluctuations at the soma have a high correlation between cells. In contrast, neurons *in vivo* have negligible spike correlation (Poulet and Petersen 2008, Gentet, Avermann et al. 2010). How then, might two neurons respond differently to similar inputs? One potential origin of spike response variability is intrinsic biophysical variability, an umbrella which includes I_{Na} density. We investigated the role of I_{Na} density variability between neurons, in lowering spike synchrony in response to fluctuating input. We found that in *Scn1b*$^{-/-}$ pyramidal neurons, response variability was impaired in several ways, including in firing rate heterogeneity, spike time correlation, and spike coherence. We then investigated the capacity of altering I_{Na} to affect spike patterning using a combination of computational modeling and experimentation using a low concentration of TTX. Experimentally, we found that blocking a fraction of VGSCs reduces spike train correlation and phase coherence to levels observed between different neurons. Computationally, we found that over a broad range, I_{Na} density affects spike patterning. This finding has immediate implications for epilepsy and neural coding. As we know that neighboring neurons *in vivo* exhibit correlated membrane potential fluctuations, a property that is likely

to be exacerbated in hypersynchronous conditions such as epilepsy, neuronal diversity in I_{Na} density can desynchronize the resulting spike output. This result also has implications for intellectual disability. The capacity of different neurons to extract unique information from the same signal may be important in the coordination of information in the nervous system.

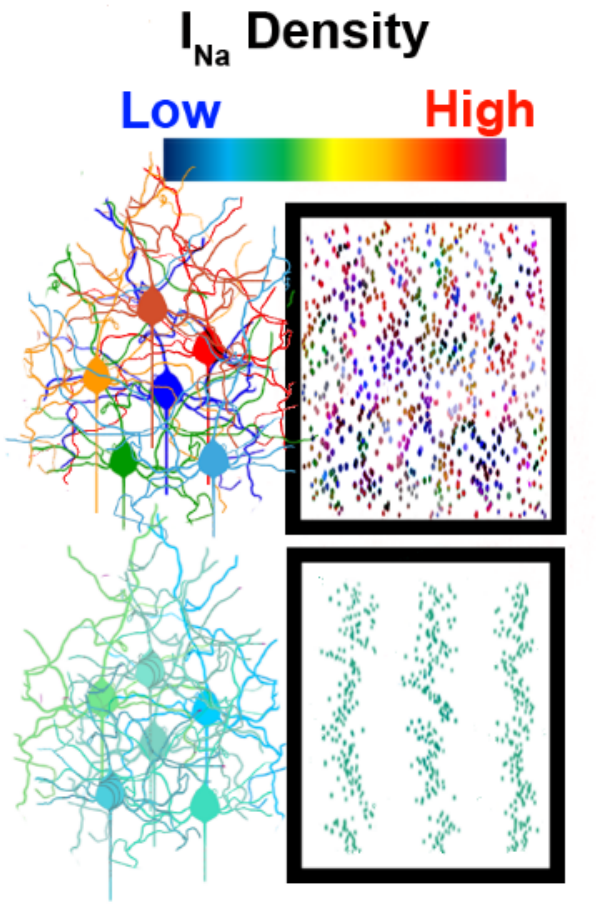


Fig. 4.1. I_{Na} Variability and Synchrony. We find high variability in I_{Na} between neurons which impairs synchrony both from external input and spontaneous synchronization

Heterogeneity and Spontaneous Synchronization

The work discussed above highlights the concept that heterogeneity in response to a shared input is a critical underlying component of synchrony. However, this form of synchrony is highly transient. There exists another, more enigmatic, form of synchronization that occurs without a central coordinator, without a large perturbation or shared external stimulus, and is persistent. This form of synchrony, as in the two friends with the shared joke above and their I_{Na} homogenous neuronal counterparts, is highly dependent on the similarity between the involved elements.

Many physical processes, including those in the brain, have oscillatory properties. Unsurprisingly, groups of oscillators are also subject to synchronization. While two identical oscillators that start in phase will forever remain synchronous unless their phase is differentially perturbed, two oscillators started out of phase can synchronize through influencing each other. This phenomenon was first described by Christian Huygens as “an odd kind of sympathy” where two pendulum clocks sharing a support, when started out of phase, undergo a gradual synchronization of their phases. When uncoupled oscillators with different intrinsic frequencies are started in phase, they will gradually disperse their phases into incoherence. When oscillators are allowed to influence each other, synchronization can occur. Synchronization depends on the strength of the coupling as well as the degree of the differences in the oscillators’ intrinsic frequencies. The diversity of autonomous oscillation frequencies and of the connection strength between oscillators has been found to be central to understanding synchrony in a vast array of fields (Strogatz 2000). A well-studied and broadly applied model of oscillator synchronization is the Kuramoto model (Acebrón, Bonilla et al. 2005) (equation 4.1).

Equation 4.1:

$$\frac{d\theta_i}{dt} = \omega_i + \frac{K}{N}\sum_{j=1}^{N} \sin(\theta_j - \theta_i), \qquad i = 1 \ldots N$$

In this model, the system is composed of N limit-cycle oscillators that have phase θ_i with coupling K and natural frequency ω_i. When coupling between oscillators (K) is low relative to the spread of natural frequencies (ω_i), synchrony is suppressed. By increasing coupling or lowering frequency diversity, spontaneous synchronization can occur in oscillators that were otherwise phase incoherent (Kuramoto 1975). This simple model captures the essential relationship between heterogeneity and coupling that was explored using Hodgkin-Huxley style model neurons in Chapter 3. We showed that I_{Na} heterogeneity is not limited to generating heterogeneity of responses between neurons to the same stimulus. It is also involved in the spontaneous synchronization of networks of neurons through the relationship between network coupling and the spread of I_{Na} density between neurons. We found that heterogeneity in I_{Na}, much like oscillator heterogeneity in the Kuramoto model, shifts the coupling requirements necessary to support network synchronization, here in the form of the number and strength of network connections. The relationship between network coupling and I_{Na} heterogeneity has immediate implications for synchrony in epilepsy. Indeed, the Kuramoto model itself is already used in the study of brain dynamics (Acebrón, Bonilla et al. 2005). Additionally, insults impacting the strength of network coupling, e.g. mossy fiber sprouting or adult neurogenesis, are also implicated as epilepsy mechanisms (Parent, Yu et al. 1997,

Santhakumar, Aradi et al. 2005, Morgan and Soltesz 2008). We have found that neuronal diversity in I_{Na} density has a powerful influence on spontaneous synchronization in the balance between coupling and heterogeneity leading to synchrony, and thus is an important consideration in the mechanisms leading to neuronal synchrony both physiologically and pathophysiologically.

Unanswered Questions and Future Directions

As in many cases in science, every answered question raises further questions. This work is no exception, and may have created more questions than it answered.

We found in Chapter 2 that deletion of *Scn1b* in PV+ neurons results in seizures and death, further, that we did not observe seizures with CAMK2α driven *Scn1b* deletion. While this is evidence that the strong phenotype of lethality and behaviorally observed convulsive seizures is not caused by the action of β1 in CAMK2α positive cells, there are numerous other seizure types that would require electrographic monitoring to detect. This may especially be the case, as patients with *SCN1B* variants also exhibit absence seizures. The detection of defects in layer 6 pyramidal neurons in fact strongly suggest a role for *Scn1b* in absence seizure generation, as it is known that defects in layer 6 pyramidal neurons can cause absence seizures. Furthermore, PV+ neurons in the thalamic reticular nucleus and throughout the rest of the brain may be involved in either convulsive or non-convulsive seizure generation. This raises another important consideration. The work presented here, while covering a relatively broad number of cell

types for an *in vitro* electrophysiological study, does not approach the myriad of known and unknown cell types in the brain, any one of which could be a contributing factor in pathology. β1 is expressed ubiquitously in the nervous system, suggesting that it plays a role in every cell. Another phenotypic feature not addressed in this work is the origin of death with *Scn1b* deletion. *Scn1b* null mice have severe malnutrition and *Scn1b* is known to be important in cardiovascular function. While the targeted deletion of *Scn1b* in mouse heart has been shown previously to not result in death, the mice do have arrhythmias, and patients with *SCN1B* variants have Brugada syndrome, which is associated with sudden cardiac death(Watanabe, Koopmann et al. 2008). In addition, the roles of the brain-heart axis and the expression of β1 in both should not be ignored.

In this work we found PV+ neurons of the *Scn1b* null cortex to be hypoexcitable and to have reduced I_{Na}. This is a result that differs from findings in hippocampal CA1 PV+ neuronal recordings in the homozygous C121W mouse model and in dissociated bipolar shaped neuron recordings from *Scn1b* null hippocampus (Patino, Claes et al. 2009, Reid, Leaw et al. 2014). One simple interpretation is that, as was a large focus of Chapter 2, β1 subunits differentially affect neurons based on network location. This may especially be the case with CA1 PV+ neuron recordings, as the pyramidal neurons in this region are found to not be hyperexcitable in homozygous C121W mutant mice (Reid, Leaw et al. 2014). This raises another important question: Why does disinhibition occur in layer 6 but not in layer 5 in *Scn1b* null brain? There is no clear circuit basis to turn to for an explanation. One possible reason could be the relative frequency of inhibition in layer 5 vs. layer 6. In this work, we found the frequency of sIPSCs to be ~6 Hz in layer 5

and ~4 Hz in layer 6. It could therefore be a matter of the robustness of inhibition, with the weaker inhibition in layer 6 failing. Alternatively, it could be that different cell types are responsible for inhibition in layer 5 and layer 6 pyramidal neurons. A useful measure would be to optogenetically silence different types of interneurons while recording sIPSCs in these regions to gather information on the relative origins of inhibitory tone.

We found that impairing *Scn8a* expression does not phenotypically rescue *Scn1b*$^{-/-}$ mice as it does with *Scn1a*$^{+/-}$ mice, despite the shared PV+ interneuron hypoexcitability (Martin, Tang et al. 2007). We have not yet provided any mechanistic reason why this might be so. One reason could be that $Na_v1.6$ expression could already be impaired in *Scn1b*$^{-/-}$ mice. In cerebellar granule neurons, we know that $Na_v1.6$ expression is reduced. We find that I_{Na} to be impaired in layer 6 and subicular pyramidal neurons and the origin of reduced current could be due to a special relationship between *Scn1b* and *Scn8a*.

I_{Na} density and I_{Na} density heterogeneity are reduced in *Scn1b* null layer 6 and subicular pyramidal neurons. Is this impairment due to an effect of disinhibition? While we did not measure sIPSCs in subiculum, the similarly depolarized resting membrane potential in these cells is suggestive that these neurons are also disinhibited. Could the effects we measured here be a compensatory down regulation of I_{Na} density to limit hyperexcitability resulting from disinhibition? Furthermore, why does increased input resistance occur in these two populations but not throughout the brain? A potential reason is that robust disinhibition in these regions could result in neuronal damage and impaired dendritic arborization. This raises a further question of how do neurons balance such a

large array of neuronal excitability mechanisms, a question for which *Scn1b*$^{-/-}$ mice may be particularly well suited for answering given that we have demonstrated degeneracy in excitability mechanisms that only compensate for a subset of neuronal excitability features.

The measured changes we found in I_{Na} density in pyramidal neurons could be due to loss of an especially I_{Na} rich cell type in the affected regions. This explanation is an intriguing one, as this may be an explanation for our previous inability to detect an effect of *Scn1b* deletion on I_{Na} in CNS neurons. It would be consistent with the primary role of β1 in regulating I_{Na} density as an on-demand I_{Na} enhancer in subsets of cells, which for the majority of neurons may be unnecessary. In pyramidal neurons, we measured I_{Na} density only in the soma. Do VGSC β1 subunits have different roles in modulating α subunits in other subcellular domains? As we know from heterologous systems, β1 subunits differentially modulate the different VGSC α subunits(Hull and Isom 2018). As such, this may be highly likely, as certain α subunits are targeted to specific subcellular domains.

An important future direction for the work presented in Chapter 3 is the investigation of the control mechanisms of I_{Na} density variability between neurons. While biological imprecision is a possibility, such an explanation seems inconsistent with the high success of the nervous system in communication and computation. An important consideration in this regard is that in the olfactory bulb, there already exists evidence that the control of a specific ionic conductance indicates network affiliation, which can be

made homogenous across neurons by genetic manipulation of neurons to be responsive to the same odorant (Angelo, Rancz et al. 2012). It is of note that neuromodulation could serve as both a source and suppressor of I_{Na} density variability between neurons. Another important consideration for the work presented in Chapter 3 is the demonstration that changes in I_{Na} density between neurons can affect neural coding and synchrony *in vivo*. Many results found *in vitro* may not be relevant under *in vivo* conditions. Alternatively, the results may be blunted *in vitro*, where neurons lack the neuromodulation and high synaptic conductances that occur *in vivo*.

In conclusion, this graduate work has made important progress in advancing our understanding of VGSC biology. The results presented here, as stated above, have many avenues for future development. The branching paths of future directions will hopefully continue to be enlightening in the function of VGSCs and aid in the treatment of those with VGSC related disorders.

References

Acebrón, J. A., L. L. Bonilla, C. J. P. Vicente, F. Ritort and R. Spigler (2005). "The Kuramoto model: A simple paradigm for synchronization phenomena." Reviews of modern physics **77**(1): 137.

Adrian, E. D. and Y. Zotterman (1926). "The impulses produced by sensory nerve endings: Part 3. Impulses set up by Touch and Pressure." The Journal of physiology **61**(4): 465-483.

Ahern, C. A., J. Payandeh, F. Bosmans and B. Chanda (2016). "The hitchhiker's guide to the voltage-gated sodium channel galaxy." The Journal of general physiology **147**(1): 1-24.

Akin, E. J., L. Solé, B. Johnson, M. el Beheiry, J.-B. Masson, D. Krapf and M. M. Tamkun (2016). "Single-Molecule Imaging of Na v 1.6 on the Surface of Hippocampal Neurons Reveals Somatic Nanoclusters." Biophysical Journal **111**(6): 1235-1247.

Alroy, G., H. Su and Y. Yaari (1999). "Protein kinase C mediates muscarinic block of intrinsic bursting in rat hippocampal neurons." The Journal of physiology **518**(Pt 1): 71.

Aman, T. K., T. M. Grieco-Calub, C. Chen, R. Rusconi, E. A. Slat, L. L. Isom and I. M. Raman (2009). "Regulation of persistent Na current by interactions between β subunits of voltage-gated Na channels." Journal of Neuroscience **29**(7): 2027-2042.

Angelo, K., E. A. Rancz, D. Pimentel, C. Hundahl, J. Hannibal, A. Fleischmann, B. Pichler and T. W. Margrie (2012). "A biophysical signature of network affiliation and sensory processing in mitral cells." Nature **488**(7411): 375.

Aronica, E., D. Troost, A. J. Rozemuller, B. Yankaya, G. H. Jansen, L. L. Isom and J. A. Gorter (2003). "Expression and regulation of voltage-gated sodium channel β1 subunit protein in human gliosis-associated pathologies." Acta neuropathologica **105**(5): 515-523.

Auld, V. J., A. L. Goldin, D. S. Krafte, J. Marshall, J. M. Dunn, W. A. Catterall, H. A. Lester, N. Davidson and R. J. Dunn (1988). "A rat brain Na+ channel α subunit with novel gating properties." Neuron **1**(6): 449-461.

Azouz, R., M. S. Jensen and Y. Yaari (1994). "Muscarinic modulation of intrinsic burst firing in rat hippocampal neurons." European Journal of Neuroscience **6**(6): 961-966.

Bant, J. S. and I. M. Raman (2010). "Control of transient, resurgent, and persistent current by open-channel block by Na channel β4 in cultured cerebellar granule neurons." Proceedings of the national academy of sciences **107**(27): 12357-12362.

Bao, Y., B. C. Willis, C. R. Frasier, L. F. Lopez-Santiago, X. Lin, R. Ramos-Mondragón, D. S. Auerbach, C. Chen, Z. Wang and J. Anumonwo (2016). "Scn2b Deletion in Mice Results in Ventricular and Atrial Arrhythmias." Circulation: Arrhythmia and Electrophysiology **9**(12): e003923.

Bastian, M., S. Heymann and M. Jacomy (2009). Gephi: an open source software for exploring and manipulating networks. Third international AAAI conference on weblogs and social media.

Bean, B. P. (2007). "The action potential in mammalian central neurons." Nature Reviews Neuroscience **8**(6): 451.

Beck, H. and C. E. Elger (2008). "Epilepsy research: a window onto function and dysfunction of the human brain." Dialogues in clinical neuroscience **10**(1): 7.

Ben-Shalom, R., C. M. Keeshen, K. N. Berrios, J. Y. An, S. J. Sanders and K. J. Bender (2017). "Opposing effects on NaV1. 2 function underlie differences between SCN2A variants observed in individuals with autism spectrum disorder or infantile seizures." Biological psychiatry **82**(3): 224-232.

Bezanilla, F. (2000). "The voltage sensor in voltage-dependent ion channels." Physiological reviews **80**(2): 555-592.

Blackburn-Munro, G. and S. Fleetwood-Walker (1999). "The sodium channel auxiliary subunits β1 and β2 are differentially expressed in the spinal cord of neuropathic rats." Neuroscience **90**(1): 153-164.

Blanchard, M. G., M. H. Willemsen, J. B. Walker, S. D. Dib-Hajj, S. G. Waxman, M. C. Jongmans, T. Kleefstra, B. P. van de Warrenburg, P. Praamstra and J. Nicolai (2015). "De novo gain-of-function and loss-of-function mutations of SCN8A in patients with intellectual disabilities and epilepsy." Journal of medical genetics **52**(5): 330-337.

Boerma, R. S., K. P. Braun, M. P. van de Broek, F. M. van Berkestijn, M. E. Swinkels, E. O. Hagebeuk, D. Lindhout, M. van Kempen, M. Boon and J. Nicolai (2016). "Remarkable phenytoin sensitivity in 4 children with SCN8A-related epilepsy: a molecular neuropharmacological approach." Neurotherapeutics **13**(1): 192-197.

Bogaard, A., J. Parent, M. Zochowski and V. Booth (2009). "Interaction of cellular and network mechanisms in spatiotemporal pattern formation in neuronal networks." Journal of Neuroscience **29**(6): 1677-1687.

Bogaard, A., J. Parent, M. Zochowski and V. Booth (2009). "Interaction of cellular and network mechanisms in spatiotemporal pattern formation in neuronal networks." J Neurosci **29**(6): 1677-1687.

Boiko, T., A. Van Wart, J. H. Caldwell, S. R. Levinson, J. S. Trimmer and G. Matthews (2003). "Functional specialization of the axon initial segment by isoform-specific sodium channel targeting." Journal of Neuroscience **23**(6): 2306-2313.

Bortone, D. S., S. R. Olsen and M. Scanziani (2014). "Translaminar inhibitory cells recruited by layer 6 corticothalamic neurons suppress visual cortex." Neuron **82**(2): 474-485.

Brackenbury, W. J., J. D. Calhoun, C. Chen, H. Miyazaki, N. Nukina, F. Oyama, B. Ranscht and L. L. Isom (2010). "Functional reciprocity between Na+ channel Nav1. 6 and β1 subunits in the coordinated regulation of excitability and neurite outgrowth." Proceedings of the National Academy of Sciences **107**(5): 2283-2288.

Brackenbury, W. J., T. H. Davis, C. Chen, E. A. Slat, M. J. Detrow, T. L. Dickendesher, B. Ranscht and L. L. Isom (2008). "Voltage-gated Na+ channel β1 subunit-mediated neurite outgrowth requires Fyn kinase and contributes to postnatal CNS development in vivo." Journal of Neuroscience **28**(12): 3246-3256.

Brackenbury, W. J. and L. L. Isom (2011). "Na Channel beta Subunits: Overachievers of the Ion Channel Family." Front Pharmacol **2**: 53.

Brackenbury, W. J. and L. L. Isom (2011). "Na+ channel β subunits: overachievers of the ion channel family." Frontiers in pharmacology **2**: 53.

Brackenbury, W. J., Y. Yuan, H. A. O'Malley, J. M. Parent and L. L. Isom (2013). "Abnormal neuronal patterning occurs during early postnatal brain development of Scn1b-null mice and precedes hyperexcitability." Proc Natl Acad Sci U S A **110**(3): 1089-1094.

Brackenbury, W. J., Y. Yuan, H. A. O'Malley, J. M. Parent and L. L. Isom (2013). "Abnormal neuronal patterning occurs during early postnatal brain development of Scn1b-null mice and

precedes hyperexcitability." Proceedings of the National Academy of Sciences **110**(3): 1089-1094.

Briggs, F. (2010). "Organizing principles of cortical layer 6." Front Neural Circuits **4**: 3.

Buffington, S. A. and M. N. Rasband (2013). "Na+ channel-dependent recruitment of Navβ4 to axon initial segments and nodes of Ranvier." Journal of Neuroscience **33**(14): 6191-6202.

Bui, A., H. K. Kim, M. Maroso and I. Soltesz (2015). "Microcircuits in epilepsy: Heterogeneity and hub cells in network synchronization." Cold Spring Harbor perspectives in medicine **5**(11): a022855.

Bunton-Stasyshyn, R. K., J. L. Wagnon, E. R. Wengert, B. S. Barker, A. Faulkner, P. K. Wagley, K. Bhatia, J. M. Jones, M. R. Maniaci and J. M. Parent (2019). "Prominent role of forebrain excitatory neurons in SCN8A encephalopathy." Brain **142**(2): 362-375.

Burgess, D. L., D. C. Kohrman, J. Galt, N. W. Plummer, J. M. Jones, B. Spear and M. H. Meisler (1995). "Mutation of a new sodium channel gene, Scn8a, in the mouse mutant 'motor endplate disease'." Nature Genetics **10**(August): 461-465.

Caldwell, J. H., K. L. Schaller, R. S. Lasher, E. Peles and S. R. Levinson (2000). "Sodium channel Nav1. 6 is localized at nodes of Ranvier, dendrites, and synapses." Proceedings of the National Academy of Sciences **97**(10): 5616-5620.

Calhoun, J. D. and L. L. Isom (2014). "The Role of Non-pore-Forming beta Subunits in Physiology and Pathophysiology of Voltage-Gated Sodium Channels." Handb Exp Pharmacol **221**: 51-89.

Calhoun, J. D. and L. L. Isom (2014). The role of non-pore-forming β subunits in physiology and pathophysiology of voltage-gated sodium channels. Voltage Gated Sodium Channels, Springer**:** 51-89.

Cantrell, A. R. and W. A. Catterall (2001). "Neuromodulation of Na+ channels: An unexpected form of cellular platicity." Nature Reviews Neuroscience **2**(6): 397.

Cantrell, A. R., J. Y. Ma, T. Scheuer and W. A. Catterall (1996). "Muscarinic modulation of sodium current by activation of protein kinase C in rat hippocampal neurons." Neuron **16**(5): 1019-1026.

Cantrell, A. R., T. Scheuer and W. A. Catterall (1999). "Voltage-dependent neuromodulation of Na+ channels by D1-like dopamine receptors in rat hippocampal neurons." Journal of Neuroscience **19**(13): 5301-5310.

Cantrell, A. R., R. D. Smith, A. L. Goldin, T. Scheuer and W. A. Catterall (1997). "Dopaminergic modulation of sodium current in hippocampal neurons via cAMP-dependent phosphorylation of specific sites in the sodium channel α subunit." Journal of Neuroscience **17**(19): 7330-7338.

Carr, D. B., M. Day, A. R. Cantrell, J. Held, T. Scheuer, W. A. Catterall and D. J. Surmeier (2003). "Transmitter modulation of slow, activity-dependent alterations in sodium channel availability endows neurons with a novel form of cellular plasticity." Neuron **39**(5): 793-806.

Catterall, W. A. (1986). "Molecular properties of voltage-sensitive sodium channels." Annual review of biochemistry **55**(1): 953-985.

Catterall, W. A. (1986). "Voltage-dependent gating of sodium channels: correlating structure and function." Trends in Neurosciences **9**: 7-10.

Catterall, W. A. (2010). "Ion channel voltage sensors: structure, function, and pathophysiology." Neuron **67**(6): 915-928.

Catterall, W. A. (2012). "Voltage-gated sodium channels at 60: structure, function and pathophysiology." J Physiol **590**(Pt 11): 2577-2589.

Catterall, W. A. (2012). "Voltage-gated sodium channels at 60: structure, function and pathophysiology." The Journal of physiology **590**(11): 2577-2589.

Catterall, W. A. (2016). Dravet syndrome: a sodium channel interneuronopathy. Ion Channels in Health and Disease, Elsevier**:** 85-111.

Catterall, W. A. (2018). "Dravet Syndrome: A Sodium Channel Interneuronopathy." Curr Opin Physiol **2**: 42-50.

Catterall WA, G. A. and S. Waxman (2005). "International union of pharmacology. xlvii. Nomenclature and structure–function relationships of voltage-gated sodium channels." Pharmacological Rev **57**: 397-409.

Catterall, W. A., A. L. Goldin and S. G. Waxman (2005). "International Union of Pharmacology. XLVII. Nomenclature and structure-function relationships of voltage-gated sodium channels." Pharmacological reviews **57**(4): 397-409.

Catterall, W. A., E. Perez-Reyes, T. P. Snutch and J. Striessnig (2005). "International Union of Pharmacology. XLVIII. Nomenclature and structure-function relationships of voltage-gated calcium channels." Pharmacological reviews **57**(4): 411-425.

Cheah, C. S., H. Y. Frank, R. E. Westenbroek, F. K. Kalume, J. C. Oakley, G. B. Potter, J. L. Rubenstein and W. A. Catterall (2012). "Specific deletion of NaV1. 1 sodium channels in inhibitory interneurons causes seizures and premature death in a mouse model of Dravet syndrome." Proceedings of the National Academy of Sciences **109**(36): 14646-14651.

Cheah, C. S., F. H. Yu, R. E. Westenbroek, F. K. Kalume, J. C. Oakley, G. B. Potter, J. L. Rubenstein and W. A. Catterall (2012). "Specific deletion of NaV1.1 sodium channels in inhibitory

interneurons causes seizures and premature death in a mouse model of Dravet syndrome." Proc Natl Acad Sci U S A **109**(36): 14646-14651.

Chen, C., V. Bharucha, Y. Chen, R. E. Westenbroek, A. Brown, J. D. Malhotra, D. Jones, C. Avery, P. J. Gillespie and K. A. Kazen-Gillespie (2002). "Reduced sodium channel density, altered voltage dependence of inactivation, and increased susceptibility to seizures in mice lacking sodium channel β2-subunits." Proceedings of the National Academy of Sciences **99**(26): 17072-17077.

Chen, C., J. D. Calhoun, Y. Zhang, L. Lopez-Santiago, N. Zhou, T. H. Davis, J. L. Salzer and L. L. Isom (2012). "Identification of the cysteine residue responsible for disulfide linkage of Na+ channel α and β2 subunits." Journal of Biological Chemistry **287**(46): 39061-39069.

Chen, C., T. L. Dickendesher, F. Oyama, H. Miyazaki, N. Nukina and L. L. Isom (2007). "Floxed allele for conditional inactivation of the voltage-gated sodium channel beta1 subunit Scn1b." Genesis **45**(9): 547-553.

Chen, C., J. K. Holth, R. Bunton-Stasyshyn, C. K. Anumonwo, M. H. Meisler, J. L. Noebels and L. L. Isom (2018). "Mapt deletion fails to rescue premature lethality in two models of sodium channel epilepsy." Ann Clin Transl Neurol **5**(8): 982-987.

Chen, C., R. E. Westenbroek, X. Xu, C. A. Edwards, D. R. Sorenson, Y. Chen, D. P. McEwen, H. A. O'Malley, V. Bharucha and L. S. Meadows (2004). "Mice lacking sodium channel β1 subunits display defects in neuronal excitability, sodium channel expression, and nodal architecture." Journal of Neuroscience **24**(16): 4030-4042.

Chen, C., R. E. Westenbroek, X. Xu, C. A. Edwards, D. R. Sorenson, Y. Chen, D. P. McEwen, H. A. O'Malley, V. Bharucha, L. S. Meadows, G. A. Knudsen, A. Vilaythong, J. L. Noebels, T. L. Saunders, T. Scheuer, P. Shrager, W. A. Catterall and L. L. Isom (2004). "Mice lacking sodium

channel beta1 subunits display defects in neuronal excitability, sodium channel expression, and nodal architecture." J Neurosci **24**(16): 4030-4042.

Chen, X., L.-L. Yuan, C. Zhao, S. G. Birnbaum, A. Frick, W. E. Jung, T. L. Schwarz, J. D. Sweatt and D. Johnston (2006). "Deletion of Kv4. 2 gene eliminates dendritic A-type K+ current and enhances induction of long-term potentiation in hippocampal CA1 pyramidal neurons." Journal of Neuroscience **26**(47): 12143-12151.

Chen, Y., H. Y. Frank, E. M. Sharp, D. Beacham, T. Scheuer and W. A. Catterall (2008). "Functional properties and differential neuromodulation of Nav1. 6 channels." Molecular and Cellular Neuroscience **38**(4): 607-615.

Chen, Y., H. Y. Frank, D. J. Surmeier, T. Scheuer and W. A. Catterall (2006). "Neuromodulation of Na+ channel slow inactivation via cAMP-dependent protein kinase and protein kinase C." Neuron **49**(3): 409-420.

Chen, Y. H., T. J. Dale, M. A. Romanos, W. R. Whitaker, X. M. Xie and J. J. Clare (2000). "Cloning, distribution and functional analysis of the type III sodium channel from human brain." European journal of neuroscience **12**(12): 4281-4289.

Clare, J. J., S. N. Tate, M. Nobbs and M. A. Romanos (2000). "Voltage-gated sodium channels as therapeutic targets." Drug discovery today **5**(11): 506-520.

Cox, D. R. (1966). The Statistical Analysis of Series of Events, Springer Netherlands.

Crill, W. E. (1996). "Persistent sodium current in mammalian central neurons." Annual review of physiology **58**(1): 349-362.

Crochet, S. and C. C. Petersen (2006). "Correlating whisker behavior with membrane potential in barrel cortex of awake mice." Nature neuroscience **9**(5): 608.

Cusdin, F. S., D. Nietlispach, J. Maman, T. J. Dale, A. J. Powell, J. J. Clare and A. P. Jackson (2010). "The sodium channel β3-subunit induces multiphasic gating in NaV1. 3 and affects fast inactivation via distinct intracellular regions." Journal of Biological Chemistry **285**(43): 33404-33412.

Das, A., G. Wallace, C. Holmes, M. L. McDowell, J. A. Smith, J. D. Marshall, L. Bonilha, J. C. Edwards, S. S. Glazier and S. K. Ray (2012). "Hippocampal tissue of patients with refractory temporal lobe epilepsy is associated with astrocyte activation, inflammation, and altered expression of channels and receptors." Neuroscience **220**: 237-246.

Das, S., J. Gilchrist, F. Bosmans and F. Van Petegem (2016). "Binary architecture of the Nav1. 2-β2 signaling complex." Elife **5**: e10960.

De Kovel, C. G., M. H. Meisler, E. H. Brilstra, F. M. van Berkestijn, R. van't Slot, S. van Lieshout, I. J. Nijman, J. E. O'Brien, M. F. Hammer and M. Estacion (2014). "Characterization of a de novo SCN8A mutation in a patient with epileptic encephalopathy." Epilepsy research **108**(9): 1511-1518.

de Lecea, L., J. A. del Rio and E. Soriano (1995). "Developmental expression of parvalbumin mRNA in the cerebral cortex and hippocampus of the rat." Brain Res Mol Brain Res **32**(1): 1-13.

De Ligt, J., M. H. Willemsen, B. W. Van Bon, T. Kleefstra, H. G. Yntema, T. Kroes, A. T. Vulto-van Silfhout, D. A. Koolen, P. De Vries and C. Gilissen (2012). "Diagnostic exome sequencing in persons with severe intellectual disability." New England Journal of Medicine **367**(20): 1921-1929.

Deschenes, I. and G. F. Tomaselli (2002). "Modulation of Kv4.3 current by accessory subunits." FEBS Lett **528**(1-3): 183-188.

Deschênes, I. and G. F. Tomaselli (2002). "Modulation of Kv4. 3 current by accessory subunits." FEBS letters **528**(1-3): 183-188.

Destexhe, A., M. Rudolph, J.-M. Fellous and T. J. Sejnowski (2001). "Fluctuating synaptic conductances recreate in vivo-like activity in neocortical neurons." Neuroscience **107**(1): 13-24.

Dilena, R., P. Striano, E. Gennaro, L. Bassi, S. Olivotto, L. Tadini, F. Mosca, S. Barbieri, F. Zara and M. Fumagalli (2017). "Efficacy of sodium channel blockers in SCN2A early infantile epileptic encephalopathy." Brain and Development **39**(4): 345-348.

Dodge, F. and J. Cooley (1973). "Action potential of the motorneuron." IBM Journal of Research and Development **17**(3): 219-229.

Drion, G., T. O'Leary and E. Marder (2015). "Ion channel degeneracy enables robust and tunable neuronal firing rates." Proceedings of the National Academy of Sciences **112**(38): E5361-E5370.

Eaholtz, G., T. Scheuer and W. A. Catterall (1994). "Restoration of inactivation and block of open sodium channels by an inactivation gate peptide." Neuron **12**(5): 1041-1048.

Ecker, A. S., P. Berens, G. A. Keliris, M. Bethge, N. K. Logothetis and A. S. Tolias (2010). "Decorrelated neuronal firing in cortical microcircuits." science **327**(5965): 584-587.

Eggermann, E., Y. Kremer, S. Crochet and C. C. Petersen (2014). "Cholinergic signals in mouse barrel cortex during active whisker sensing." Cell reports **9**(5): 1654-1660.

Ellerkmann, R., S. Remy, J. Chen, D. Sochivko, C. Elger, B. Urban, A. Becker and H. Beck (2003). "Molecular and functional changes in voltage-dependent Na+ channels following pilocarpine-induced status epilepticus in rat dentate granule cells." Neuroscience **119**(2): 323-333.

Errington, A. C., T. Stöhr, C. Heers and G. Lees (2008). "The investigational anticonvulsant lacosamide selectively enhances slow inactivation of voltage-gated sodium channels." Molecular pharmacology **73**(1): 157-169.

Estacion, M., A. Gasser, S. D. Dib-Hajj and S. G. Waxman (2010). "A sodium channel mutation linked to epilepsy increases ramp and persistent current of Nav1. 3 and induces hyperexcitability in hippocampal neurons." Experimental neurology **224**(2): 362-368.

Estacion, M., J. E. O'Brien, A. Conravey, M. F. Hammer, S. G. Waxman, S. D. Dib-Hajj and M. H. Meisler (2014). "A novel de novo mutation of SCN8A (Nav1. 6) with enhanced channel activation in a child with epileptic encephalopathy." Neurobiology of disease **69**: 117-123.

Farzan, M., C. E. Schnitzler, N. Vasilieva, D. Leung and H. Choe (2000). "BACE2, a β-secretase homolog, cleaves at the β site and within the amyloid-β region of the amyloid-β precursor protein." Proceedings of the National Academy of Sciences **97**(17): 9712-9717.

Favero, M., N. P. Sotuyo, E. Lopez, J. A. Kearney and E. M. Goldberg (2018). "A transient developmental window of fast-spiking interneuron dysfunction in a mouse model of Dravet syndrome." Journal of Neuroscience **38**(36): 7912-7927.

Featherstone, D. E., J. E. Richmond and P. C. Ruben (1996). "Interaction between fast and slow inactivation in Skm1 sodium channels." Biophysical Journal **71**(6): 3098-3109.

Fisher, R. S., C. Acevedo, A. Arzimanoglou, A. Bogacz, J. H. Cross, C. E. Elger, J. Engel, L. Forsgren, J. A. French and M. Glynn (2014). "ILAE official report: a practical clinical definition of epilepsy." Epilepsia **55**(4): 475-482.

Fleidervish, I. A., A. Friedman and M. Gutnick (1996). "Slow inactivation of Na+ current and slow cumulative spike adaptation in mouse and guinea-pig neocortical neurones in slices." The Journal of physiology **493**(1): 83-97.

Fleidervish, I. A., N. Lasser-Ross, M. J. Gutnick and W. N. Ross (2010). "Na+ imaging reveals little difference in action potential–evoked Na+ influx between axon and soma." Nature neuroscience **13**(7): 852.

Frank, H. Y. and W. A. Catterall (2003). "Overview of the voltage-gated sodium channel family." Genome biology **4**(3): 207.

Frank, H. Y., M. Mantegazza, R. E. Westenbroek, C. A. Robbins, F. Kalume, K. A. Burton, W. J. Spain, G. S. McKnight, T. Scheuer and W. A. Catterall (2006). "Reduced sodium current in GABAergic interneurons in a mouse model of severe myoclonic epilepsy in infancy." Nature neuroscience **9**(9): 1142.

Gajewiak, J., L. Azam, J. Imperial, A. Walewska, B. R. Green, P. K. Bandyopadhyay, S. Raghuraman, B. Ueberheide, M. Bern and H. M. Zhou (2014). "A disulfide tether stabilizes the block of sodium channels by the conotoxin μO § -GVIIJ." Proceedings of the National Academy of Sciences **111**(7): 2758-2763.

Galán, R. F., G. B. Ermentrout and N. N. Urban (2008). "Optimal time scale for spike-time reliability: theory, simulations, and experiments." Journal of neurophysiology **99**(1): 277-283.

Gardella, E., F. Becker, R. S. Møller, J. Schubert, J. R. Lemke, L. H. Larsen, H. Eiberg, M. Nothnagel, H. Thiele and J. Altmüller (2016). "Benign infantile seizures and paroxysmal dyskinesia caused by an SCN8A mutation." Annals of neurology **79**(3): 428-436.

Gassen, V., L. Koen, M. De Wit, M. J. Koerkamp, M. G. Rensen, P. C. Van Rijen, F. C. Holstege, D. Lindhout and P. N. De Graan (2008). "Possible role of the innate immunity in temporal lobe epilepsy." Epilepsia **49**(6): 1055-1065.

Gastaldi, M., A. Robaglia-Schlupp, A. Massacrier, R. Planells and P. Cau (1998). "mRNA coding for voltage-gated sodium channel β2 subunit in rat central nervous system: cellular distribution and changes following kainate-induced seizures." Neuroscience letters **249**(1): 53-56.

Gawne, T. J., T. W. Kjaer, J. A. Hertz and B. J. Richmond (1996). "Adjacent visual cortical complex cells share about 20% of their stimulus-related information." Cerebral Cortex **6**(3): 482-489.

Gentet, L. J., M. Avermann, F. Matyas, J. F. Staiger and C. C. Petersen (2010). "Membrane potential dynamics of GABAergic neurons in the barrel cortex of behaving mice." Neuron **65**(3): 422-435.

Gersbacher, M. T., D. Y. Kim, R. Bhattacharyya and D. M. Kovacs (2010). "Identification of BACE1 cleavage sites in human voltage-gated sodium channel beta 2 subunit." Molecular neurodegeneration **5**(1): 61.

Gheyara, A. L., R. Ponnusamy, B. Djukic, R. J. Craft, K. Ho, W. Guo, M. M. Finucane, P. E. Sanchez and L. Mucke (2014). "Tau reduction prevents disease in a mouse model of Dravet syndrome." Ann Neurol **76**(3): 443-456.

Gilchrist, J., S. Das, F. Van Petegem and F. Bosmans (2013). "Crystallographic insights into sodium-channel modulation by the β4 subunit." Proceedings of the National Academy of Sciences **110**(51): E5016-E5024.

Gjorgjieva, J., G. Drion and E. Marder (2016). "Computational implications of biophysical diversity and multiple timescales in neurons and synapses for circuit performance." Curr Opin Neurobiol **37**: 44-52.

Goff, K. M. and E. M. Goldberg (2019). "Vasoactive intestinal peptide-expressing interneurons are impaired in a mouse model of Dravet syndrome." eLife **8**.

Goldin, A. L., T. Snutch, H. Lübbert, A. Dowsett, J. Marshall, V. Auld, W. Downey, L. C. Fritz, H. A. Lester and R. Dunn (1986). "Messenger RNA coding for only the alpha subunit of the rat brain Na channel is sufficient for expression of functional channels in Xenopus oocytes." Proceedings of the National Academy of Sciences **83**(19): 7503-7507.

Gong, B., K. J. Rhodes, Z. Bekele-Arcuri and J. S. Trimmer (1999). "Type I and type II Na+ channel α-subunit polypeptides exhibit distinct spatial and temporal patterning, and association with auxiliary subunits in rat brain." Journal of Comparative Neurology **412**(2): 342-352.

Gorter, J. A., E. A. Van Vliet, F. H. L. Da Silva, L. L. Isom and E. Aronica (2002). "SHORT COMMUNICATION Sodium channel β1-subunit expression is increased in reactive astrocytes in a rat model for mesial temporal lobe epilepsy." European Journal of Neuroscience **16**(2): 360-364.

Grieco, T. M., J. D. Malhotra, C. Chen, L. L. Isom and I. M. Raman (2005). "Open-channel block by the cytoplasmic tail of sodium channel β4 as a mechanism for resurgent sodium current." Neuron **45**(2): 233-244.

Grinton, B. E., S. E. Heron, J. T. Pelekanos, S. M. Zuberi, S. Kivity, Z. Afawi, T. C. Williams, D. M. Casalaz, S. Yendle and I. Linder (2015). "Familial neonatal seizures in 36 families: clinical and genetic features correlate with outcome." Epilepsia **56**(7): 1071-1080.

GuY, H. R. and P. Seetharamulu (1986). "Molecular model of the action potential sodium channel." Proceedings of the National Academy of Sciences **83**(2): 508-512.

Hakim, P., N. Brice, R. Thresher, J. Lawrence, Y. Zhang, A. Jackson, A. Grace and C. H. Huang (2010). "Scn3b knockout mice exhibit abnormal sino-atrial and cardiac conduction properties." Acta physiologica **198**(1): 47-59.

Hakim, P., I. S. Gurung, T. H. Pedersen, R. Thresher, N. Brice, J. Lawrence, A. A. Grace and C. L.-H. Huang (2008). "Scn3b knockout mice exhibit abnormal ventricular electrophysiological properties." Progress in biophysics and molecular biology **98**(2): 251-266.

Haley, J. A., D. Hampton and E. Marder (2018). "Two central pattern generators from the crab, Cancer borealis, respond robustly and differentially to extreme extracellular pH." eLife **7**: e41877.

Han, S., C. Tai, R. E. Westenbroek, H. Y. Frank, C. S. Cheah, G. B. Potter, J. L. Rubenstein, T. Scheuer, O. Horacio and W. A. Catterall (2012). "Autistic-like behaviour in Scn1a+/-mice and rescue by enhanced GABA-mediated neurotransmission." Nature **489**(7416): 385-390.

Hartshorne, R., D. Messner, J. Coppersmith and W. A. Catterall (1982). "The saxitoxin receptor of the sodium channel from rat brain. Evidence for two nonidentical beta subunits." Journal of Biological Chemistry **257**(23): 13888-13891.

Hartshorne, R. P., D. J. Messner, J. C. Coppersmith and W. A. Catterall (1982). "The saxitoxin receptor of the sodium channel from rat brain Evidence for two nonidentical beta subunits." J.Biol.Chem. **257**: 13888-13891.

Heinemann, S. H., H. Terlau, W. Stühmer, K. Imoto and S. Numa (1992). "Calcium channel characteristics conferred on the sodium channel by single mutations." Nature **356**(6368): 441.

Heron, S. E., K. M. Crossland, E. Andermann, H. A. Phillips, A. J. Hall, A. Bleasel, M. Shevell, S. Mercho, M.-H. Seni and M.-C. Guiot (2002). "Sodium-channel defects in benign familial neonatal-infantile seizures." The Lancet **360**(9336): 851-852.

Higurashi, N., T. Uchida, C. Lossin, Y. Misumi, Y. Okada, W. Akamatsu, Y. Imaizumi, B. Zhang, K. Nabeshima and M. X. Mori (2013). "A human Dravet syndrome model from patient induced pluripotent stem cells." Molecular brain **6**(1): 19.

Hille, B. (2001). Ion Channels of Excitable Membranes. Sunderland, MA, Sinauer Associates, Inc.

Hille, B. (2001). Ion channels of excitable membranes, Sinauer Sunderland, MA.

Holland, K. D., J. A. Kearney, T. A. Glauser, G. Buck, M. Keddache, J. R. Blankston, I. W. Glaaser, R. S. Kass and M. H. Meisler (2008). "Mutation of sodium channel SCN3A in a patient with cryptogenic pediatric partial epilepsy." Neuroscience letters **433**(1): 65-70.

Hu, W., C. Tian, T. Li, M. Yang, H. Hou and Y. Shu (2009). "Distinct contributions of Na v 1.6 and Na v 1.2 in action potential initiation and backpropagation." Nature neuroscience **12**(8): 996.

Hu, W., C. Tian, T. Li, M. Yang, H. Hou and Y. Shu (2009). "Distinct contributions of Na(v)1.6 and Na(v)1.2 in action potential initiation and backpropagation." Nat Neurosci **12**(8): 996-1002.

Hull, J. M. and L. L. Isom (2017). "Voltage-gated sodium channel beta subunits: The power outside the pore in brain development and disease." Neuropharmacology.

Hull, J. M. and L. L. Isom (2018). "Voltage-gated sodium channel β subunits: the power outside the pore in brain development and disease." Neuropharmacology **132**: 43-57.

Huth, T., A. Rittger, P. Saftig and C. Alzheimer (2011). "β-Site APP-cleaving enzyme 1 (BACE1) cleaves cerebellar Na+ channel β4-subunit and promotes Purkinje cell firing by slowing the decay of resurgent Na+ current." Pflügers Archiv-European Journal of Physiology **461**(3): 355-371.

Isom, L., D. Ragsdale, K. De Jongh, R. E. Westenbroek, B. Reber, T. Scheuer and W. A. Catterall (1995). "Structure and function of the β2 subunit of brain sodium channels, a transmembrane glycoprotein with a CAM motif." Cell **83**(3): 433-442.

Isom, L. L. and W. A. Catterall (1996). "Na+ channel subunits and Ig domains." Nature **383**(6598): 307.

Isom, L. L. and W. A. Catterall (1996). "Na^+ channel subunits and Ig domains." Nature **383**: 307-308.

Isom, L. L. and K. De Jongh (1992). "Primary Structure and Functional Expression of the (Beta1) Subunit of the Rat Brain Sodium Channel." Science **256**(5058): 839.

Isom, L. L., K. S. De Jongh and W. A. Catterall (1994). "Auxiliary subunits of voltage-gated ion channels." Neuron **12**(6): 1183-1194.

Isom, L. L., T. Scheuer, A. B. Brownstein, D. S. Ragsdale, B. J. Murphy and W. A. Catterall (1995). "Functional co-expression of the b1 and type IIA a subunits of sodium channels in a mammalian cell line." J. Biol. Chem. **270**: 3306-3312.

Jan, L. Y. and Y. N. Jan (2012). "Voltage-gated potassium channels and the diversity of electrical signalling." The Journal of physiology **590**(11): 2591-2599.

Johnson, D. and E. S. Bennett (2006). "Isoform-specific effects of the β2 subunit on voltage-gated sodium channel gating." Journal of Biological Chemistry **281**(36): 25875-25881.

Johnson, D., M. L. Montpetit, P. J. Stocker and E. S. Bennett (2004). "The sialic acid component of the β1 subunit modulates voltage-gated sodium channel function." Journal of Biological Chemistry **279**(43): 44303-44310.

Johnson, K. W., K. F. Herold, T. A. Milner, H. C. Hemmings Jr and J. Platholi (2017). "Sodium channel subtypes are differentially localized to pre-and post-synaptic sites in rat hippocampus." Journal of Comparative Neurology **525**(16): 3563-3578.

Joho, R. H., J. R. Moorman, A. M. Vandongen, G. E. Kirsch, H. Silberberg, G. Schuster and A. M. Brown (1990). "Toxin and kinetic profile of rat brain type III sodium channels expressed in Xenopus oocytes." Molecular Brain Research **7**(2): 105-113.

Jones, S. L. and T. M. Svitkina (2016). "Axon initial segment cytoskeleton: architecture, development, and role in neuron polarity." Neural plasticity **2016**.

Jung, H.-Y., T. Mickus and N. Spruston (1997). "Prolonged sodium channel inactivation contributes to dendritic action potential attenuation in hippocampal pyramidal neurons." Journal of Neuroscience **17**(17): 6639-6646.

Kalume, F., J. C. Oakley, R. E. Westenbroek, J. Gile, O. Horacio, T. Scheuer and W. A. Catterall (2015). "Sleep impairment and reduced interneuron excitability in a mouse model of Dravet Syndrome." Neurobiology of disease **77**: 141-154.

Katz, E., O. Stoler, A. Scheller, Y. Khrapunsky, S. Goebbels, F. Kirchhoff, M. J. Gutnick, F. Wolf and I. A. Fleidervish (2018). "Role of sodium channel subtype in action potential generation by neocortical pyramidal neurons." Proceedings of the National Academy of Sciences **115**(30): E7184-E7192.

Kazarinova-Noyes, K., J. D. Malhotra, D. P. McEwen, L. N. Mattei, E. O. Berglund, B. Ranscht, S. R. Levinson, M. Schachner, P. Shrager and L. L. Isom (2001). "Contactin associates with Na+ channels and increases their functional expression." Journal of Neuroscience **21**(19): 7517-7525.

Kazarinova-Noyes, K., J. D. Malhotra, D. P. McEwen, L. N. Mattei, E. O. Berglund, B. Ranscht, S. R. Levinson, M. Schachner, P. Shrager, L. L. Isom and Z.-C. Xiao (2001). "Contactin associates with Na^+ channels and increases their functional expression." J. Neurosci. **21**: 7517-7525.

Kazen-Gillespie, K. A., D. S. Ragsdale, M. R. D'Andrea, L. N. Mattei, K. E. Rogers and L. L. Isom (2000). "Cloning, localization, and functional expression of sodium channel β1A subunits." Journal of Biological Chemistry **275**(2): 1079-1088.

Kearney, J., N. Plummer, M. Smith, J. Kapur, T. Cummins, S. Waxman, A. Goldin and M. Meisler (2001). "A gain-of-function mutation in the sodium channel gene Scn2a results in seizures and behavioral abnormalities." Neuroscience **102**(2): 307-317.

Kim, D. Y., B. W. Carey, H. Wang, L. A. Ingano, A. M. Binshtok, M. H. Wertz, W. H. Pettingell, P. He, V. M.-Y. Lee and C. J. Woolf (2007). "BACE1 regulates voltage-gated sodium channels and neuronal activity." Nature cell biology **9**(7): 755-764.

Kim, D. Y., L. A. M. Ingano, B. W. Carey, W. H. Pettingell and D. M. Kovacs (2005). "Presenilin/γ-secretase-mediated cleavage of the voltage-gated sodium channel β2-subunit regulates cell adhesion and migration." Journal of Biological Chemistry **280**(24): 23251-23261.

Kim, J., C. J. Matney, A. Blankenship, S. Hestrin and S. P. Brown (2014). "Layer 6 corticothalamic neurons activate a cortical output layer, layer 5a." J Neurosci **34**(29): 9656-9664.

Kiss, T. (2008). "Persistent Na-channels: Origin and function: A review János Salánki memory lecture." Acta Biologica Hungarica **59**(Supplement 2): 1-12.

Ko, S.-H., P. W. Lenkowski, H. C. Lee, J. P. Mounsey and M. K. Patel (2005). "Modulation of Nav1. 5 by β1-and β3-subunit co-expression in mammalian cells." Pflügers Archiv **449**(4): 403-412.

Kole, M. H., S. U. Ilschner, B. M. Kampa, S. R. Williams, P. C. Ruben and G. J. Stuart (2008). "Action potential generation requires a high sodium channel density in the axon initial segment." Nature neuroscience **11**(2): 178.

Kontis, K. J., A. Rounaghi and A. L. Goldin (1997). "Sodium channel activation gating is affected by substitutions of voltage sensor positive charges in all four domains." The Journal of general physiology **110**(4): 391-401.

Krafte, D. S., T. P. Snutch, J. P. Leonard, N. Davidson and H. A. Lester (1988). "Evidence for the involvement of more than one mRNA species in controlling the inactivation process of rat and rabbit brain Na channels expressed in Xenopus oocytes." Journal of Neuroscience **8**(8): 2859-2868.

Krahe, R. and F. Gabbiani (2004). "Burst firing in sensory systems." Nature Reviews Neuroscience **5**(1): 13-23.

Kruger, L. C., H. A. O'Malley, J. M. Hull, A. Kleeman, G. A. Patino and L. L. Isom (2016). "β1-C121W Is Down But Not Out: Epilepsy-Associated Scn1b-C121W Results in a Deleterious Gain-of-Function." Journal of Neuroscience **36**(23): 6213-6224.

Krzemien, D. M., K. L. Schaller, S. R. Levinson and J. H. Caldwell (2000). "Immunolocalization of sodium channel isoform NaCh6 in the nervous system." Journal of Comparative Neurology **420**(1): 70-83.

Kuramoto, Y. (1975). Self-entrainment of a population of coupled non-linear oscillators. Berlin, Heidelberg, Springer.

Kwan, P. and M. J. Brodie (2000). "Early identification of refractory epilepsy." New England Journal of Medicine **342**(5): 314-319.

Laedermann, C. J., N. Syam, I. Decosterd and H. Abriel (2013). "β1-and β3-voltage-gated sodium channel subunits modulate cell surface expression and glycosylation of Nav1. 7 in HEK293 cells." Frontiers in cellular neuroscience **7**: 137.

Lai, H. C. and L. Y. Jan (2006). "The distribution and targeting of neuronal voltage-gated ion channels." Nature Reviews Neuroscience **7**(7): 548.

Larsen, J., G. L. Carvill, E. Gardella, G. Kluger, G. Schmiedel, N. Barisic, C. Depienne, E. Brilstra, Y. Mang and J. E. K. Nielsen (2015). "The phenotypic spectrum of SCN8A encephalopathy." Neurology **84**(5): 480-489.

Lau, C., A. B. Ettinger, S. Hamberger, K. Fanning and M. L. Reed (2012). "Do mood instability symptoms in epilepsy represent formal bipolar disorder?" Epilepsia **53**(2): e37-e40.

Lauxmann, S., N. Boutry-Kryza, C. Rivier, S. Mueller, U. B. Hedrich, S. Maljevic, P. Szepetowski, H. Lerche and G. Lesca (2013). "An SCN2A mutation in a family with infantile seizures from Madagascar reveals an increased subthreshold N a+ current." Epilepsia **54**(9): e117-e121.

Lein, E. S., M. J. Hawrylycz, N. Ao, M. Ayres, A. Bensinger, A. Bernard, A. F. Boe, M. S. Boguski, K. S. Brockway and E. J. Byrnes (2007). "Genome-wide atlas of gene expression in the adult mouse brain." Nature **445**(7124): 168-176.

Lenkowski, P. W., B. S. Shah, A. E. Dinn, K. Lee and M. K. Patel (2003). "Lidocaine block of neonatal Na v 1.3 is differentially modulated by co-expression of β1 and β3 subunits." European journal of pharmacology **467**(1): 23-30.

Leterrier, C. (2018). "The axon initial segment: an updated viewpoint." Journal of Neuroscience **38**(9): 2135-2145.

Levisohn, P. M. (2007). "The autism-epilepsy connection." Epilepsia **48**(s9): 33-35.

Lewis, A. H. and I. M. Raman (2011). "Cross-species conservation of open-channel block by Na channel β4 peptides reveals structural features required for resurgent Na current." Journal of Neuroscience **31**(32): 11527-11536.

Lewis, A. H. and I. M. Raman (2014). "Resurgent current of voltage-gated Na+ channels." The Journal of physiology **592**(22): 4825-4838.

Li, M., J. W. West, R. Numann, B. J. Murphy, T. Scheuer and W. A. Catterall (1993). "Convergent regulation of sodium channels by protein kinase C and cAMP-dependent protein kinase." Science **261**(5127): 1439-1442.

Li, T., C. Tian, P. Scalmani, C. Frassoni, M. Mantegazza, Y. Wang, M. Yang, S. Wu and Y. Shu (2014). "Action potential initiation in neocortical inhibitory interneurons." PLoS biology **12**(9): e1001944.

Liao, Y., A.-K. Anttonen, E. Liukkonen, E. Gaily, S. Maljevic, S. Schubert, A. Bellan-Koch, S. Petrou, V. Ahonen and H. Lerche (2010). "SCN2A mutation associated with neonatal epilepsy, late-onset episodic ataxia, myoclonus, and pain." Neurology **75**(16): 1454-1458.

Lipkind, G. M. and H. A. Fozzard (2008). "Voltage-gated Na channel selectivity: the role of the conserved domain III lysine residue." The Journal of general physiology **131**(6): 523-529.

Liu, Y., L. F. Lopez-Santiago, Y. Yuan, J. M. Jones, H. Zhang, H. A. O'Malley, G. A. Patino, J. E. O'Brien, R. Rusconi and A. Gupta (2013). "Dravet syndrome patient-derived neurons suggest a novel epilepsy mechanism." Annals of neurology **74**(1): 128-139.

Lopez-Santiago, L. F., W. J. Brackenbury, C. Chen and L. L. Isom (2011). "Na+ channel Scn1b gene regulates dorsal root ganglion nociceptor excitability in vivo." Journal of Biological Chemistry **286**(26): 22913-22923.

Lopez-Santiago, L. F., M. Pertin, X. Morisod, C. Chen, S. Hong, J. Wiley, I. Decosterd and L. L. Isom (2006). "Sodium channel β2 subunits regulate tetrodotoxin-sensitive sodium channels in small dorsal root ganglion neurons and modulate the response to pain." Journal of Neuroscience **26**(30): 7984-7994.

Lopez-Santiago, L. F., Y. Yuan, J. L. Wagnon, J. M. Hull, C. R. Frasier, H. A. O'Malley, M. H. Meisler and L. L. Isom (2017). "Neuronal hyperexcitability in a mouse model of SCN8A epileptic encephalopathy." Proc Natl Acad Sci U S A.

Lopez-Santiago, L. F., Y. Yuan, J. L. Wagnon, J. M. Hull, C. R. Frasier, H. A. O'Malley, M. H. Meisler and L. L. Isom (2017). "Neuronal hyperexcitability in a mouse model of SCN8A epileptic encephalopathy." Proceedings of the National Academy of Sciences **114**(9): 2383-2388.

Lorincz, A. and Z. Nusser (2010). "Molecular identity of dendritic voltage-gated sodium channels." Science **328**(5980): 906-909.

Louis, E. K. S. (2011). "Sleep and epilepsy: strange bedfellows no more." Minerva pneumologica **50**(3): 159.

Lucas, P. T., L. S. Meadows, J. Nicholls and D. S. Ragsdale (2005). "An epilepsy mutation in the β1 subunit of the voltage-gated sodium channel results in reduced channel sensitivity to phenytoin." Epilepsy research **64**(3): 77-84.

Mainen, Z. F., J. Joerges, J. R. Huguenard and T. J. Sejnowski (1995). "A model of spike initiation in neocortical pyramidal neurons." Neuron **15**(6): 1427-1439.

Mainen, Z. F. and T. J. Sejnowski (1995). "Reliability of spike timing in neocortical neurons." Science **268**(5216): 1503-1506.

Mainen, Z. F. and T. J. Sejnowski (1996). "Influence of dendritic structure on firing pattern in model neocortical neurons." Nature **382**(6589): 363.

Makinson, C. D., B. S. Tanaka, J. M. Sorokin, J. C. Wong, C. A. Christian, A. L. Goldin, A. Escayg and J. R. Huguenard (2017). "Regulation of thalamic and cortical network synchrony by Scn8a." Neuron **93**(5): 1165-1179. e1166.

Makita, N., P. B. Bennett and A. L. George Jr (1996). "Molecular determinants of β1 subunit-induced gating modulation in voltage-dependent Na+ channels." Journal of Neuroscience **16**(22): 7117-7127.

Malhotra, J. D., C. Chen, I. Rivolta, H. Abriel, R. Malhotra, L. N. Mattei, F. C. Brosius, R. S. Kass and L. L. Isom (2001). "Characterization of sodium channel α-and β-subunits in rat and mouse cardiac myocytes." Circulation **103**(9): 1303-1310.

Malhotra, J. D., K. Kazen-Gillespie, M. Hortsch and L. L. Isom (2000). "Sodium channel β subunits mediate homophilic cell adhesion and recruit ankyrin to points of cell-cell contact." Journal of Biological Chemistry **275**(15): 11383-11388.

Malhotra, J. D., M. C. Koopmann, K. A. Kazen-Gillespie, N. Fettman, M. Hortsch and L. L. Isom (2002). "Structural requirements for interaction of sodium channel β1 subunits with ankyrin." Journal of Biological Chemistry **277**(29): 26681-26688.

Malhotra, J. D., V. Thyagarajan, C. Chen and L. L. Isom (2004). "Tyrosine-phosphorylated and nonphosphorylated sodium channel β1 subunits are differentially localized in cardiac myocytes." Journal of Biological Chemistry **279**(39): 40748-40754.

Marin, O. (2012). "Interneuron dysfunction in psychiatric disorders." Nat Rev Neurosci **13**(2): 107-120.

Marini, C., I. E. Scheffer, R. Nabbout, A. Suls, P. De Jonghe, F. Zara and R. Guerrini (2011). "The genetics of Dravet syndrome." Epilepsia **52 Suppl 2**: 24-29.

Marionneau, C., Y. Carrasquillo, A. J. Norris, R. R. Townsend, L. L. Isom, A. J. Link and J. M. Nerbonne (2012). "The sodium channel accessory subunit Navbeta1 regulates neuronal excitability through modulation of repolarizing voltage-gated K(+) channels." J Neurosci **32**(17): 5716-5727.

Marionneau, C., Y. Carrasquillo, A. J. Norris, R. R. Townsend, L. L. Isom, A. J. Link and J. M. Nerbonne (2012). "The sodium channel accessory subunit Navβ1 regulates neuronal excitability through modulation of repolarizing voltage-gated K+ channels." Journal of Neuroscience **32**(17): 5716-5727.

Martin, M. S., B. Tang, L. A. Papale, F. H. Yu, W. A. Catterall and A. Escayg (2007). "The voltage-gated sodium channel Scn8a is a genetic modifier of severe myoclonic epilepsy of infancy." Hum Mol Genet **16**(23): 2892-2899.

Martin, M. S., B. Tang, L. A. Papale, F. H. Yu, W. A. Catterall and A. Escayg (2007). "The voltage-gated sodium channel Scn8a is a genetic modifier of severe myoclonic epilepsy of infancy." Human molecular genetics **16**(23): 2892-2899.

Matalon, D., E. Goldberg, L. Medne and E. D. Marsh (2014). "Confirming an expanded spectrum of SCN2A mutations: a case series." Epileptic Disorders **16**(1): 13-18.

Maurice, N., T. Tkatch, M. Meisler, L. K. Sprunger and D. J. Surmeier (2001). "D1/D5 dopamine receptor activation differentially modulates rapidly inactivating and persistent sodium currents in prefrontal cortex pyramidal neurons." Journal of Neuroscience **21**(7): 2268-2277.

McCormick, K. A., L. L. Isom, D. Ragsdale, D. Smith, T. Scheuer and W. A. Catterall (1998). "Molecular determinants of Na+ channel function in the extracellular domain of the β1 subunit." Journal of Biological Chemistry **273**(7): 3954-3962.

McCormick, K. A., J. Srinivasan, K. White, T. Scheuer and W. A. Catterall (1999). "The extracellular domain of the β1 subunit is both necessary and sufficient for β1-like modulation of sodium channel gating." Journal of Biological Chemistry **274**(46): 32638-32646.

McEwen, D. P., C. Chen, L. S. Meadows, L. Lopez-Santiago and L. L. Isom (2009). "The voltage-gated Na+ channel β3 subunit does not mediate trans homophilic cell adhesion or associate with the cell adhesion molecule contactin." Neuroscience letters **462**(3): 272-275.

McEwen, D. P. and L. L. Isom (2004). "Heterophilic interactions of sodium channel β1 subunits with axonal and glial cell adhesion molecules." Journal of Biological Chemistry **279**(50): 52744-52752.

McEwen, D. P., L. S. Meadows, C. Chen, V. Thyagarajan and L. L. Isom (2004). "Sodium channel β1 subunit-mediated modulation of Nav1. 2 currents and cell surface density is dependent on interactions with contactin and ankyrin." Journal of Biological Chemistry **279**(16): 16044-16049.

Meadows, L. S., J. Malhotra, A. Loukas, V. Thyagarajan, K. A. Kazen-Gillespie, M. C. Koopman, S. Kriegler, L. L. Isom and D. S. Ragsdale (2002). "Functional and biochemical analysis of a sodium channel β1 subunit mutation responsible for generalized epilepsy with febrile seizures plus type 1." Journal of Neuroscience **22**(24): 10699-10709.

Meisler, M. H., G. Helman, M. F. Hammer, B. E. Fureman, W. D. Gaillard, A. L. Goldin, S. Hirose, A. Ishii, B. L. Kroner and C. Lossin (2016). "SCN8A encephalopathy: research progress and prospects." Epilepsia **57**(7): 1027-1035.

Meisler, M. H., G. Helman, M. F. Hammer, B. E. Fureman, W. D. Gaillard, A. L. Goldin, S. Hirose, A. Ishii, B. L. Kroner, C. Lossin, H. C. Mefford, J. M. Parent, M. Patel, J. Schreiber, R. Stewart, V. Whittemore, K. Wilcox, J. L. Wagnon, P. L. Pearl, A. Vanderver and I. E. Scheffer (2016). "SCN8A encephalopathy: Research progress and prospects." Epilepsia **57**(7): 1027-1035.

Meisler, M. H. and J. A. Kearney (2005). "Sodium channel mutations in epilepsy and other neurological disorders." The Journal of clinical investigation **115**(8): 2010-2017.

Mercimek-Mahmutoglu, S., J. Patel, D. Cordeiro, S. Hewson, D. Callen, E. J. Donner, C. D. Hahn, P. Kannu, J. Kobayashi and B. A. Minassian (2015). "Diagnostic yield of genetic testing in epileptic encephalopathy in childhood." Epilepsia **56**(5): 707-716.

Merrick, E. C., C. L. Kalmar, S. L. Snyder, F. S. Cusdin, J. Y. Ester, J. J. Sando, B. E. Isakson, A. P. Jackson and M. K. Patel (2010). "The importance of serine 161 in the sodium channel β3 subunit for modulation of NaV1. 2 gating." Pflügers Archiv-European Journal of Physiology **460**(4): 743-753.

Messner, D. J. and W. A. Catterall (1985). "The sodium channel from rat brain. Separation and characterization of subunits." Journal of Biological Chemistry **260**(19): 10597-10604.

Metherate, R., C. L. Cox and J. H. Ashe (1992). "Cellular bases of neocortical activation: modulation of neural oscillations by the nucleus basalis and endogenous acetylcholine." Journal of Neuroscience **12**(12): 4701-4711.

Mistry, A. M., C. H. Thompson, A. R. Miller, C. G. Vanoye, A. L. George, Jr. and J. A. Kearney (2014). "Strain- and age-dependent hippocampal neuron sodium currents correlate with epilepsy severity in Dravet syndrome mice." Neurobiol Dis **65**: 1-11.

Mistry, A. M., C. H. Thompson, A. R. Miller, C. G. Vanoye, A. L. George Jr and J. A. Kearney (2014). "Strain-and age-dependent hippocampal neuron sodium currents correlate with epilepsy severity in Dravet syndrome mice." Neurobiology of disease **65**: 1-11.

Mitrovic, N., A. L. George and R. Horn (2000). "Role of domain 4 in sodium channel slow inactivation." The Journal of general physiology **115**(6): 707-718.

Mitzdorf, U. (1985). "Current source-density method and application in cat cerebral cortex: investigation of evoked potentials and EEG phenomena." Physiological reviews **65**(1): 37-100.

Miyazaki, H., F. Oyama, R. Inoue, T. Aosaki, T. Abe, H. Kiyonari, Y. Kino, M. Kurosawa, J. Shimizu and I. Ogiwara (2014). "Singular localization of sodium channel β4 subunit in unmyelinated fibres and its role in the striatum." Nature Communications **5**: 5525.

Moore, J., N. Stockbridge and M. Westerfield (1983). "On the site of impulse initiation in a neurone." The Journal of Physiology **336**(1): 301-311.

Morgan, K., E. B. Stevens, B. Shah, P. J. Cox, A. K. Dixon, K. Lee, R. D. Pinnock, J. Hughes, P. J. Richardson and K. Mizuguchi (2000). "β3: an additional auxiliary subunit of the voltage-

sensitive sodium channel that modulates channel gating with distinct kinetics." Proceedings of the National Academy of Sciences **97**(5): 2308-2313.

Morgan, R. J. and I. Soltesz (2008). "Nonrandom connectivity of the epileptic dentate gyrus predicts a major role for neuronal hubs in seizures." Proc Natl Acad Sci U S A **105**(16): 6179-6184.

Moubarak, E., D. Engel, M. A. Dufour, M. Tapia, F. Tell and J.-M. Goaillard (2019). "Robustness to axon initial segment variation is explained by somatodendritic excitability in rat substantia nigra dopaminergic neurons." Journal of Neuroscience **39**(26): 5044-5063.

Nakamura, K., M. Kato, H. Osaka, S. Yamashita, E. Nakagawa, K. Haginoya, J. Tohyama, M. Okuda, T. Wada and S. Shimakawa (2013). "Clinical spectrum of SCN2A mutations expanding to Ohtahara syndrome." Neurology **81**(11): 992-998.

Namadurai, S., D. Balasuriya, R. Rajappa, M. Wiemhöfer, K. Stott, J. Klingauf, J. M. Edwardson, D. Y. Chirgadze and A. P. Jackson (2014). "Crystal structure and molecular imaging of the Nav channel β3 subunit indicates a trimeric assembly." Journal of Biological Chemistry **289**(15): 10797-10811.

Neale, B. M., Y. Kou, L. Liu, A. Ma'Ayan, K. E. Samocha, A. Sabo, C.-F. Lin, C. Stevens, L.-S. Wang and V. Makarov (2012). "Patterns and rates of exonic de novo mutations in autism spectrum disorders." Nature **485**(7397): 242.

Nelson, A. D. and P. M. Jenkins (2017). "Axonal membranes and their domains: assembly and function of the axon initial segment and node of Ranvier." Frontiers in cellular neuroscience **11**: 136.

Nguyen, H. M., H. Miyazaki, N. Hoshi, B. J. Smith, N. Nukina, A. L. Goldin and K. G. Chandy (2012). "Modulation of voltage-gated K+ channels by the sodium channel beta1 subunit." Proc Natl Acad Sci U S A **109**(45): 18577-18582.

Nguyen, H. M., H. Miyazaki, N. Hoshi, B. J. Smith, N. Nukina, A. L. Goldin and K. G. Chandy (2012). "Modulation of voltage-gated K+ channels by the sodium channel β1 subunit." Proceedings of the National Academy of Sciences **109**(45): 18577-18582.

Noda, M., T. Ikeda, H. Suzuki, H. Takeshima, T. Takahashi, M. Kuno and S. Numa (1986). "Expression of functional sodium channels from cloned cDNA." Nature **322**(6082): 826-828.

Noda, M., H. Suzuki, S. Numa and W. Stühmer (1989). "A single point mutation confers tetrodotoxin and saxitoxin insensitivity on the sodium channel II." FEBS letters **259**(1): 213-216.

Nusser, Z. (2009). "Variability in the subcellular distribution of ion channels increases neuronal diversity." Trends in neurosciences **32**(5): 267-274.

O'Brien, J. E. and M. H. Meisler (2013). "Sodium channel SCN8A (Nav1. 6): properties and de novo mutations in epileptic encephalopathy and intellectual disability." Frontiers in genetics **4**: 213.

O'Malley, H. A., J. M. Hull, B. C. Clawson, C. Chen, G. Owens-Fiestan, M. B. Jameson, S. J. Aton, J. M. Parent and L. L. Isom (2019). "Scn1b deletion in adult mice results in seizures and SUDEP." Ann Clin Transl Neurol **6**(6): 1121-1126.

O'Malley, H. A., J. M. Hull, B. C. Clawson, C. Chen, G. Owens-Fiestan, M. B. Jameson, S. J. Aton, J. M. Parent and L. L. Isom (2019). "Scn1b deletion in adult mice results in seizures and SUDEP." Annals of clinical and translational neurology **6**(6): 1121-1126.

O'Malley, H. A. and L. L. Isom (2015). "Sodium Channel beta Subunits: Emerging Targets in Channelopathies." Annu Rev Physiol **77**: 481-504.

O'Malley, H. A. and L. L. Isom (2015). "Sodium channel β subunits: emerging targets in channelopathies." Annual review of physiology **77**: 481-504.

O'Malley, H. A., A. B. Shreiner, G.-H. Chen, G. B. Huffnagle and L. L. Isom (2009). "Loss of Na+ channel β2 subunits is neuroprotective in a mouse model of multiple sclerosis." Molecular and Cellular Neuroscience **40**(2): 143-155.

O'Roak, B. J., L. Vives, S. Girirajan, E. Karakoc, N. Krumm, B. P. Coe, R. Levy, A. Ko, C. Lee and J. D. Smith (2012). "Sporadic autism exomes reveal a highly interconnected protein network of de novo mutations." Nature **485**(7397): 246.

Ogiwara, I., T. Iwasato, H. Miyamoto, R. Iwata, T. Yamagata, E. Mazaki, Y. Yanagawa, N. Tamamaki, T. K. Hensch and S. Itohara (2013). "Nav1. 1 haploinsufficiency in excitatory neurons ameliorates seizure-associated sudden death in a mouse model of Dravet syndrome." Human molecular genetics **22**(23): 4784-4804.

Ogiwara, I., T. Iwasato, H. Miyamoto, R. Iwata, T. Yamagata, E. Mazaki, Y. Yanagawa, N. Tamamaki, T. K. Hensch, S. Itohara and K. Yamakawa (2013). "Nav1.1 haploinsufficiency in excitatory neurons ameliorates seizure-associated sudden death in a mouse model of Dravet syndrome." Hum Mol Genet **22**(23): 4784-4804.

Ogiwara, I., H. Miyamoto, N. Morita, N. Atapour, E. Mazaki, I. Inoue, T. Takeuchi, S. Itohara, Y. Yanagawa and K. Obata (2007). "Nav1. 1 localizes to axons of parvalbumin-positive inhibitory interneurons: a circuit basis for epileptic seizures in mice carrying an Scn1a gene mutation." Journal of Neuroscience **27**(22): 5903-5914.

Ogiwara, I., H. Miyamoto, N. Morita, N. Atapour, E. Mazaki, I. Inoue, T. Takeuchi, S. Itohara, Y. Yanagawa, K. Obata, T. Furuichi, T. K. Hensch and K. Yamakawa (2007). "Na(v)1.1 localizes to axons of parvalbumin-positive inhibitory interneurons: a circuit basis for epileptic seizures in mice carrying an Scn1a gene mutation." J Neurosci **27**(22): 5903-5914.

Ogiwara, I., T. Nakayama, T. Yamagata, H. Ohtani, E. Mazaki, S. Tsuchiya, Y. Inoue and K. Yamakawa (2012). "A homozygous mutation of voltage-gated sodium channel beta(I) gene SCN1B in a patient with Dravet syndrome." Epilepsia **53**(12): e200-203.

Ogiwara, I., T. Nakayama, T. Yamagata, H. Ohtani, E. Mazaki, S. Tsuchiya, Y. Inoue and K. Yamakawa (2012). "A homozygous mutation of voltage-gated sodium channel βI gene SCN1B in a patient with Dravet syndrome." Epilepsia **53**(12): e200-e203.

Okaty, B. W., M. N. Miller, K. Sugino, C. M. Hempel and S. B. Nelson (2009). "Transcriptional and electrophysiological maturation of neocortical fast-spiking GABAergic interneurons." Journal of Neuroscience **29**(21): 7040-7052.

Olsen, S. R., D. S. Bortone, H. Adesnik and M. Scanziani (2012). "Gain control by layer six in cortical circuits of vision." Nature **483**(7387): 47-52.

Ong, B.-H., G. F. Tomaselli and J. R. Balser (2000). "A structural rearrangement in the sodium channel pore linked to slow inactivation and use dependence." The Journal of general physiology **116**(5): 653-662.

Osorio, N., G. Alcaraz, F. Padilla, F. Couraud, P. Delmas and M. Crest (2005). "Differential targeting and functional specialization of sodium channels in cultured cerebellar granule cells." The Journal of physiology **569**(3): 801-816.

Ottolini, M., B. S. Barker, R. P. Gaykema, M. H. Meisler and M. K. Patel (2017). "Aberrant sodium channel currents and hyperexcitability of medial entorhinal cortex neurons in a mouse model of SCN8A encephalopathy." Journal of Neuroscience **37**(32): 7643-7655.

Padmanabhan, K. and N. N. Urban (2010). "Intrinsic biophysical diversity decorrelates neuronal firing while increasing information content." Nature neuroscience **13**(10): 1276.

Padmanabhan, K. and N. N. Urban (2010). "Intrinsic biophysical diversity decorrelates neuronal firing while increasing information content." Nat Neurosci **13**(10): 1276-1282.

Papale, L. A., B. Beyer, J. M. Jones, L. M. Sharkey, S. Tufik, M. Epstein, V. A. Letts, M. H. Meisler, W. N. Frankel and A. Escayg (2009). "Heterozygous mutations of the voltage-gated sodium channel SCN8A are associated with spike-wave discharges and absence epilepsy in mice." Human molecular genetics **18**(9): 1633-1641.

Parent, J. M., T. W. Yu, R. T. Leibowitz, D. H. Geschwind, R. S. Sloviter and D. H. Lowenstein (1997). "Dentate granule cell neurogenesis is increased by seizures and contributes to aberrant network reorganization in the adult rat hippocampus." J Neurosci **17**(10): 3727-3738.

Patino, G. A., W. J. Brackenbury, Y. Bao, L. F. Lopez-Santiago, H. A. O'Malley, C. Chen, J. D. Calhoun, R. G. Lafrenière, P. Cossette and G. A. Rouleau (2011). "Voltage-gated Na+ channel β1B: a secreted cell adhesion molecule involved in human epilepsy." Journal of Neuroscience **31**(41): 14577-14591.

Patino, G. A., L. R. Claes, L. F. Lopez-Santiago, E. A. Slat, R. S. Dondeti, C. Chen, H. A. O'Malley, C. B. Gray, H. Miyazaki and N. Nukina (2009). "A functional null mutation of SCN1B in a patient with Dravet syndrome." Journal of Neuroscience **29**(34): 10764-10778.

Patino, G. A., L. R. Claes, L. F. Lopez-Santiago, E. A. Slat, R. S. Dondeti, C. Chen, H. A. O'Malley, C. B. Gray, H. Miyazaki, N. Nukina, F. Oyama, P. De Jonghe and L. L. Isom (2009). "A functional null mutation of SCN1B in a patient with Dravet syndrome." J Neurosci **29**(34): 10764-10778.

Paul, J. R., D. DeWoskin, L. J. McMeekin, R. M. Cowell, D. B. Forger and K. L. Gamble (2016). "Regulation of persistent sodium currents by glycogen synthase kinase 3 encodes daily rhythms of neuronal excitability." Nature Communications **7**.

Petersen, C. C. (2017). "Whole-cell recording of neuronal membrane potential during behavior." Neuron **95**(6): 1266-1281.

Poulet, J. F. and C. C. Petersen (2008). "Internal brain state regulates membrane potential synchrony in barrel cortex of behaving mice." Nature **454**(7206): 881.

Prettejohn, B. J., M. J. Berryman and M. D. McDonnell (2011). "Methods for generating complex networks with selected structural properties for simulations: a review and tutorial for neuroscientists." Frontiers in computational neuroscience **5**: 11.

Qu, Y., R. Curtis, D. Lawson, K. Gilbride, P. Ge, P. DiStefano, I. Silos-Santiago, W. A. Catterall and T. Scheuer (2001). "Differential modulation of sodium channel gating and persistent sodium currents by the β1, β2, and β3 subunits." Molecular and Cellular Neuroscience **18**(5): 570-580.

Qu, Y., J. C. Rogers, S.-F. Chen, K. A. McCormick, T. Scheuer and W. A. Catterall (1999). "Functional roles of the extracellular segments of the sodium channel α subunit in voltage-dependent gating and modulation by β1 subunits." Journal of Biological Chemistry **274**(46): 32647-32654.

Ramadan, W., N. Patel, S. Anazi, A. Y. Kentab, F. A. Bashiri, M. H. Hamad, L. Jad, M. A. Salih, H. Alsaif and M. Hashem (2017). "Confirming the recessive inheritance of SCN1B mutations in developmental epileptic encephalopathy." Clinical Genetics (doi: 10.1111/cge.12999.).

Ramadan, W., N. Patel, S. Anazi, A. Y. Kentab, F. A. Bashiri, M. H. Hamad, L. Jad, M. A. Salih, H. Alsaif, M. Hashem, E. Faqeih, H. E. Shamseddin and F. S. Alkuraya (2017). "Confirming the recessive inheritance of SCN1B mutations in developmental epileptic encephalopathy." Clin Genet.

RAMON, S. C. (1952). "Structure and connections of neurons." Bulletin of the Los Angeles Neurological Society **17**(1-2): 5-46.

Rapp, M., Y. Yarom and I. Segev (1996). "Modeling back propagating action potential in weakly excitable dendrites of neocortical pyramidal cells." Proceedings of the National Academy of Sciences **93**(21): 11985-11990.

Ratcliffe, C. F., Y. Qu, K. A. McCormick, V. C. Tibbs, J. E. Dixon, T. Scheuer and W. A. Catterall (2000). "A sodium channel signaling complex: modulation by associated receptor protein tyrosine phosphatase β." Nature neuroscience **3**(5): 437-444.

Ratcliffe, C. F., R. E. Westenbroek, R. Curtis and W. A. Catterall (2001). "Sodium channel β1 and β3 subunits associate with neurofascin through their extracellular immunoglobulin-like domain." J Cell Biol **154**(2): 427-434.

Rauch, A., D. Wieczorek, E. Graf, T. Wieland, S. Endele, T. Schwarzmayr, B. Albrecht, D. Bartholdi, J. Beygo and N. Di Donato (2012). "Range of genetic mutations associated with severe non-syndromic sporadic intellectual disability: an exome sequencing study." The Lancet **380**(9854): 1674-1682.

Recio-Pinto, E., D. S. Duch, S. R. Levinson and B. W. Urban (1987). "Purified and unpurified sodium channels from eel electroplax in planar lipid bilayers." The Journal of general physiology **90**(3): 375-395.

Reid, C. A., B. Leaw, K. L. Richards, R. Richardson, V. Wimmer, C. Yu, E. L. Hill-Yardin, H. Lerche, I. E. Scheffer and S. F. Berkovic (2014). "Reduced dendritic arborization and hyperexcitability of pyramidal neurons in a Scn1b-based model of Dravet syndrome." Brain **137**(6): 1701-1715.

Reid, C. A., B. Leaw, K. L. Richards, R. Richardson, V. Wimmer, C. Yu, E. L. Hill-Yardin, H. Lerche, I. E. Scheffer, S. F. Berkovic and S. Petrou (2014). "Reduced dendritic arborization and hyperexcitability of pyramidal neurons in a Scn1b-based model of Dravet syndrome." Brain.

Rubinstein, M., S. Han, C. Tai, R. E. Westenbroek, A. Hunker, T. Scheuer and W. A. Catterall (2015). "Dissecting the phenotypes of Dravet syndrome by gene deletion." Brain **138**(Pt 8): 2219-2233.

Rudy, B. (1978). "Slow inactivation of the sodium conductance in squid giant axons. Pronase resistance." The Journal of physiology **283**(1): 1-21.

Sanders, S. J., M. T. Murtha, A. R. Gupta, J. D. Murdoch, M. J. Raubeson, A. J. Willsey, A. G. Ercan-Sencicek, N. M. DiLullo, N. N. Parikshak and J. L. Stein (2012). "De novo mutations revealed by whole-exome sequencing are strongly associated with autism." Nature **485**(7397): 237.

Santhakumar, V., I. Aradi and I. Soltesz (2005). "Role of mossy fiber sprouting and mossy cell loss in hyperexcitability: a network model of the dentate gyrus incorporating cell types and axonal topography." J Neurophysiol **93**(1): 437-453.

Sashihara, S., C. A. Greer, Y. Oh and S. G. Waxman (1996). "Cell-Specific Differential Expression of Na+-Channel b1-Subunit mRNA in the Olfactory System during Postnatal Development and after Denervation." Journal of Neuroscience **16**(2): 702-713.

Schauf, C., T. Pencek and F. Davis (1976). "Slow sodium inactivation in Myxicola axons. Evidence for a second inactive state." Biophysical journal **16**(7): 771-778.

Scheffer, I. E., Y. H. Zhang, J. Gecz and L. Dibbens (2010). "Genetics of the epilepsies: Genetic twists in the channels and other tales." Epilepsia **51**(s1): 33-36.

Scheuer, T. (2011). Regulation of sodium channel activity by phosphorylation. Seminars in cell & developmental biology, Elsevier.

Schmidt, J., S. Rossie and W. A. Catterall (1985). "A large intracellular pool of inactive Na channel alpha subunits in developing rat brain." Proceedings of the National Academy of Sciences **82**(14): 4847-4851.

Schmidt, J. W. and W. A. Catterall (1986). "Biosynthesis and processing of the α subunit of the voltage-sensitive sodium channel in rat brain neurons." Cell **46**(3): 437-445.

Schulz, D. J., J.-M. Goaillard and E. Marder (2006). "Variable channel expression in identified single and electrically coupled neurons in different animals." Nature neuroscience **9**(3): 356.

Shah, B., E. Stevens, R. Pinnock, A. Dixon and K. Lee (2001). "Developmental expression of the novel voltage-gated sodium channel auxiliary subunit β3, in rat CNS." The Journal of physiology **534**(3): 763-776.

Shimizu, H., H. Miyazaki, N. Ohsawa, S. Shoji, Y. Ishizuka-Katsura, A. Tosaki, F. Oyama, T. Terada, K. Sakamoto and M. Shirouzu (2016). "Structure-based site-directed photo-crosslinking

analyses of multimeric cell-adhesive interactions of voltage-gated sodium channel β subunits." Scientific reports **6**(doi: 10.1038/srep26618.).

Skluzacek, J. V., K. P. Watts, O. Parsy, B. Wical and P. Camfield (2011). "Dravet syndrome and parent associations: the IDEA League experience with comorbid conditions, mortality, management, adaptation, and grief." Epilepsia **52**(s2): 95-101.

Smith, R. S., C. J. Kenny, V. Ganesh, A. Jang, R. Borges-Monroy, J. N. Partlow, R. S. Hill, T. Shin, A. Y. Chen and R. N. Doan (2018). "Sodium channel SCN3A (NaV1. 3) regulation of human cerebral cortical folding and oral motor development." Neuron **99**(5): 905-913. e907.

Softky, W. R. and C. Koch (1993). "The highly irregular firing of cortical cells is inconsistent with temporal integration of random EPSPs." Journal of Neuroscience **13**(1): 334-350.

Soltesz, I. and A. Losonczy (2018). "CA1 pyramidal cell diversity enabling parallel information processing in the hippocampus." Nat Neurosci **21**(4): 484-493.

Soltesz, I. and A. Losonczy (2018). "CA1 pyramidal cell diversity enabling parallel information processing in the hippocampus." Nature neuroscience **21**(4): 484.

Spampanato, J., J. Kearney, G. De Haan, D. McEwen, A. Escayg, I. Aradi, B. MacDonald, S. Levin, I. Soltesz and P. Benna (2004). "A novel epilepsy mutation in the sodium channel SCN1A identifies a cytoplasmic domain for β subunit interaction." Journal of Neuroscience **24**(44): 10022-10034.

Sporns, O. and J. D. Zwi (2004). "The small world of the cerebral cortex." Neuroinformatics **2**(2): 145-162.

Srinivasan, J., M. Schachner and W. A. Catterall (1998). "Interaction of voltage-gated sodium channels with the extracellular matrix molecules tenascin-C and tenascin-R." Proceedings of the National Academy of Sciences **95**(26): 15753-15757.

Steffenburg, S., C. Gillberg and U. Steffenburg (1996). "Psychiatric disorders in children and adolescents with mental retardation and active epilepsy." Archives of Neurology **53**(9): 904-912.

Strogatz, S. H. (2000). "From Kuramoto to Crawford: exploring the onset of synchronization in populations of coupled oscillators." Physica D: Nonlinear Phenomena **143.1-4**: 1-20.

Stühmer, W., F. Conti, H. Suzuki, X. Wang, M. Noda, N. Yahagi, H. Kubo and S. Numa (1989). "Structural parts involved in activation and inactivation of the sodium channel." Nature **339**(6226): 597.

Sugawara, T., Y. Tsurubuchi, K. L. Agarwala, M. Ito, G. Fukuma, E. Mazaki-Miyazaki, H. Nagafuji, M. Noda, K. Imoto and K. Wada (2001). "A missense mutation of the Na+ channel αII subunit gene Nav1. 2 in a patient with febrile and afebrile seizures causes channel dysfunction." Proceedings of the National Academy of Sciences **98**(11): 6384-6389.

Sutkowski, E. and W. A. Catterall (1990). "Beta 1 subunits of sodium channels. Studies with subunit-specific antibodies." Journal of Biological Chemistry **265**(21): 12393-12399.

Tai, C., Y. Abe, R. E. Westenbroek, T. Scheuer and W. A. Catterall (2014). "Impaired excitability of somatostatin- and parvalbumin-expressing cortical interneurons in a mouse model of Dravet syndrome." Proc Natl Acad Sci U S A **111**(30): E3139-3148.

Tai, C., Y. Abe, R. E. Westenbroek, T. Scheuer and W. A. Catterall (2014). "Impaired excitability of somatostatin-and parvalbumin-expressing cortical interneurons in a mouse model of Dravet syndrome." Proceedings of the National Academy of Sciences **111**(30): E3139-E3148.

Tammaro, P., F. Conti and O. Moran (2002). "Modulation of sodium current in mammalian cells by an epilepsy-correlated β1-subunit mutation." Biochemical and biophysical research communications **291**(4): 1095-1101.

Terlau, H., S. H. Heinemann, W. Stühmer, M. Pusch, F. Conti, K. Imoto and S. Numa (1991). "Mapping the site of block by tetrodotoxin and saxitoxin of sodium channel II." FEBS letters **293**(1-2): 93-96.

Todt, H., S. C. Dudley Jr, J. W. Kyle, R. J. French and H. A. Fozzard (1999). "Ultra-slow inactivation in μ1 Na+ channels is produced by a structural rearrangement of the outer vestibule." Biophysical journal **76**(3): 1335-1345.

Tomiko, S. A., R. L. Rosenberg, M. C. Emerick and W. S. Agnew (1986). "Fluorescence assay for neurotoxin-modulated ion transport by the reconstituted voltage-activated sodium channel isolated from eel electric organ." Biochemistry **25**(8): 2162-2174.

Trimmer, J. S., S. S. Cooperman, S. A. Tomiko, J. Zhou, S. M. Crean, M. B. Boyle, R. G. Kalen, Z. Sheng, R. L. Barchi and F. J. Sigworth (1989). "Primary structure and functional expression of a mammalian skeletal muscle sodium channel." Neuron **3**(1): 33-49.

Tsien, J. Z., D. F. Chen, D. Gerber, C. Tom, E. H. Mercer, D. J. Anderson, M. Mayford, E. R. Kandel and S. Tonegawa (1996). "Subregion- and cell type-restricted gene knockout in mouse brain." Cell **87**(7): 1317-1326.

Uebachs, M., C. Albus, T. Opitz, L. Isom, I. Niespodziany, C. Wolff and H. Beck (2012). "Loss of β1 accessory Na+ channel subunits causes failure of carbamazepine, but not of lacosamide, in blocking high-frequency firing via differential effects on persistent Na+ currents." Epilepsia **53**(11): 1959-1967.

Uebachs, M., T. Opitz, M. Royeck, G. Dickhof, M.-T. Horstmann, L. L. Isom and H. Beck (2010). "Efficacy loss of the anticonvulsant carbamazepine in mice lacking sodium channel β subunits via paradoxical effects on persistent sodium currents." Journal of Neuroscience **30**(25): 8489-8501.

Usluer, S., M. A. Kayserili, A. G. Eken, U. Yiş, C. Leu, J. Altmüller, H. Thiele, P. Nürnberg, T. Sander and S. H. Çağlayan (2017). "Association of a synonymous SCN1B variant affecting splicing efficiency with Benign Familial Infantile Epilepsy (BFIE)." European Journal of Paediatric Neurology.

Van Wart, A., J. S. Trimmer and G. Matthews (2007). "Polarized distribution of ion channels within microdomains of the axon initial segment." Journal of Comparative Neurology **500**(2): 339-352.

Vargas, E., V. Yarov-Yarovoy, F. Khalili-Araghi, W. A. Catterall, M. L. Klein, M. Tarek, E. Lindahl, K. Schulten, E. Perozo and F. Bezanilla (2012). "An emerging consensus on voltage-dependent gating from computational modeling and molecular dynamics simulations." The Journal of general physiology **140**(6): 587-594.

Vassilev, P. M., T. Scheuer and W. A. Catterall (1988). "Identification of an intracellular peptide segment involved in sodium channel inactivation." Science **241**(4873): 1658-1661.

Vedantham, V. and S. C. Cannon (1998). "Slow inactivation does not affect movement of the fast inactivation gate in voltage-gated Na+ channels." The Journal of general physiology **111**(1): 83-93.

Veeramah, K. R., J. E. O'Brien, M. H. Meisler, X. Cheng, S. D. Dib-Hajj, S. G. Waxman, D. Talwar, S. Girirajan, E. E. Eichler and L. L. Restifo (2012). "De novo pathogenic SCN8A mutation identified by whole-genome sequencing of a family quartet affected by infantile epileptic encephalopathy and SUDEP." The American Journal of Human Genetics **90**(3): 502-510.

Vijayaragavan, K., A. J. Powell, I. J. Kinghorn and M. Chahine (2004). "Role of auxiliary β 1-, β 2-, and β 3-subunits and their interaction with Na v 1.8 voltage-gated sodium channel." Biochemical and biophysical research communications **319**(2): 531-540.

Villeneuve, N., V. Laguitton, M. Viellard, A. Lépine, B. Chabrol, C. Dravet and M. Milh (2014). "Cognitive and adaptive evaluation of 21 consecutive patients with Dravet syndrome." Epilepsy & behavior **31**: 143-148.

Wagnon, J. L., B. S. Barker, M. Ottolini, Y. Park, A. Volkheimer, P. Valdez, M. E. Swinkels, M. K. Patel and M. H. Meisler (2017). "Loss-of-function variants of SCN8A in intellectual disability without seizures." Neurology Genetics **3**(4): e170.

Wagnon, J. L. and M. H. Meisler (2015). "Recurrent and non-recurrent mutations of SCN8A in epileptic encephalopathy." Frontiers in neurology **6**: 104.

Wallace, A., E. Wirrell and D. L. Kenney-Jung (2016). "Pharmacotherapy for Dravet syndrome." Pediatric Drugs **18**(3): 197-208.

Wallace, R. H., D. W. Wang, R. Singh, I. E. Scheffer, A. L. George, H. A. Phillips, K. Saar, A. Reis, E. W. Johnson and G. R. Sutherland (1998). "Febrile seizures and generalized epilepsy associated with a mutation in the Na+-channel ß1 subunit gene SCN1B." Nature genetics **19**(4): 366-370.

Wang, Y., X. Du, R. Bin, S. Yu, Z. Xia, G. Zheng, J. Zhong, Y. Zhang, Y.-h. Jiang and Y. Wang (2017). "Genetic variants identified from epilepsy of unknown etiology in chinese children by targeted exome sequencing." Scientific reports **7**: 40319.

Watanabe, H., T. T. Koopmann, S. Le Scouarnec, T. Yang, C. R. Ingram, J.-J. Schott, S. Demolombe, V. Probst, F. Anselme and D. Escande (2008). "Sodium channel β1 subunit

mutations associated with Brugada syndrome and cardiac conduction disease in humans." The Journal of clinical investigation **118**(6): 2260-2268.

Watts, D. J. and S. H. Strogatz (1998). "Collective dynamics of 'small-world'networks." nature **393**(6684): 440.

Westenbroek, R. E., D. K. Merrick and W. A. Catterall (1989). "Differential subcellular localization of the RI and RII Na+ channel subtypes in central neurons." Neuron **3**(6): 695-704.

Wilson, M. J., M.-M. Zhang, L. Azam, B. M. Olivera, G. Bulaj and D. Yoshikami (2011). "Navβ subunits modulate the inhibition of Nav1. 8 by the analgesic gating modifier μO-conotoxin MrVIB." Journal of Pharmacology and Experimental Therapeutics **338**(2): 687-693.

Wilson, M. J., M.-M. Zhang, J. Gajewiak, L. Azam, J. E. Rivier, B. M. Olivera and D. Yoshikami (2015). "α-And β-subunit composition of voltage-gated sodium channels investigated with μ-conotoxins and the recently discovered μO § -conotoxin GVIIJ." Journal of neurophysiology **113**(7): 2289-2301.

Wimmer, V. C., R. C. Harty, K. L. Richards, A. M. Phillips, H. Miyazaki, N. Nukina and S. Petrou (2015). "Sodium channel β1 subunit localizes to axon initial segments of excitatory and inhibitory neurons and shows regional heterogeneity in mouse brain." Journal of Comparative Neurology **523**(5): 814-830.

Wimmer, V. C., C. A. Reid, S. Mitchell, K. L. Richards, B. B. Scaf, B. T. Leaw, E. L. Hill, M. Royeck, M.-T. Horstmann and B. A. Cromer (2010). "Axon initial segment dysfunction in a mouse model of genetic epilepsy with febrile seizures plus." The Journal of clinical investigation **120**(8): 2661-2671.

Wisedchaisri, G., L. Tonggu, E. McCord, T. M. G. El-Din, L. Wang, N. Zheng and W. A. Catterall (2019). "Resting-State Structure and Gating Mechanism of a Voltage-Gated Sodium Channel." Cell.

Wolff, M., K. M. Johannesen, U. B. Hedrich, S. Masnada, G. Rubboli, E. Gardella, G. Lesca, D. Ville, M. Milh and L. Villard (2017). "Genetic and phenotypic heterogeneity suggest therapeutic implications in SCN2A-related disorders." Brain **140**(5): 1316-1336.

Wollner, D. A. and W. A. Catterall (1986). "Localization of sodium channels in axon hillocks and initial segments of retinal ganglion cells." Proceedings of the National Academy of Sciences **83**(21): 8424-8428.

Wong, H.-K., T. Sakurai, F. Oyama, K. Kaneko, K. Wada, H. Miyazaki, M. Kurosawa, B. De Strooper, P. Saftig and N. Nukina (2005). "β Subunits of voltage-gated sodium channels are novel substrates of β-site amyloid precursor protein-cleaving enzyme (BACE1) and γ-secretase." Journal of Biological Chemistry **280**(24): 23009-23017.

Xiao, Z.-C., D. S. Ragsdale, J. D. Malhotra, L. N. Mattei, P. E. Braun, M. Schachner and L. L. Isom (1999). "Tenascin-R is a functional modulator of sodium channel β subunits." Journal of Biological Chemistry **274**(37): 26511-26517.

Yan, Z., Q. Zhou, L. Wang, J. Wu, Y. Zhao, G. Huang, W. Peng, H. Shen, J. Lei and N. Yan (2017). "Structure of the Nav1. 4-β1 Complex from Electric Eel." Cell **170**(3): 470-482. e411.

Yereddi, N. R., F. S. Cusdin, S. Namadurai, L. C. Packman, T. P. Monie, P. Slavny, J. J. Clare, A. J. Powell and A. P. Jackson (2013). "The immunoglobulin domain of the sodium channel β3 subunit contains a surface-localized disulfide bond that is required for homophilic binding." The FASEB Journal **27**(2): 568-580.

Yin, L., M. J. Rasch, Q. He, S. Wu, F. Dou and Y. Shu (2017). "Selective modulation of axonal sodium channel subtypes by 5-HT1A receptor in cortical pyramidal neuron." Cerebral Cortex **27**(1): 509-521.

Yizhar, O., L. E. Fenno, M. Prigge, F. Schneider, T. J. Davidson, D. J. O'shea, V. S. Sohal, I. Goshen, J. Finkelstein and J. T. Paz (2011). "Neocortical excitation/inhibition balance in information processing and social dysfunction." Nature **477**(7363): 171.

Yu, F. H., M. Mantegazza, R. E. Westenbroek, C. A. Robbins, F. Kalume, K. A. Burton, W. J. Spain, G. S. McKnight, T. Scheuer and W. A. Catterall (2006). "Reduced sodium current in GABAergic interneurons in a mouse model of severe myoclonic epilepsy in infancy." Nat Neurosci **9**(9): 1142-1149.

Yu, F. H., R. E. Westenbroek, I. Silos-Santiago, K. A. McCormick, D. Lawson, P. Ge, H. Ferriera, J. Lilly, P. S. DiStefano and W. A. Catterall (2003). "Sodium channel beta4, a new disulfide-linked auxiliary subunit with similarity to beta2." The Journal of neuroscience: the official journal of the Society for Neuroscience **23**(20): 7577-7585.

Zaman, T., I. Helbig, I. B. Božović, S. D. DeBrosse, A. C. Bergqvist, K. Wallis, L. Medne, A. Maver, B. Peterlin and K. L. Helbig (2018). "Mutations in SCN3A cause early infantile epileptic encephalopathy." Annals of neurology **83**(4): 703-717.

Zhang, M. M., M. J. Wilson, L. Azam, J. Gajewiak, J. E. Rivier, G. Bulaj, B. M. Olivera and D. Yoshikami (2013). "Co-expression of NaVβ subunits alters the kinetics of inhibition of voltage-gated sodium channels by pore-blocking μ-conotoxins." British journal of pharmacology **168**(7): 1597-1610.

Zhang, Z.-N., Q. Li, C. Liu, H.-B. Wang, Q. Wang and L. Bao (2008). "The voltage-gated Na+ channel Nav1. 8 contains an ER-retention/retrieval signal antagonized by the β3 subunit." Journal of cell science **121**(19): 3243-3252.

Zhao, J., M. E. O'Leary and M. Chahine (2011). "Regulation of Nav1. 6 and Nav1. 8 peripheral nerve Na+ channels by auxiliary β-subunits." Journal of neurophysiology **106**(2): 608-619.

Zimmer, T. and K. Benndorf (2007). "The Intracellular Domain of the β2 Subunit Modulates the Gating of Cardiac Na v 1.5 Channels." Biophysical journal **92**(11): 3885-3892.